CRBRP-ARD -0154

cy. 3

[redacted]

CLINCH RIVER BREEDER REACTOR PLANT

11:1 SCALE WIRE WRAPPED ROD BUNDLE AIR FLOW TEST, CORNER SUBCHANNEL

Oak Ridge National Laboratory
Research Library
4500N, MS-6191
LIBRARY LOAN COPY
DO NOT TRANSFER TO ANOTHER PERSON.
If you wish someone else to see this report, send in name with report and the library will arrange a loan.
ORNL-118(10-05)
(3 5-60)

JANUARY, 1977

TOPICAL REPORT

LMFBR

Follow release per DOE 9/19/2012

~~APPLIED TECHNOLOGY~~

~~Any Further Distribution By Any Holder Of This Document Or Of The Data Thereon To Third Parties Representing Foreign Interest, Foreign Governments, Foreign Companies, And Foreign Subsidiaries Or Foreign Division Of U.S. Companies Should Be Coordinated With The Director, Division Of Reactor Development And Demonstration, U.S. Energy Research And Development Administration.~~

WESTINGHOUSE ELECTRIC CORPORATION
ADVANCED REACTORS DIVISION

Prepared for Project Management Corporation and the U.S. Energy Research and Development Administration Under Contracts 49-18-12-3 and EY-76-C-15-2395

TECHNICAL INFORMATION CENTER
UNITED STATES ENERGY RESEARCH AND DEVELOPMENT ADMINISTRATION

NOTICE

This report was prepared as an account of work sponsored by the United States Government. Neither the United States nor the United States Energy Research and Development Administration, nor any of their employees, nor any of their contractors, subcontractors, or their employees, makes any warranty, express or implied, or assumes any legal liability or responsibility for the accuracy, completeness or usefulness of any information, apparatus, product or process disclosed, or represents that its use would not infringe privately owned rights.

This report has been reproduced directly from the best available copy.

Available from USERDA Technical Information Center, P. O. Box 62, Oak Ridge, TN 37830

Price: Paper Copy $5.50 (domestic)

Printed in the United States of America
USERDA Technical Information Center, Oak Ridge, Tennessee

CRBRP-ARD-0154
Distribution Category UC-79e

CLINCH RIVER BREEDER REACTOR PLANT

11:1 SCALE WIRE WRAPPED ROD BUNDLE AIR FLOW TEST, CORNER SUBCHANNEL

TOPICAL REPORT

T.G. BARTHOLET
R.M. ROIDT
J.E. ROMANO

Prepared for Project Management Corporation and the U.S. Energy Research and Development Administration under Contracts 49-18-12-3 and EY-76-C-15-2395

Westinghouse Electric Corporation
Advanced Reactors Division
P.O. Box 158
Madison, Pennsylvania 15663

TABLE OF CONTENTS

	Page
LIST OF FIGURES	v
1.0 EXPERIMENTAL PROGRAM	1
1.1 Introduction and Summary	1
1.2 Background	1
2.0 DESCRIPTION OF EXPERIMENTAL APPARATUS	4
2.1 Overall Test Assembly	4
2.2 Side Subchannel Configuration	8
2.3 Test Sequence	8
3.0 PRELIMINARY EXPERIMENTS	19
3.1 Introduction	19
3.2 Axial Flow Development	19
3.3 Friction Factor Calculation	22
4.0 TRACER GAS EXPERIMENTS	25
4.1 Experimental Procedure	25
4.2 Experimental Results	25
5.0 GAP CROSSFLOW EXPERIMENTS	27
5.1 Experimental Procedure	27
5.2 Experimental Results	31
6.0 AXIAL FLOW EXPERIMENTS	35
6.1 Experimental Procedure	35
6.2 Experimental Results	35
7.0 CONCLUSIONS	38
REFERENCES	40

TABLE OF CONTENTS (cont'd)

Page

APPENDIX A - Tracer Gas Distribution Contours 42

APPENDIX B - Gap Crossflow Profiles 57

APPENDIX C - Axial Velocity Contours. 90

LIST OF FIGURES

Figure		Page
1-1	Corner Subchannel Configuration as Seen in the Downstream Direction	2
2-1	217-Pin Fuel Assembly with 10.87:1 Scale Model Cross Section Superimposed	5
2-2	Cross Section of Test Section (Dimensions in Inches)	6
2-3	Axial Layout of Test Section (Dimensions in Inches)	7
2-4	Measured Model Rod Diameters from Downstream End of Test Section in Inches	9
2-5	Clearance Gap Spacings 55.0 Inches from Downstream End of Test Section in Inches, Before Repair	10
2-6	Clearance Gap Spacings 93.5 Inches from Downstream End of Test Section in Inches, Before Repair	11
2-7	Clearance Gap Spacings 132.0 Inches from Downstream End of Test Section in Inches, Before Repair	12
2-8	Clearance Gap Spacings 55.0 Inches from Downstream End of Test Section in Inches, After Repair	13
2-9	Clearance Gap Spacings 93.5 Inches from Downstream End of Test Section in Inches, After Repair	14
2-10	Clearance Gap Spacings 132.0 Inches from Downstream End of Test Section in Inches, After Repair	15
2-11	Corner Subchannel Notation as Seen in The Downstream Direction	17
3-1	Experimental Determination of Angular Location of Wire Wrap	20
3-2	Axial Development of Axial Velocity	21
3-3	Static Pressure Drop Along the Duct	23
5-1	Schematic of Cobra Probe Calibration Procedure	28
5-2	Cobra Probe Calibration Curve: Cobra Probe $\Delta P/P_{Dynamic}$ vs. Transverse Flow Angle	29

LIST OF FIGURES (cont'd)

Figure		Page
5-3	Angle Between Cobra Probe and Instrumented Rod as a Function of Probe Height	30
5-4	$\overline{\phi}$ (α) as a Function of Wire Wrap Function for Gap at α=0°	33
5-5	$\overline{\phi}$ (α) as a Function of Wire Wrap Angle for Three Gaps	34
6-1	Subchannel Average Axial Velocities at Each Axial Plane	37
A-1	Tracer Gas Experiment One, 27 Inch Axial Location	43
A-2	Tracer Gas Experiment One, 21 Inch Axial Location	44
A-3	Tracer Gas Experiment One, 15 Inch Axial Location	45
A-4	Tracer Gas Experiment One, 9 Inch Axial Location	46
A-5	Tracer Gas Experiment Two, 39 Inch Axial Location	47
A-6	Tracer Gas Experiment Two, 33 Inch Axial Location	48
A-7	Tracer Gas Experiment Two, 27 Inch Axial Location	49
A-8	Tracer Gas Experiment Two, 21 Inch Axial Location	50
A-9	Tracer Gas Experiment Three, 27 Inch Axial Location	51
A-10	Tracer Gas Experiment Three, 21 Inch Axial Location	52
A-11	Tracer Gas Experiment Three, 15 Inch Axial Location	53
A-12	Tracer Gas Experiment Three, 9 Inch Axial Location	54
A-13	Tracer Gas Experiment Four, 27 Inch Axial Location	55
A-14	Tracer Gas Experiment Four, 21 Inch Axial Location	56
B-1	Dimensionless Crossflow Coefficient ϕ (ξ), α = -79.0°	58
B-2	Dimensionless Crossflow Coefficient ϕ (ξ), α = -76.5°	59
B-3	Dimensionless Crossflow Coefficient ϕ (ξ), α = -72.0°	60
B-4	Dimensionless Crossflow Coefficient ϕ (ξ), α = -69.5°	61
B-5	Dimensionless Crossflow Coefficient ϕ (ξ), α = -65.0°	62

LIST OF FIGURES (cont'd)

Figure		Page
B-6	Dimensionless Crossflow Coefficient ϕ (ξ), α = -61.5°	63
B-7	Dimensionless Crossflow Coefficient ϕ (ξ), α = -58.2°	64
B-8	Dimensionless Crossflow Coefficient ϕ (ξ), α = -55.0°	65
B-9	Dimensionless Crossflow Coefficient ϕ (ξ), α = -51.2°	66
B-10	Dimensionless Crossflow Coefficient ϕ (ξ), α = -47.5°	67
B-11	Dimensionless Crossflow Coefficient ϕ (ξ), α = -44.0°	68
B-12	Dimensionless Crossflow Coefficient ϕ (ξ), α = -40.5°	69
B-13	Dimensionless Crossflow Coefficient ϕ (ξ), α = -37.7°	70
B-14	Dimensionless Crossflow Coefficient ϕ (ξ), α = -34.2°	71
B-15	Dimensionless Crossflow Coefficient ϕ (ξ), α = -31.2°	72
B-16	Dimensionless Crossflow Coefficient ϕ (ξ), α = -28.0°	73
B-17	Dimensionless Crossflow Coefficient ϕ (ξ), α = -26.0°	74
B-18	Dimensionless Crossflow Coefficient ϕ (ξ), α = -22.7°	75
B-19	Dimensionless Crossflow Coefficient ϕ (ξ), α = -20.2°	76
B-20	Dimensionless Crossflow Coefficient ϕ (ξ), α = -16.7°	77
B-21	Dimensionless Crossflow Coefficient ϕ (ξ), α = -14.5°	78
B-22	Dimensionless Crossflow Coefficient ϕ (ξ), α = -11.7°	79
B-23	Dimensionless Crossflow Coefficient ϕ (ξ), α = 12.5°	80
B-24	Dimensionless Crossflow Coefficient ϕ (ξ), α = 14.5°	81
B-25	Dimensionless Crossflow Coefficient ϕ (ξ), α = 17.5°	82
B-26	Dimensionless Crossflow Coefficient ϕ (ξ), α = 22.0°	83
B-27	Dimensionless Crossflow Coefficient ϕ (ξ) for Three Gaps at α = -79.0°	84
B-28	Dimensionless Crossflow Coefficient ϕ (ξ) for Three Gaps at α = -72.0°	85

LIST OF FIGURES (Cont'd.)

Figure		Page
B-29	Dimensionless Crossflow Coefficient $\phi(\xi)$ for Three Gaps at $\alpha = -65.0°$	86
B-30	Dimensionless Crossflow Coefficient $\phi(\xi)$ for Three Gaps at $\alpha = -58.2°$	87
B-31	Dimensionless Crossflow Coefficient $\phi(\xi)$ for Three gaps at $\alpha = -51.2°$	88
B-32	Dimensionless Crossflow Coefficient $\phi(\xi)$ for Three Gaps at $\alpha = -44.0°$	89
C-1	Axial Velocity Distribution (Ft/Sec) 33 Inches From Downstream End of Pitot Tube Travel	91
C-2	Axial Velocity Distribution (Ft/Sec) 27 Inches From Downstream End of Pitot Tube Travel	92
C-3	Axial Velocity Distribution (Ft/Sec) 21 Inches From Downstream End of Pitot Tube Travel	93
C-4	Axial Velocity Distribution (Ft/Sec) 15 Inches From Downstream End of Pitot Tube Travel	94
C-5	Axial Velocity Distribution (Ft/Sec) 9 Inches From Downstream End of Pitot Tube Travel	95

1.0 EXPERIMENTAL PROGRAM

1.1 Introduction and Summary

This document is a report of the concluding experimental work conducted with the 10.87 to 1 scale air flow test facility at the Westinghouse Research Laboratories for the Energy Research and Development Administration under contract E(11-1)-2395. Experimental results for interior and side subchannels of the wire wrapped rod bundle have been previously reported[1,2]. Results of a similar test series for the corner subchannel region of the same test assembly are reported here.

The test assembly itself is an unheated 10.87:1 scale model of a portion of a Clinch River Breeder Reactor fuel assembly. As such, it offers a unique opportunity to make detailed measurements of mixing and flow behavior within the rod bundle. The experimental results described in this report cover identification of flow development characteristics, tracer gas mixing tests, gap crossflow mappings, and detailed axial flow measurements for the corner subchannel region of the test assembly. The test procedures are similar to those used in interior and side subchannel tests. The data obtained complement the previous test results in interior and side subchannels as a basis for further development of analytical techniques modeling the hydrodynamics of wire wrapped rod bundles.

1.2 Background

An LMFBR core is composed of parallel arrays of cylindrical fuel rods enclosed in ducts through which coolant flows axially. In the case of rods arranged on a triangular pitch within a hexagonal duct, this produces a corner subchannel configuration as shown in Figure 1-1. Transport of mass, momentum and energy takes place laterally through the clearance gaps as well as in the axial direction, which results in transverse distribution of these quantities. These distributions have considerable importance with respect to core design in determining flow and temperature characteristics.

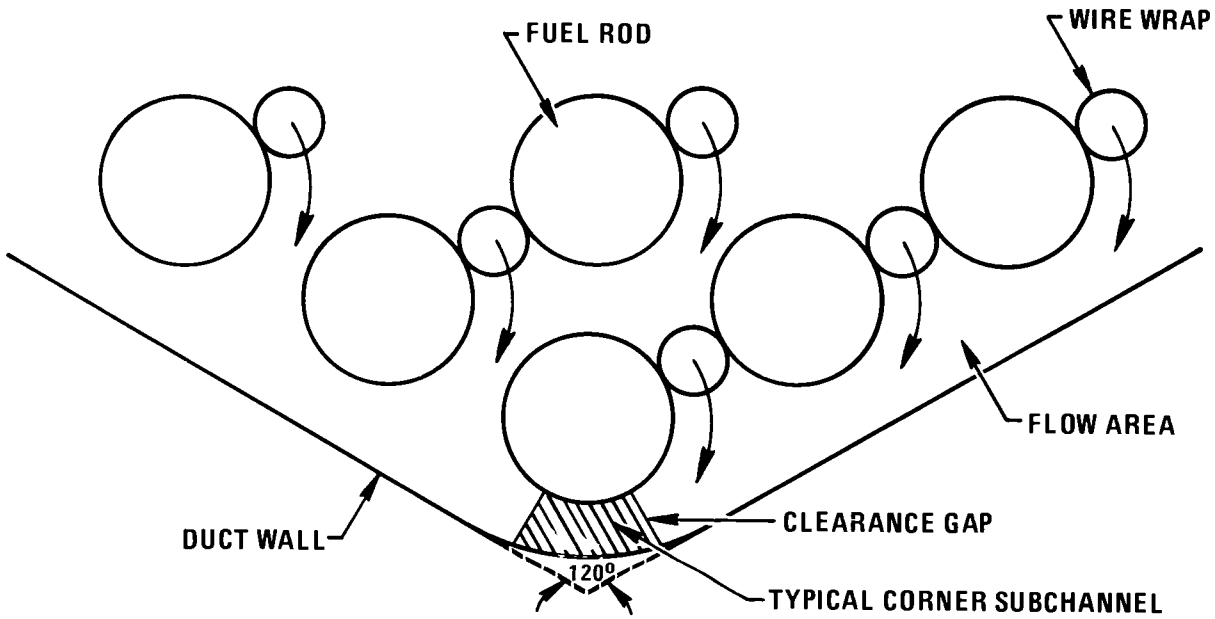

Figure 1-1. Corner Subchannel Configuration As Seen In The Downstream Direction

8786-1

At present, various analytical computer codes are used and are being developed to predict the hydrodynamic and thermal behavior of core assemblies. In general, these codes divide the rod array into subchannels and calculate values of pertinent, lumped parameters for the subchannels. They employ a variety of approximations for the purposes of representing physical data within the limitations of computer memory space and execution time.

The experimental data obtained through this test series at steady state, nominal flow conditions, as previously reported[1,2] and as described on the following pages, provide information on detailed hydrodynamic behavior of the coolant within the wire wrapped rod bundle. This test series is the only one which provides such data for interior, side and corner subchannels under the same conditions and in much detail. The data are important for evaluating and improving the approximations used in the analytical codes. Reduction and better quantification of the uncertainties in these calculational techniques are needed to provide a reliable and cost effective design of wire wrapped rod bundles.

2.0 DESCRIPTION OF EXPERIMENTAL APPARATUS

2.1 Overall Test Assembly

The asymmetric portion of the Clinch River Breeder Reactor fuel assembly design represented by the test assembly is indicated in Figure 2-1. Within the test assembly, four rods can accommodate flow sampling devices. These rods, which can be rotated or moved axially within their wire wrap are numbered in Figure 2-2. Figure 2-2 also gives the major dimensions of the test assembly cross-section.

Figure 2-3 presents an axial view of the entire test duct. One of the three instrumented rods is shown, which can receive either a pitot-static tube (United Sensor Corporation, Type PDA-12-F-10-KL) for pressure drop, tracer gas and axial flow measurements, or a two-dimensional Cobra probe (United Sensor Corporation, Type CA-120-12-CD) for recording gap cross-flow data. The 100 inch length of instrument travel is also indicated. All flow test data indicated as functions of axial distance reference the downstream end of instrument travel as "0" inches and measure upstream.

In addition to the allowable axial and circumferential motion of the instrumented rods, the pitot-static tubes can be extended or retracted radially. Dial indicators measure the axial position of a screw actuated push-pull connector rod which, through a yoke, drives a wedge inside the instrumented rod to position the pitot-static tube radially. A linkage is incorporated to maintain the pitot-static tube parallel to the rod surface against the torque of its plastic tubing leading out the upstream end of the instrumented rod.

The test assembly scale of 10.87:1 is based on the nominal dimensions of a 217-pin Clinch River Breeder Reactor fuel assembly. These are:

Rod Diameter (OD)	0.230 Inches
Wire Wrap Diameter (OD)	0.056 Inches
Rod Pitch	0.288 Inches
Wire Wrap Lead	11.9 Inches

Dwg. 6354A30

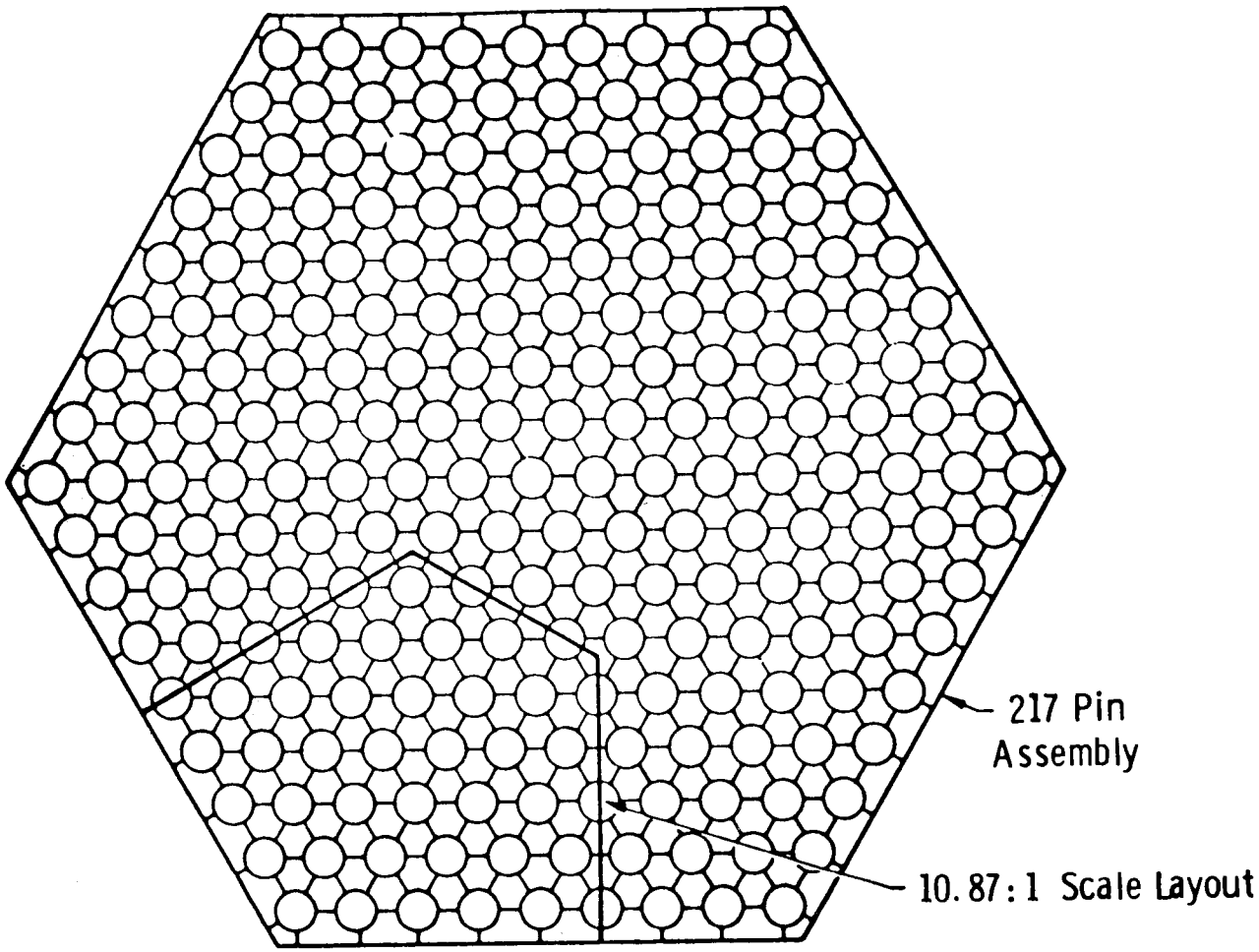

FIGURE 2-1

217-PIN FUEL ASSEMBLY WITH 10.87:1 SCALE MODEL
CROSS SECTION SUPER IMPOSED

Dwg. 6354A29

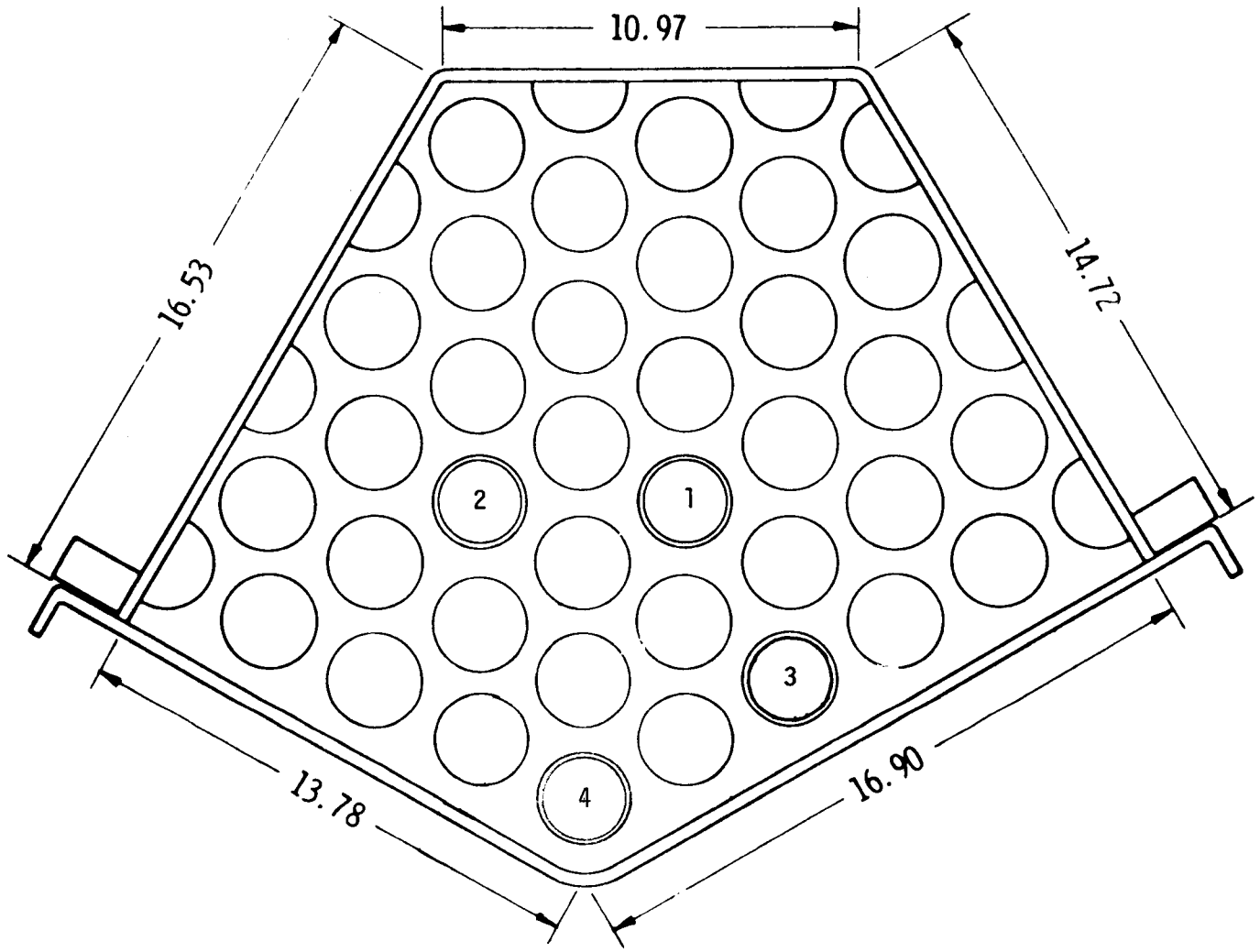

FIGURE 2-2
CROSS SECTION OF TEST SECTION (DIMENSIONS IN INCHES)

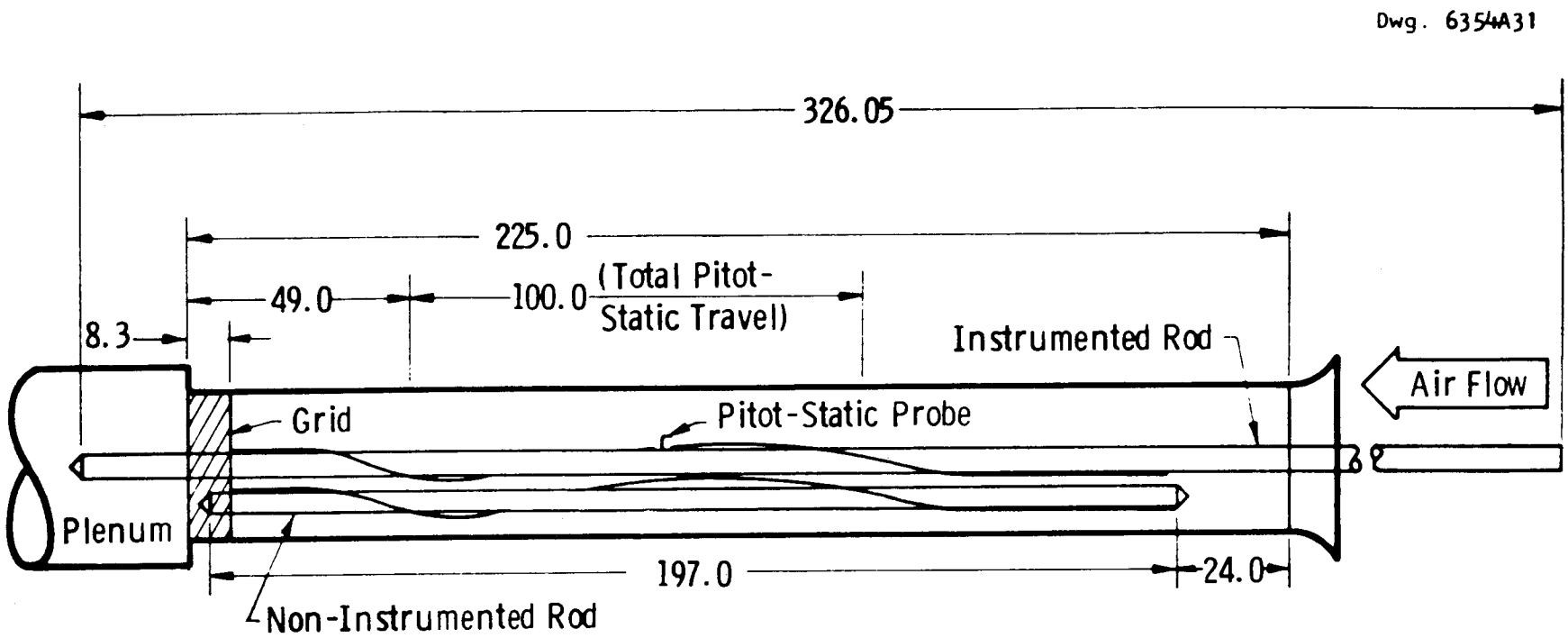

FIGURE 2-3
AXIAL LAYOUT OF TEST SECTION (DIMENSIONS IN INCHES)

As-built dimensions of the rod diameters (OD) within the test assembly are shown in Figure 2-4. These dimensions are the same as those for the interior and side subchannel tests[1,2]. Figures 2-5 through 2-10 present two sets of measured gap widths within the test assembly at three axial locations. Two sets are given since disassembly, repair and reassembly of the test section were necessary during testing and effected gap width measurement had to be repeated. The test sequence is described in Section 2.3 of this report. Copper pipe 0.625 inches in diameter (OD) wrapped around the rods with a lead of 129.4 inches as the wire wrap completes the scale model as the wire wrap. The test section flow area (147.6 square inches) and wetted perimeter (421.6 inches) remain unchanged and yield a hydraulic diameter of 1.400 inches for the overall assembly[1].

Flow leaves the test assembly through the exit plenum and a 20 x 18 inch rectangular duct located above the test section. A 40 HP, radially bladed blower with an adjustable throttling plate exhausts the air through the laboratory roof. Within the rectangular duct, a group of nine pitot-static tubes arranged on Gaussian quadrature coordinates monitor total flow rate through the assembly.

2.2 Side Subchannel Configuration

The configuration of the subchannels surrounding instrumented rod number four is shown in Figure 2-11. These are the subchannels in which the experiments are conducted. Subchannel labels and the wire wrap reference angle, α, are also indicated for use throughout the rest of this report. At the inlet of the rod bundle, the wire wrap angle α equals -30°.

2.3 Test Sequence

The planned test sequence was twice interrupted by the need for repairs to the test section. In each case, equipment failure was caused by excessive loads on instrumented rod number four during rod movement to reposition the test instrumentation. In the first instance, the

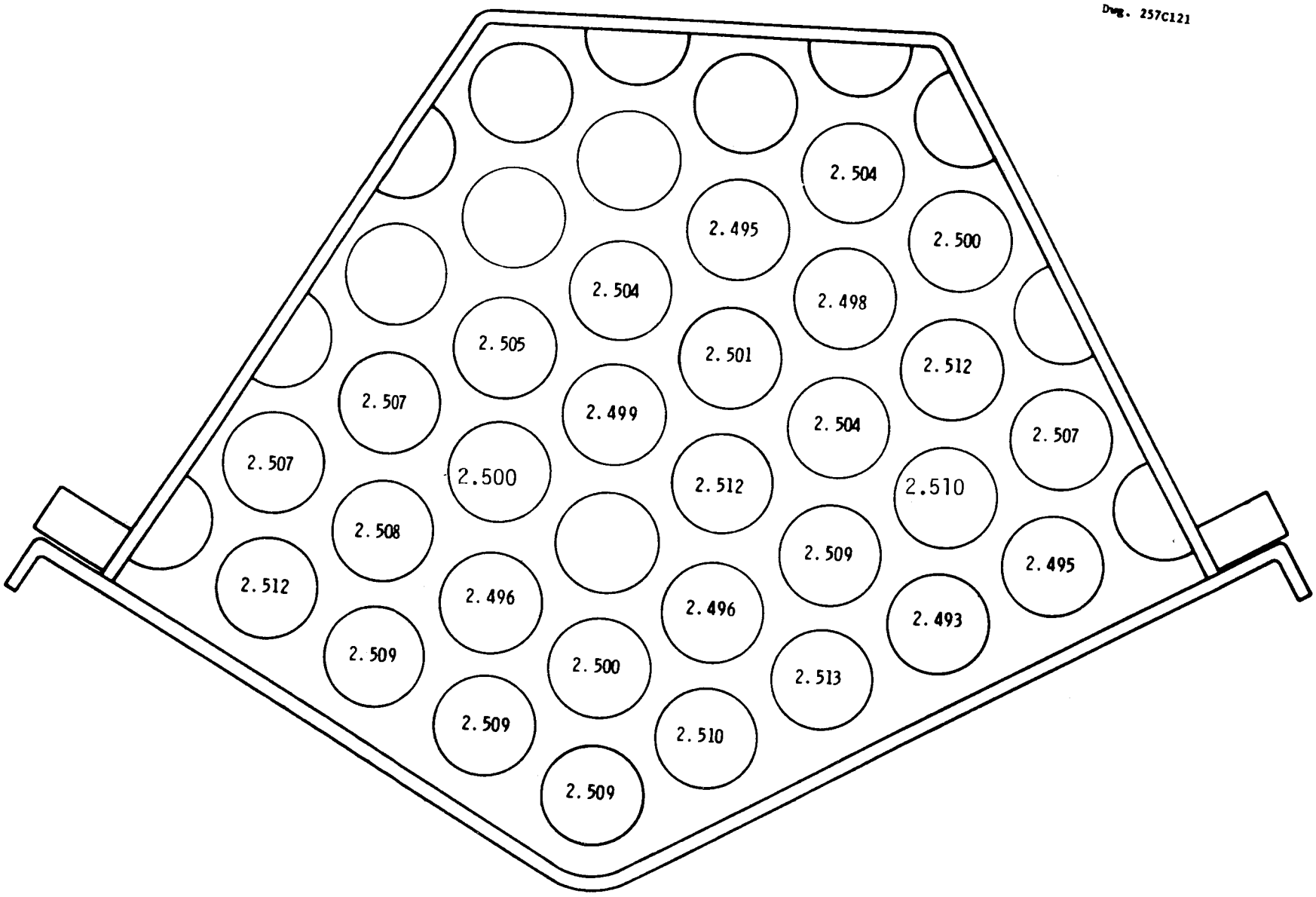

MEASURED MODEL ROD DIAMETERS 93.5 INCHES FROM DOWNSTREAM END OF TEST SECTION IN INCHES

Figure 2-4

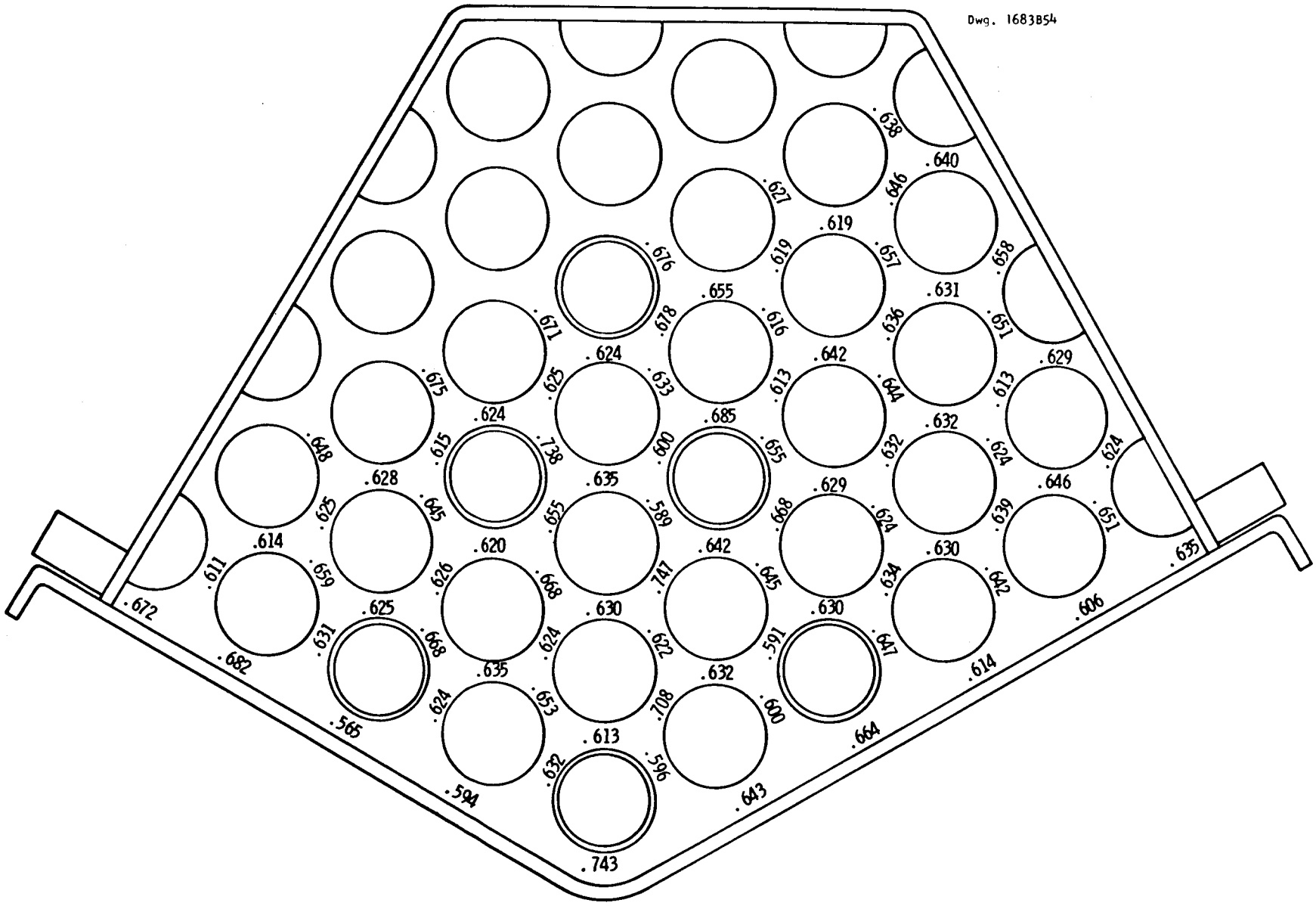

FIGURE 2-5 Clearance Gap Spacings 55.0 Inches from Downstream End of Test Section in Inches, Before Repair

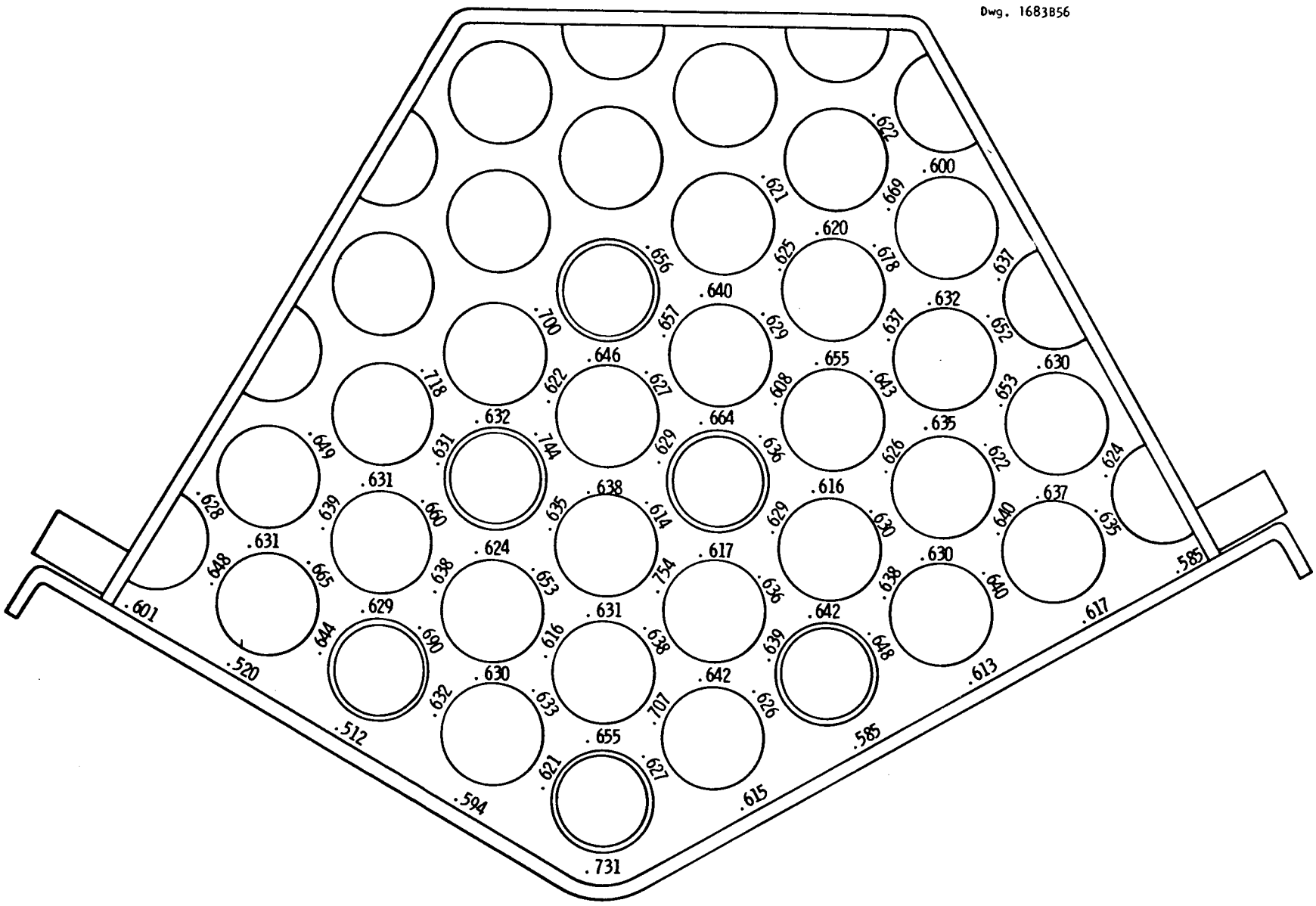

FIGURE 2-6 Clearance Gap Spacings 93.5 Inches from Downstream End of Test Section in Inches, Before Repair

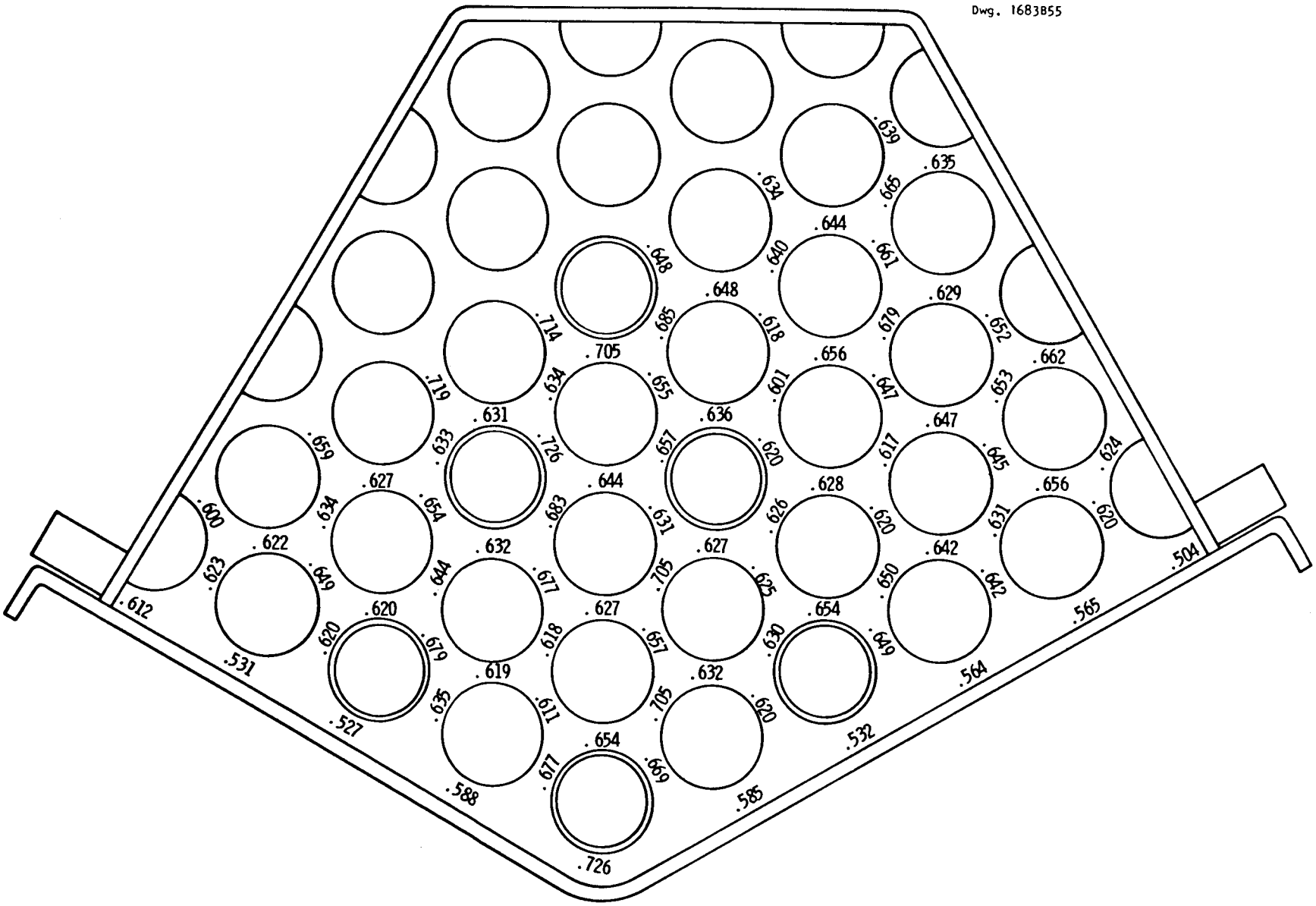

FIGURE 2-7 Clearance Gap Spacings 132.0 Inches from Downstream End of Test Section in Inches, Before Repair

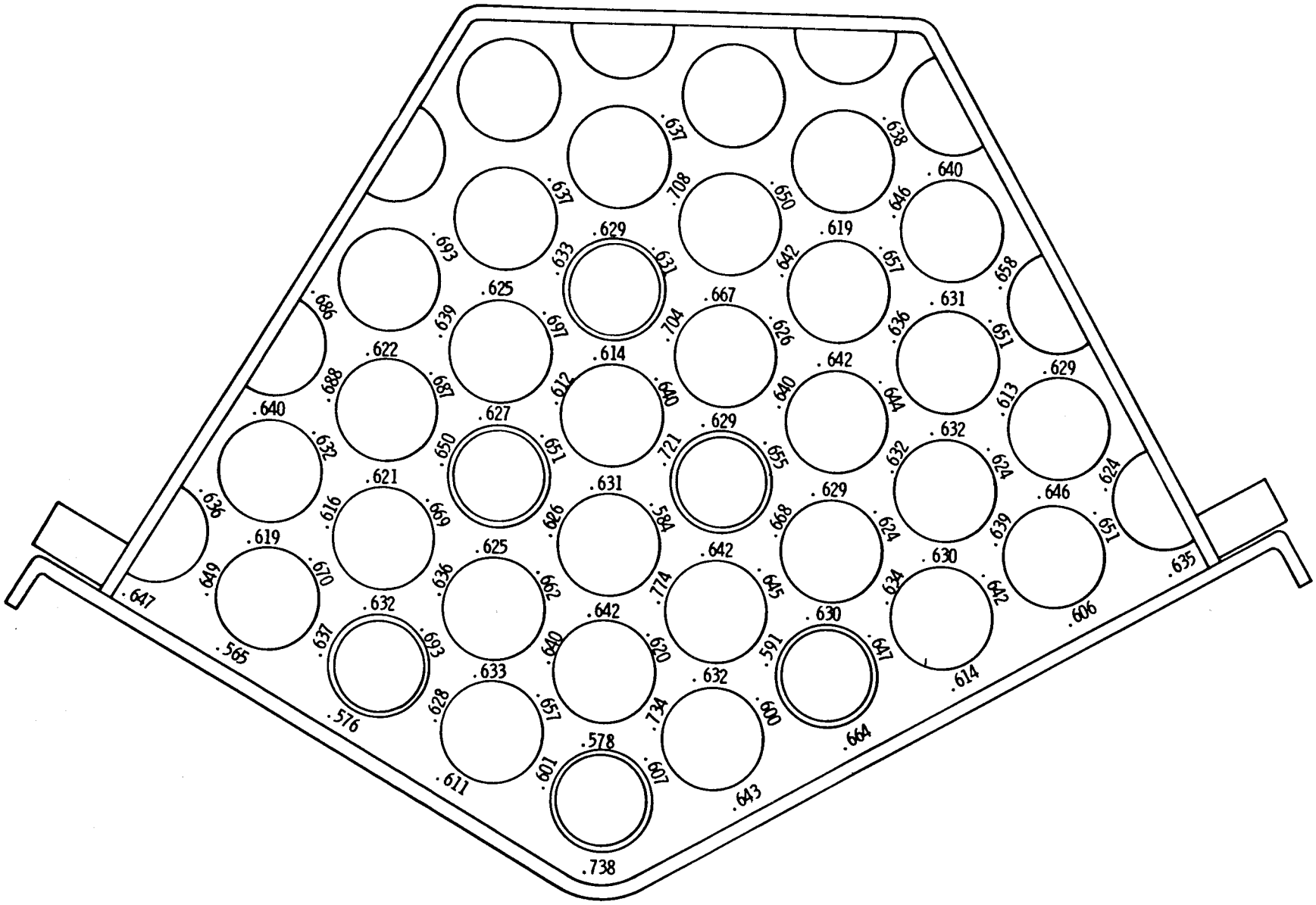

FIGURE 2-8 Remeasured Clearance Gap Spacings 55.0 Inches from Downstream End of Test Section, After Repair

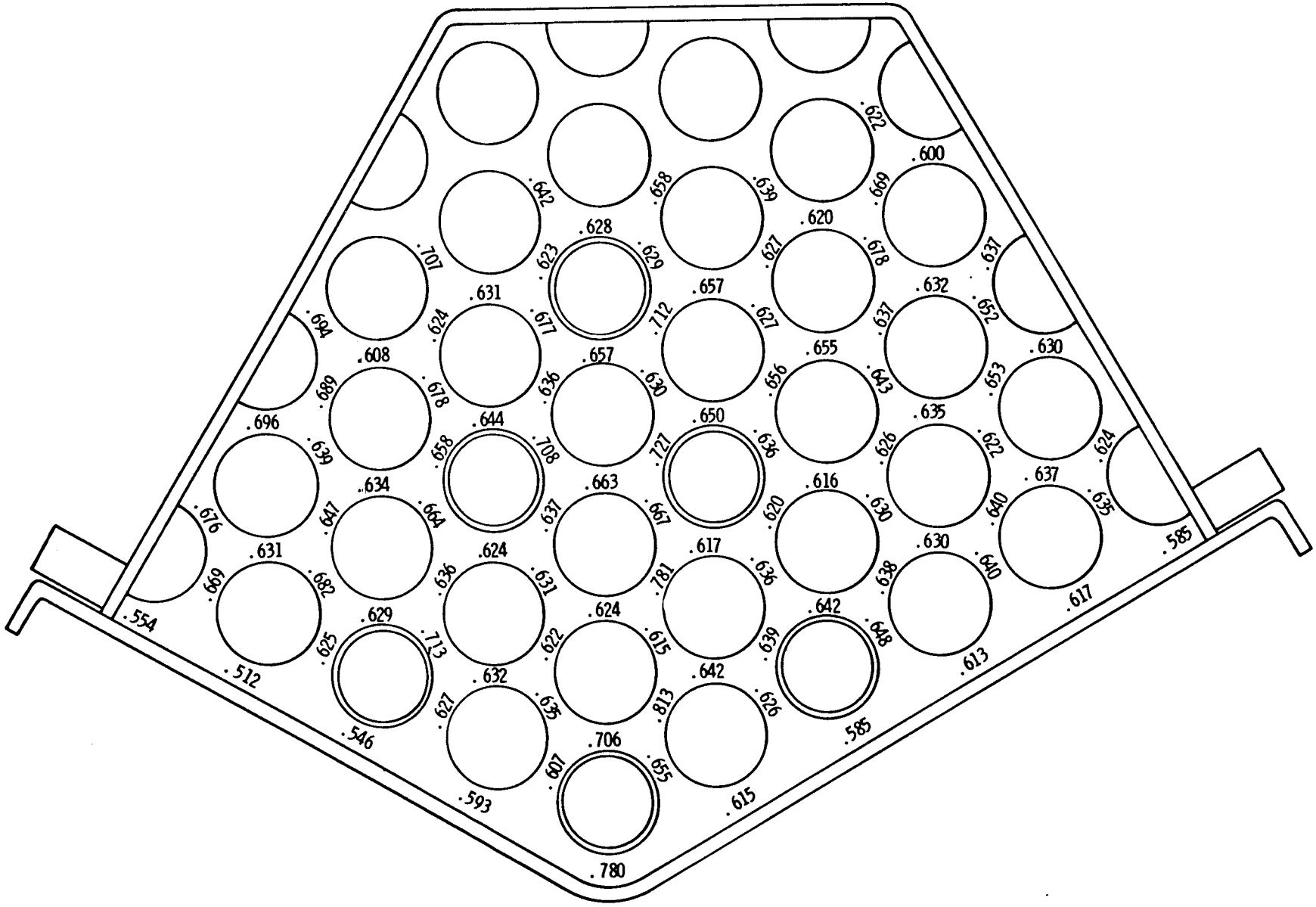

FIGURE 2-9 Remeasured Clearance Gap Spacings 93.5 Inches from Downstream End of Test Section, After Repair

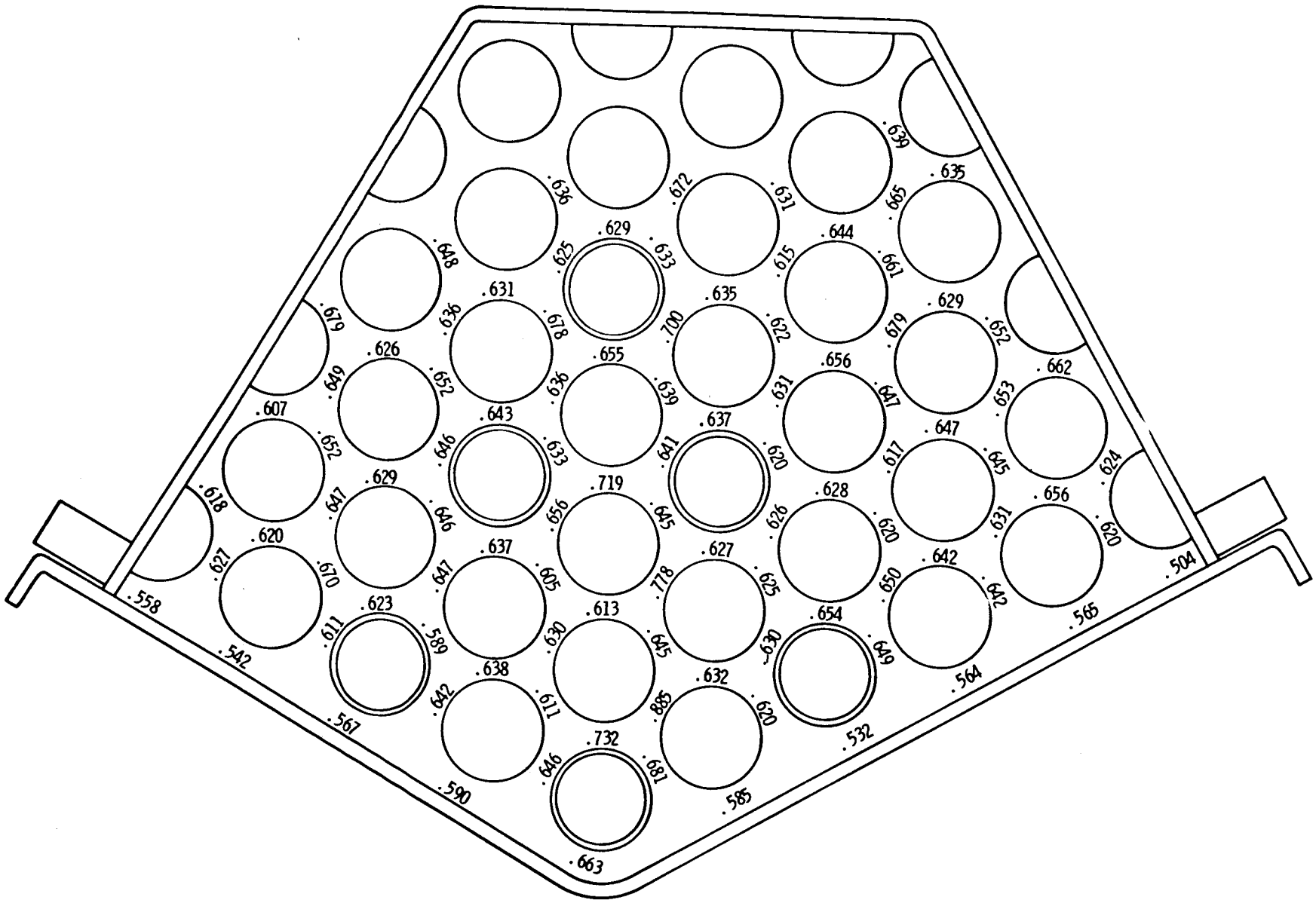

FIGURE 2-10 Remeasured Clearance Gap Spacings 132.0 Inches from Downstream End of Test Section, After Repair

wire wrap around the instrumented rod broke loose from the adjacent rods to which it was fastened, after gap width measurements (Figures 2-5 through 2-7) and preliminary experiments had been performed. Disassembly, repair and reassembly of the test section were necessary to assure that the wire wrap would remain in place during testing. After the repair, a new set of gap widths was recorded (Figures 2-8 through 2-10) and the preliminary experiments rerun.

Later, after the axial velocity data and two sets of tracer gas data had been recorded, screw fasteners of the instrumentation section within the instrumented rod broke, requiring removal of that rod from the test section for repair. A Cobra probe was installed to perform gap crossflow measurements, but the need for recalibration of the probe was apparent upon resumption of testing so the rod was again withdrawn, recalibrated and reinserted. After gap crossflow testing was repeated, the rod was once more removed for replacement of the pitot-static tube and then reinserted into the test section for completion of the tracer gas tests.

A summary description of the resultant test sequence is as follows:

1) Test section initially prepared for corner subchannel tests with pitot-static tube mounted in instrumented rod number four and gap width measurements recorded (Figures 2-5 through 2-7).

2) Preliminary experiments performed to determine uniformity of wire wrap curvature and axial development of static pressure and axial velocity.

3) Test section disassembled, loose wire wrap refastened to adjacent rods, test section reassembled and new gap widths recorded (Figures 2-8 through 2-10).

4) Additional preliminary experiments performed.

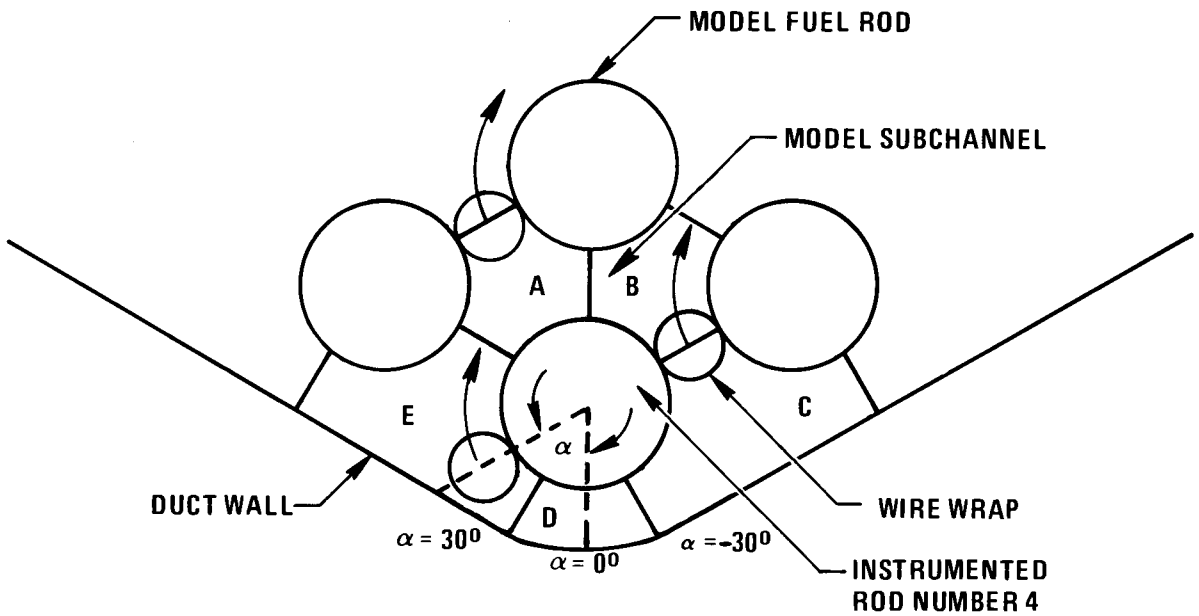

Figure 2-11. Corner Subchannel Notation As Seen In The Downstream Direction

8786-2

5) Axial velocity and initial tracer gas data recorded.

6) Broken instrumented rod removed, repaired and reinserted with Cobra probe.

7) First set of gap crossflow data recorded.

8) Instrumented rod removed to recalibrate Cobra probe, then reinserted into test section.

9) Gap crossflow measurements repeated.

10) Instrumented rod removed for reinstallation of pitot-static tube and reinserted into test section.

11) Tracer gas tests completed.

3.0 PRELIMINARY EXPERIMENTS

3.1 Introduction

Prior to performance of mixing and flow tests, several preliminary tests are necessary to characterize flow development within the corner subchannels. Principal among these are measurements of axial development of both axial flow and static pressure as an indication of flow development within the experimental length of the test assembly. Measurements of the uniformity of the wire wrap curvature have also been made and are shown in Figure 3-1. The wire wrap curvature averages 2.9 degress per inch with estimated limits of ± 5.0 percent. Assembly flow rate for all tests remains unchanged at 112.6 ft^3/sec. This produces an assembly-wide average velocity of 109.8 ft/sec and Reynolds number of 73,000 based on 75°F air. The previously reported variations in flow rate of $\pm$ 4.0 percent maximum and ± 2.0 percent nominal also apply[1].

3.2 Axial Flow Development

Axial development of axial flow is mapped with a pitot-static tube in the subchannels surrounding instrumented rod number four over the downstream portion of the 100 inch instrument travel shown in Figure 2-3. This is done by locating the movable pitot tube at a uniform 60 degrees clockwise from the wire wrap and at a radial distance of one-half the wire wrap diameter from the rod surface. This technique assures that measurements are made well away from wall surfaces.

The measured axial velocities are shown in Figure 3-2. Data from Run 1 were recorded prior to the first repair to the test section. Data from Run 2 were recorded after the repair and extended in range. The dramatic increase in axial velocity beginning at the 18-inch location is coincident with the approach of the wire wrap to the rod-duct wall gap at α=0°. The wire wrap is centered in that gap at about the 13-inch location. At upstream locations, the axial velocity varies around 112 ft/sec. The most definite statement that can be made about axial development of axial velocity

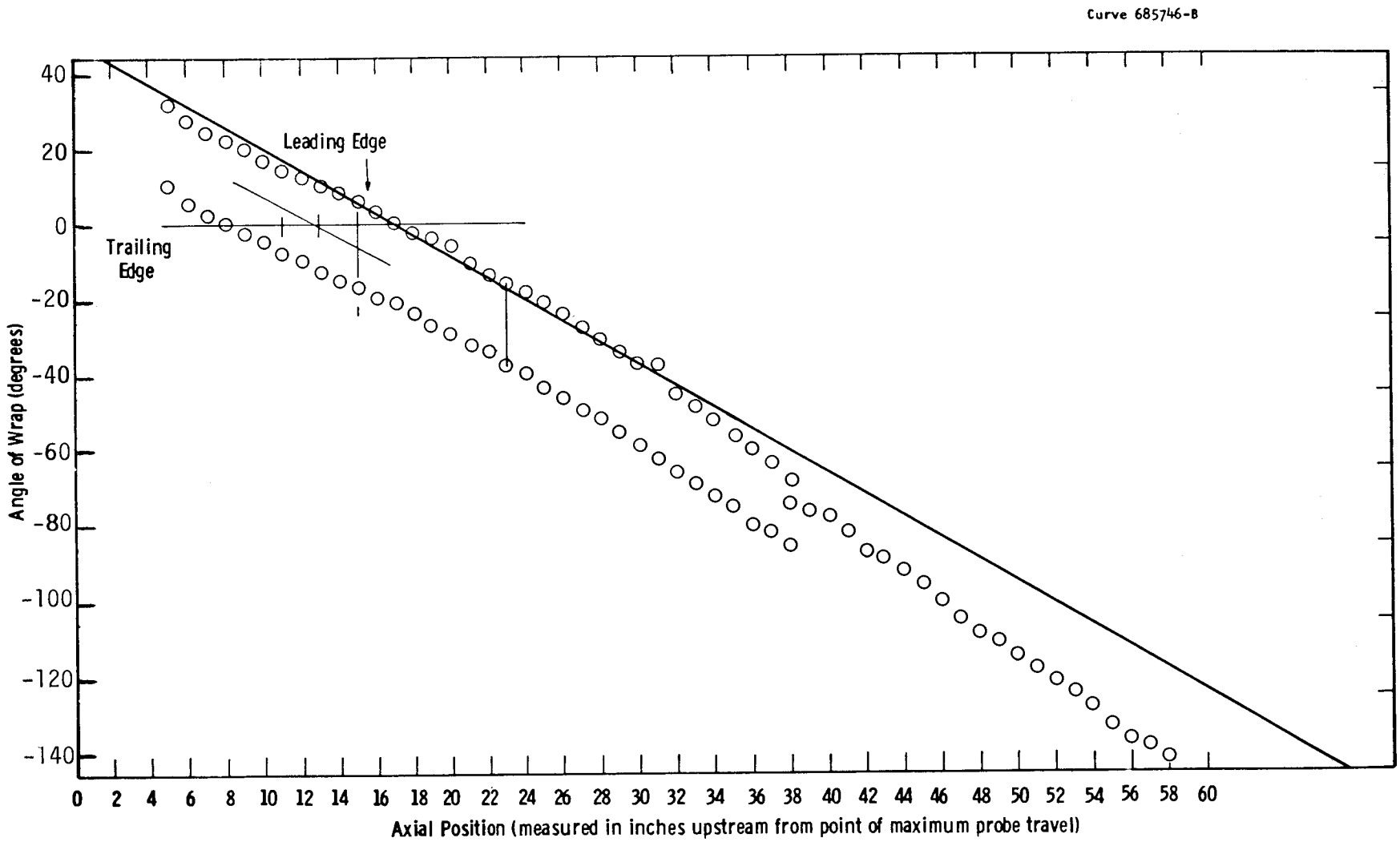

Fig. 3-1 – Experimental determination of angular location of wire wrap

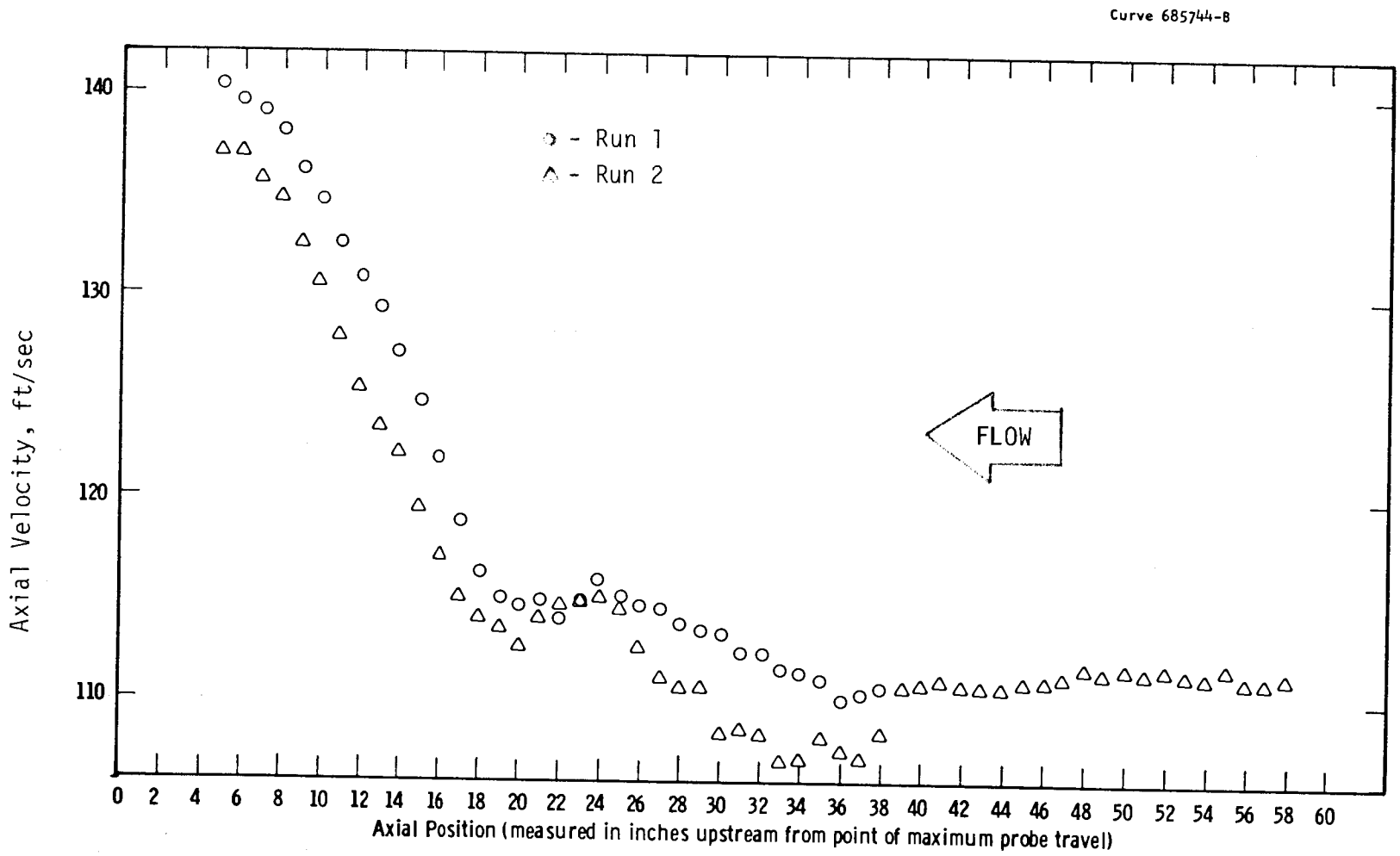

Fig. 3-2 – Axial development of axial velocity

is that full development is the least certain in the corner subchannel as compared to that observed in the interior and side subchannels. The effect of the wire wrap entering the corner subchannel seems to be dominate, and without more data for other ranges of wire wrap angle, firm conclusions are impossible. It must be remembered that less than one-half of a wire wrap pitch is represented in Figure 3-2.

3.3 Friction Factor Calculation

An axial profile of static pressure has also been developed from the experiment described in the previous section. Pressures are read in increments of 0.005 inches of water on a 0.834 s.g. oil manometer inclined at 15° from the horizontal plane. The manometer had previously been checked against a differential micromanometer accurate to ± 0.0002 inches of alcohol. The two readings agreed to within 0.6 percent over the range of interest in the present work and to within 0.8 percent overall. The variations were not systematic so no correction factor was determined.[1]

The pressure profile is shown in Figure 3-3. A check on flow development can be made from this data by calculating the friction factor f defined as(*)

$$\frac{\Delta P}{\Delta L} = \frac{f}{d_h} \frac{\rho \bar{u}^2}{2g}$$

where
- ΔP = pressure drop due to friction over ΔL
- ΔL = increment in axial length
- d_h = hydraulic diameter of test section
- ρ = density of air
- g = gravitational constant
- $\bar{u}$ = average axial flow of test section.

Based on the straight line drawn in Figure 3-3, the friction factor for the corner subchannel has been determined as 0.0388. The friction factor for side subchannels ranged from 0.0251 to 0.0297.[2] The friction factor for the interior subchannels had been calculated as 0.0206[1]. The higher range of experimental values for the friction factor in both the corner and side subchannels may indicate that the flow is not as fully developed as that in

(*) The friction factor is based on the Blasius rather than the Fanning correlation.

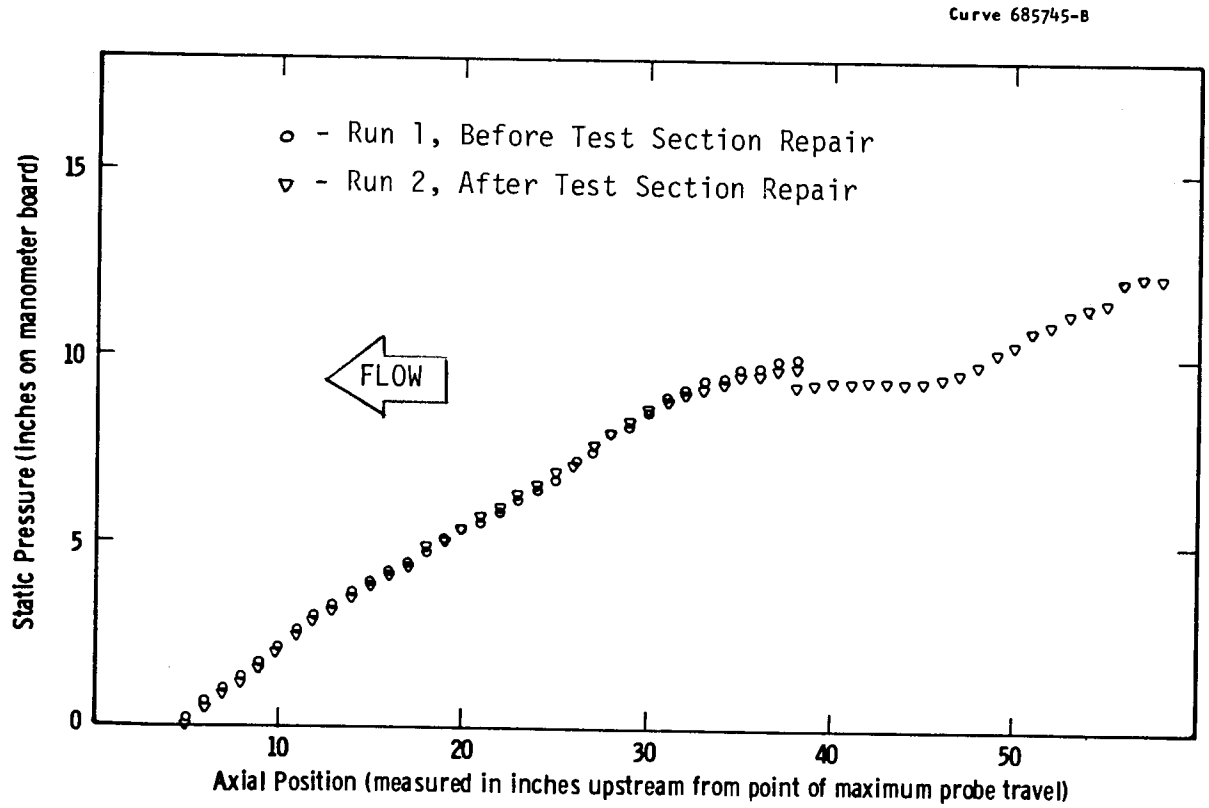

Fig. 3-3 — Static pressure drop along the duct

the interior subchannels at the same axial locations. They may also indicate an effect of subchannel geometry on the value of the friction factor for fully developed flow.

Preceding the final inches of instrument travel for which a relatively constant $\Delta P/\Delta X$ can be calculated, is a region where $\Delta P/\Delta X$ is decidedly less constant. This is also shown in Figure 3-3. Flow development in this upstream region is less than full. Whether fully developed flow has been attained in the downstream region or not cannot be definitely stated in light of the unusual axial velocity trace of Figure 3-2 and the limited range of wire wrap angle observed.

4.0 TRACER GAS EXPERIMENTS

4.1 Experimental Procedure

Mixing characteristics within the corner subchannel region have been investigated by means of a series of tracer gas experiments. The general approach is that of injecting a small amount of ethane tracer gas through the duct wall into the corner subchannel region and mapping downstream concentration distributions. The dynamic pressure tap of the pitot-static tube mounted in instrumented rod number four is used as a gas sampling port which can be extended throughout the subchannels. The sample collection is routed through a dessicant to a MSA Model 300 infra-red analyzer, which is factory calibrated to read 0 to 2000 ppm ethane at atmospheric pressure with a maximum scale non-linearity of 2.5 percent. Ethane (C_2H_6) is used in these experiments since its molecular weight of 30.07 approximates that of air, rendering buoyancy effects negligible.

The ethane enters the corner subchannel region through a 0.0625 inch OD port in the duct wall. A 0.043 inch diameter orifice with a 0.834 S.G. oil manometer mounted differentially across the orifice meters the ethane through the injector. The ethane volumetric flow rate is determined by calibrating the orifice pressure drop against a precision volumetric displacement type wet test meter.

A vacuum pump is necessary to draw the sample gas through the analyzer. To increase the sample withdrawal rate, the specimen chamber is held at 22.2 inches of Hg below atmospheric pressure. The exhaust from the vacuum pump is then piped back into the test section just ahead of the blower.

4.2 Experimental Results

Mappings of downstream tracer gas concentrations are given in Appendix A. These have been determined by graphic interpolation between data points on 5:1 scale drawings. Approximately 40-50 data points were recorded per side and interior subchannel along with about 20 data points in the

small corner subchannel itself. The numerical values assigned to the contours represent percent of full deflection of the infra-red analyzer where 100 percent deflection is equivalent to a concentration of about 2400 ppm in the test section. Tracer gas distributions are shown at six inch intervals of axial length where six inches of axial length correspond to approximately 17.4 degrees of wire wrap angular displacement. The remaining features of the drawings are self-explanatory.

Experiment one, represented in Figures A-1 through A-4, was performed prior to the failure and subsequent repair of the instrumented rod mentioned in Section 2.3. In this experiment, injection takes place in the gap where α equals zero degrees. Only normally expected crossflow ahead of the wire wrap is observed.

Experiment two, and all subsequent experiments were performed after all repairs to the test section and all other tests had been completed. Experiment two (see Figures A-5 through A-8) fails to show any backflow in the gap between the wire wrap and duct wall. Such backflow had been observed in side subchannel tests[2]. The tracer gas in this instance, however, has been injected well in advance of the wire wrap and appears to have been strongly swept into the corner gap. Experiment three (see Figures A-9 and A-12) also fails to show any backflow even though injection is made much closer to the approaching wire wrap. Experiment three does show, beginning at the 15-inch axial location (see Figure A-11), a strong crossflow behind the wire wrap as the tracer gas expands into the wake of the wire wrap. This effect had been previously seen in side subchannel tests[2]. The fourth and last experiment shown in Figures A-13 and A-14 does show some tracer gas behind the wire wrap but even this does not represent backflow as seen in the side subchannels.

5.0 GAP CROSSFLOW EXPERIMENTS

5.1 Experimental Procedure

Detailed gap crossflow measurements have also been made in the three gaps between the rod surface and duct wall in the corner subchannel. The gaps are located at $\alpha = -30°$, $0°$ and $30°$ as shown in Figure 2-11. A two-dimensional Cobra probe is used in the instrumented rod rather than a pitot-static tube. The Cobra probe has a central dynamic pressure tap with an angled tap on each side such that the pressure difference between the angled taps yields a measure of the flow angle across the probe. By positioning the Cobra probe at several locations across each gap, a detailed profile of crossflow across the width of the gap can be obtained for any given wire wrap angle so long as the wire wrap does not interfere with the probe.

Calibration of the Cobra probe determines the relationship between flow angle and the pressure difference between the outer taps of the probe. This is done in the device shown in Figure 5-1. For different dynamic pressures as measured with a pitot tube, the Cobra probe pressure tap differences are recorded as a function of the flow angle β over the range $-6° \leq \beta \leq 6°$. The final recalibrated results are given in Figure 5-2 for a given probe height. A subsequent check of the Cobra probe reveals a systematic variation with probe extension from the rod surface as seen in Figure 5-3. These two calibration curves have been used to reduce all data from both sets of crossflow experiments, both before and after recalibration of the probe. The previously experienced uncertainty in probe orientation of $\pm 2\delta = \pm 0.36°$[1,2] remains suitable as an error band.

Data from the Cobra probe is represented as a ratio of transverse velocity to axial velocity, $\phi(\alpha)$, where

$$\phi(\alpha) = \frac{v(\alpha)}{\bar{u} \tan\theta}$$

and α = clockwise wire wrap angular displacement from the central gap (see Figure 2-11)

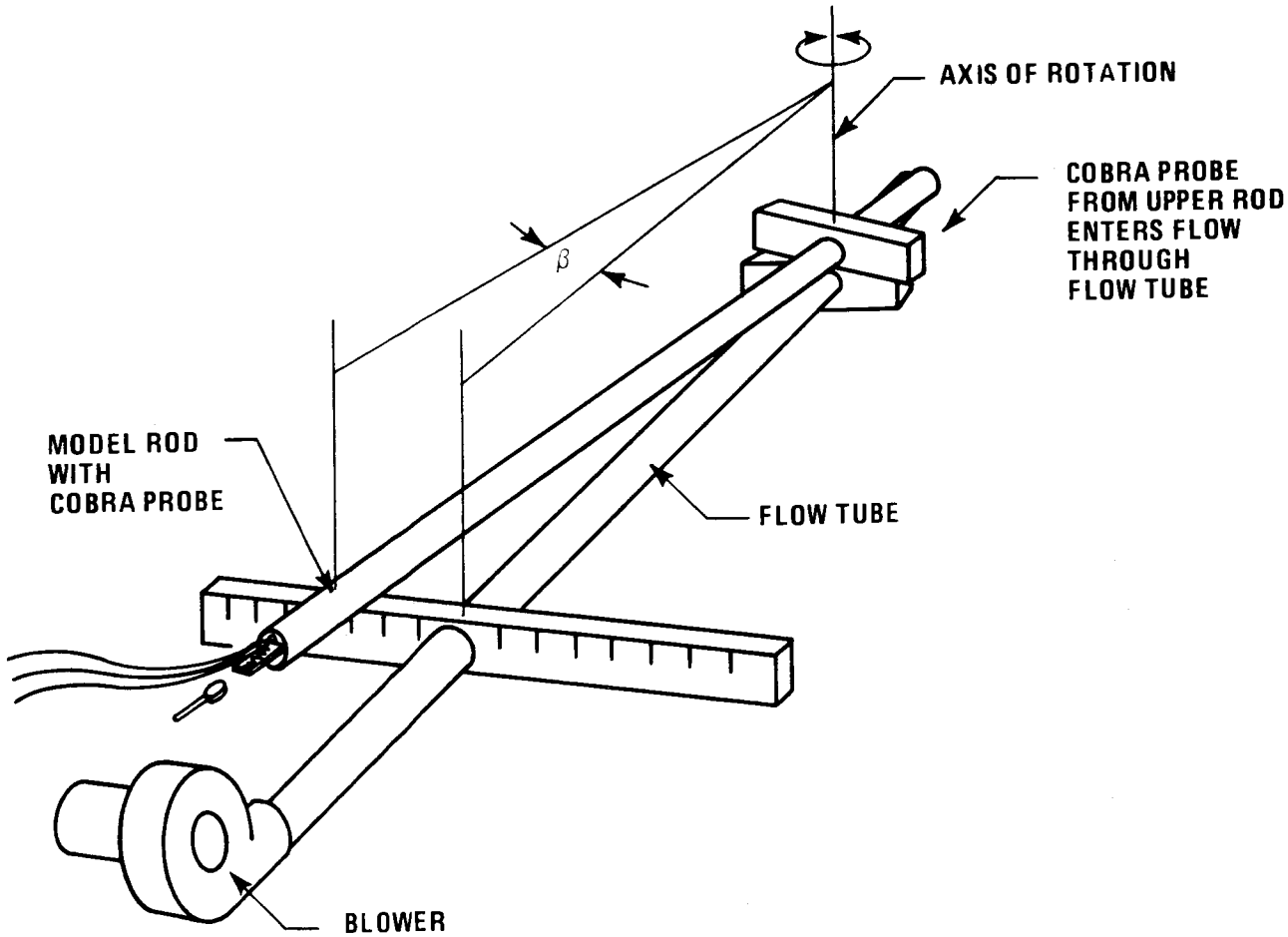

Figure 5-1 Schematic of Cobra Probe Calibration Procedure

7686-27

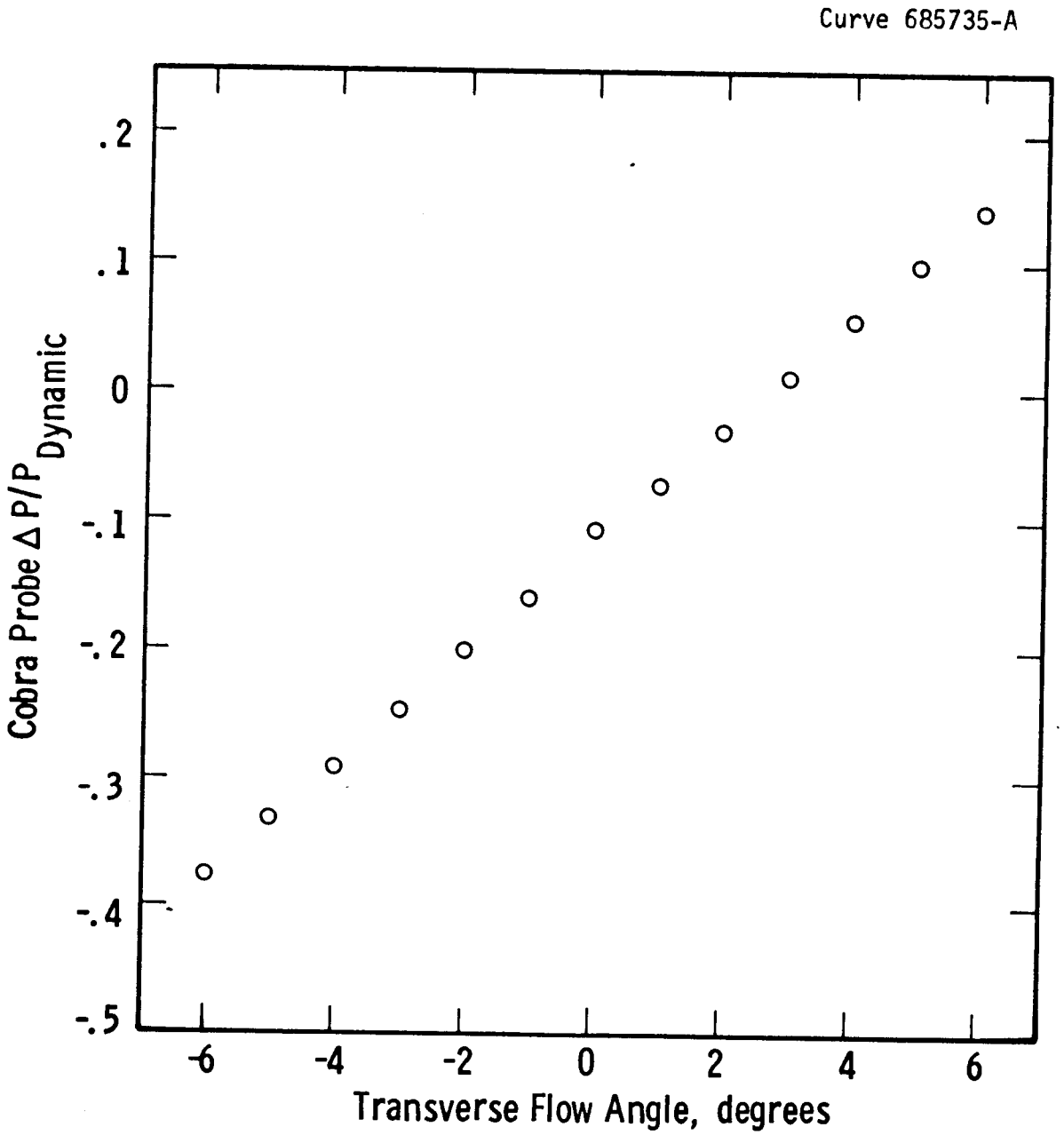

Fig. 5-2 — Cobra probe calibration curve: cobra probe $\Delta P/P_{Dynamic}$ vs. transverse flow angle

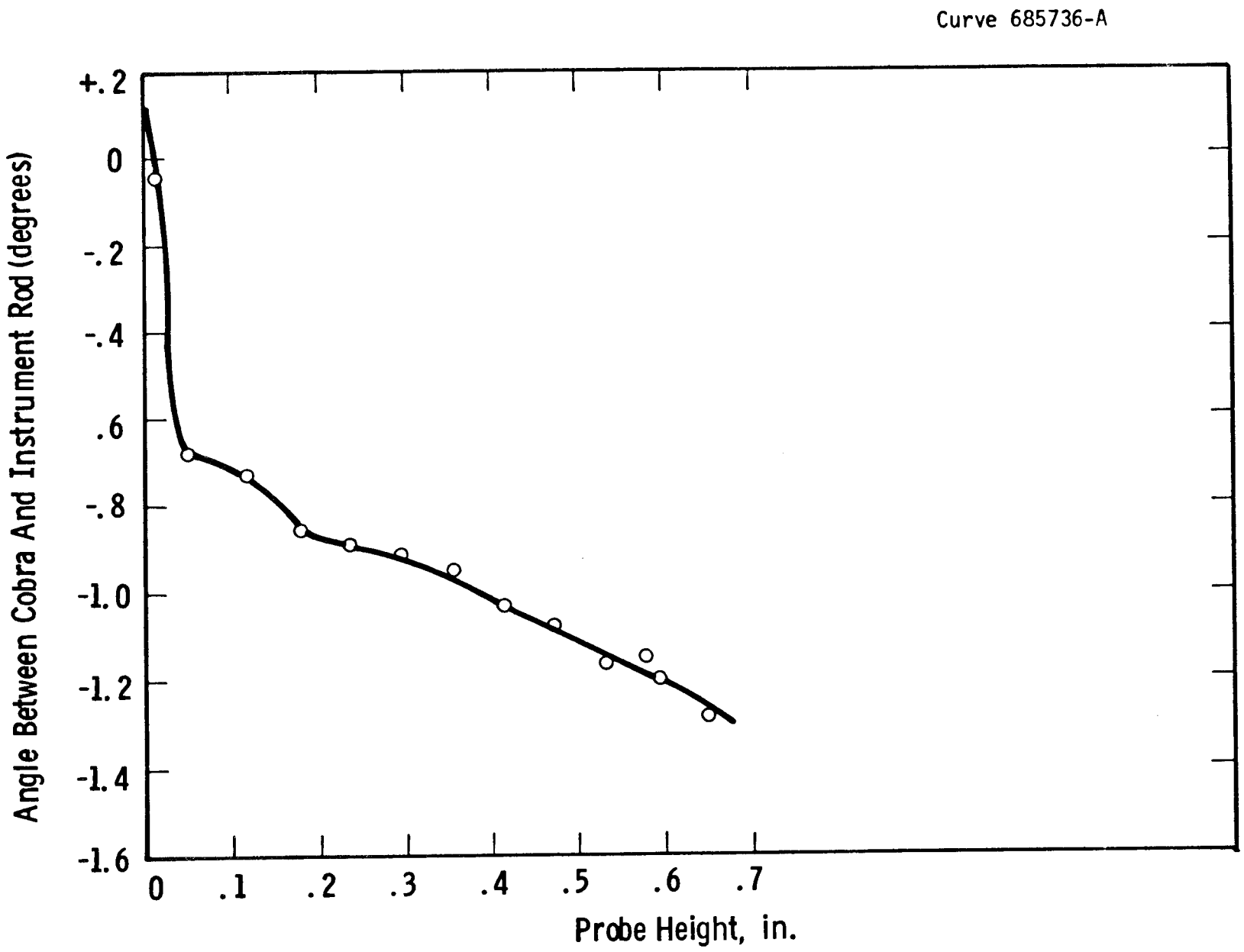

Fig. 5-3 — Angle between cobra probe and instrumented rod as a function of probe height

$v(\alpha)$ = transverse fluid velocity through the gap, positive in the direction of wire wrap revolution

$\overline{u}$ = test section average axial fluid velocity, 109.8 ft/sec.

θ = angle of projection of wire wrap centerline on axis of rod.

Profiles of $\phi(\alpha)$ are then plotted across the gap. An average of $\phi(\alpha)$ across the gap is also calculated such that

$$\overline{\phi}(\alpha) = \frac{\overline{v}(\alpha)}{\overline{u}\ \tan\theta} \ .$$

The function $\overline{\phi}(\alpha)$ is then plotted over the range of the wire wrap angular displacement, α.

5.2 Experimental Results

Two sets of gap crossflow data have been obtained in the corner subchannel gap at α equals zero degrees. The first set (Run 1) was recorded prior to recalibration of the Cobra probe; the second set (Run 2) after recalibration. In addition, Run 2 includes measurements in the gaps between corner rod and duct wall where $\alpha = \pm 30°$ (see Figure 2-11). Both sets of data have been reduced using the recalibrated parameters of the Cobra probe. The gap crossflow profiles are represented in Appendix B as functions of ϕ over a range of $-79.0° \leq \alpha \leq 22.0°$ for the wire wrap angle. This range of wire wrap angle corresponds to a range of axial location from 39 to 5 inches from the downstream end of instrument travel. The function ϕ is defined as positive for crossflow in the direction of wire wrap revolution. The variation of ϕ between the two sets is an indication of experimental error. The standard deviation calculated between the two runs represented in Appendix B in terms of the dimensionless function $\phi(\alpha)$ is 0.053. Uncertainty in the probe location is ± 0.010 inches[2].

The ϕ profiles show a strong, positive crossflow with only minor and highly localized backflow in the gap. As the wire wrap approaches and enters the corner subchannel from an angle of -79° to -20°, the maximum local crossflow consistently occurs at a normalized distance of 0.4 from the rod surface. The local maximum then shifts dramatically toward the duct wall and increases

significantly over the range of wire wrap angle from -20° to 22°. Figures B-27 through B-32 present a comparison of all three gaps over a range of wire wrap angle from -79° to -44°. This added comparison has been limited by wire wrap locations where all three gaps are simultaneously unobstructed and, therefore, available for measurements.

From these ϕ profiles, gap averaged values of ϕ have been calculated for all three gaps as functions of the wire wrap angle. Figure 5-4 gives $\overline{\phi}(\alpha)$ for the gap at $\alpha = 0°$ as determined from both sets of data. The standard deviation calculated between the two runs in terms of the dimensionless function $\overline{\phi}(\alpha)$ is 0.025.

The curve for $\overline{\phi}(\alpha)$ for the corner subchannel gap at $\alpha = 0°$ compares favorably with the corresponding curve for side subchannel gaps[2]. A local minimum is shown by both sets of data as a minor perturbation at $\alpha = -25°$. Two major differences can be noted. First, the corner subchannel gap is oriented thirty degress clockwise from the side subchannel gap. The minimum ϕ in the corner subchannel gap at $\alpha = -52°$ is comparable to that observed in the side subchannel gap at $\alpha = 330°$ or, equivalently, $\alpha = 30°$[2]. Secondly, the value of $\overline{\phi}$ just preceding the entrance of the wire wrap into the corner subchannel gap decreases sharply from a local maximum of about 0.6. In the side subchannel gap, the value of $\overline{\phi}$ had been observed to continue to increase and approach 0.8 just prior to entrance of the wire wrap into that gap[2].

Figure 5-5 graphically presents the calculated $\overline{\phi}$ for the corner subchannel gaps at $\alpha = \pm 30°$. The curve for $\overline{\phi}(\alpha)$ in the gap at $\alpha = 0°$ is also shown for comparison. Over the observed range of wire wrap angle, the behavior of $\overline{\phi}(\alpha)$ is closely similar in all three gaps. There does seem to be slightly stronger average crossflow in the two gaps at $\alpha = \pm 30°$ as compared to the gap at $\alpha = 0°$. Also, the gap at $\alpha = -30°$ shows the strongest average crossflow and is the closest to the approaching wire wrap. In fact, as the wire wrap approaches the gaps, the values of $\overline{\phi}$ seem to order themselves in increasing values as the closeness of the respective gaps to the wire wrap.

Curve 685734-A

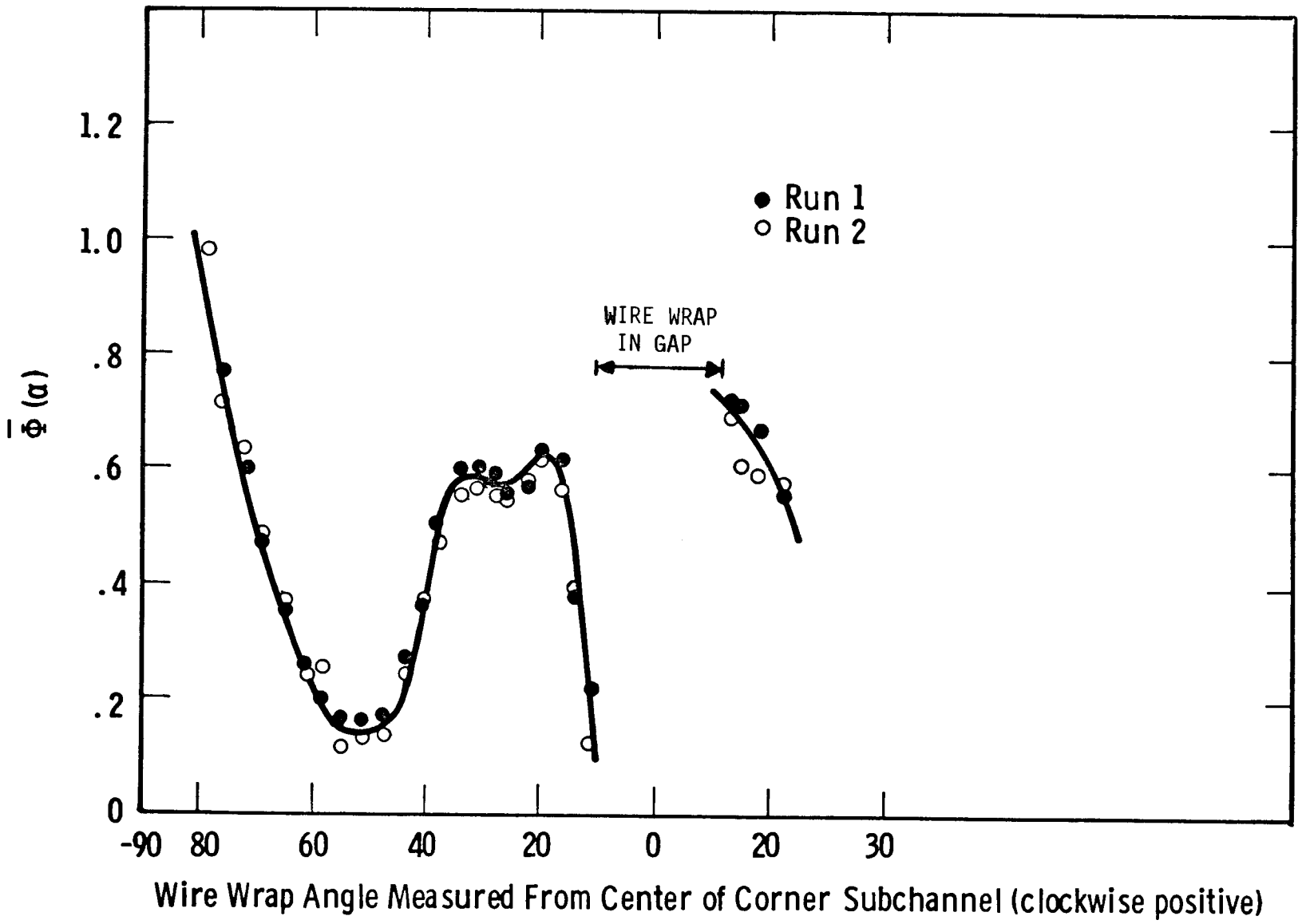

Fig. 5-4 — $\bar{\Phi}(\alpha)$ as a function of wire wrap angle FOR GAP AT $\alpha = 0°$

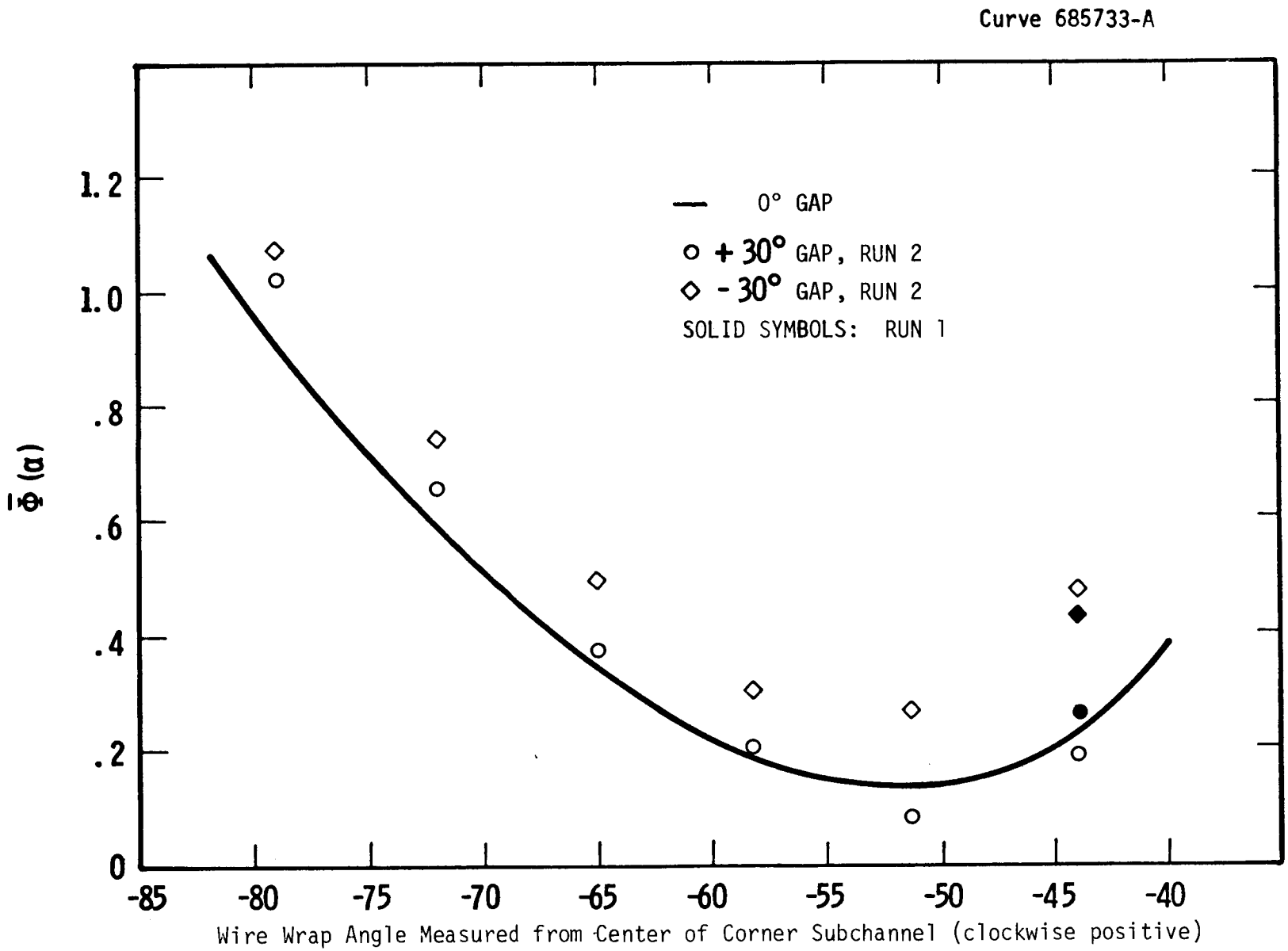

Fig. 5-5 — $\bar{\Phi}(\alpha)$ as a function of wire wrap angle for three gaps

6.0 AXIAL FLOW EXPERIMENTS

6.1 Experimental Procedure

Axial flow measurements are made using a pitot-static tube mounted in instrumented rod number four. The measurements are made in five axial planes in the surrounding subchannels at locations of 33, 27, 21, 15 and 9 inches from the downstream end of allowable pitot tube travel. In each interior and side subchannel, data are taken at 40 to 50 points, along with about 20 data points recorded in the small corner subchannel itself. Locations of data points have been spaced throughout the subchannels but allow for intervening wire wrap. The need for more data points in a given area to better define the flow patterns has also influenced the location of data points.

The pitot-static tube measurements are used to calculate the dynamic pressure head as follows:

$$\Delta P_{dynamic} = P_{static} - P_{total} \cdot$$

This subtraction is reversed from the normal order since measurements are taken in a suction. The axial velocity is then calculated from this pressure head. Finally, axial velocity contours are determined by interpolating radially and circumferentially between data points. Estimated error in velocity magnitudes is ±5%. From these contours, average axial velocities are calculated for each subchannel at each axial plane.

6.2 Experimental Results

The axial velocity contours are shown for each axial location in Figures C-1 through C-5 of Appendix C. The viewpoint is looking downstream.

Flow patterns in subchannel C look much the same as side subchannels CD and EF in WARD-D-0129[2]. The axial flow contours in subchannel C seem to have

slightly higher values. Subchannel E cannot be compared to other side subchannels since the wire wrap angle covers a different range. Interior subchannel B is equivalent to subchannel B of WARD-D-0129, and the flow patterns of the two subchannels are similar. Strong comparison of the two subchannels is difficult for lack of distinctive features of the axial velocity contours. The A subchannels of this report and WARD-D-0129 are equivalent except that the A subchannel of WARD-D-0129 is joined to another interior subchannel where the A subchannel of this report connects to a side subchannel. Despite this difference, there is a strong resemblence between the axial flow patterns of these two subchannels. The corner subchannel (D) appears as an extended connection between side subchannels involving a phase shift of sixty degrees in the wire wrap angle. Except for contours directly behind the wire wrap, the axial flow contours seem to parallel the curvature of the rod surface and duct wall.

Area weighted averages of axial velocity are plotted for each subchannel in Figure 6-1. Corner subchannel D seems fairly constant over this range of wire wrap angle. All other subchannels significantly increase in average axial velocity. The average axial velocity of the corner subchannel over the experimental range of wire wrap angle is 103.2 ft/sec. The averages for the other subchannels in the corner region vary from 108.7 to 115.2 ft/sec. The assembly wide and side subchannel average axial velocity has previously been determined as 109.8 ft/sec[1,2] and the interior subchannel average as 104.5 ft/sec[1] over the same portion of wire wrap revolution.

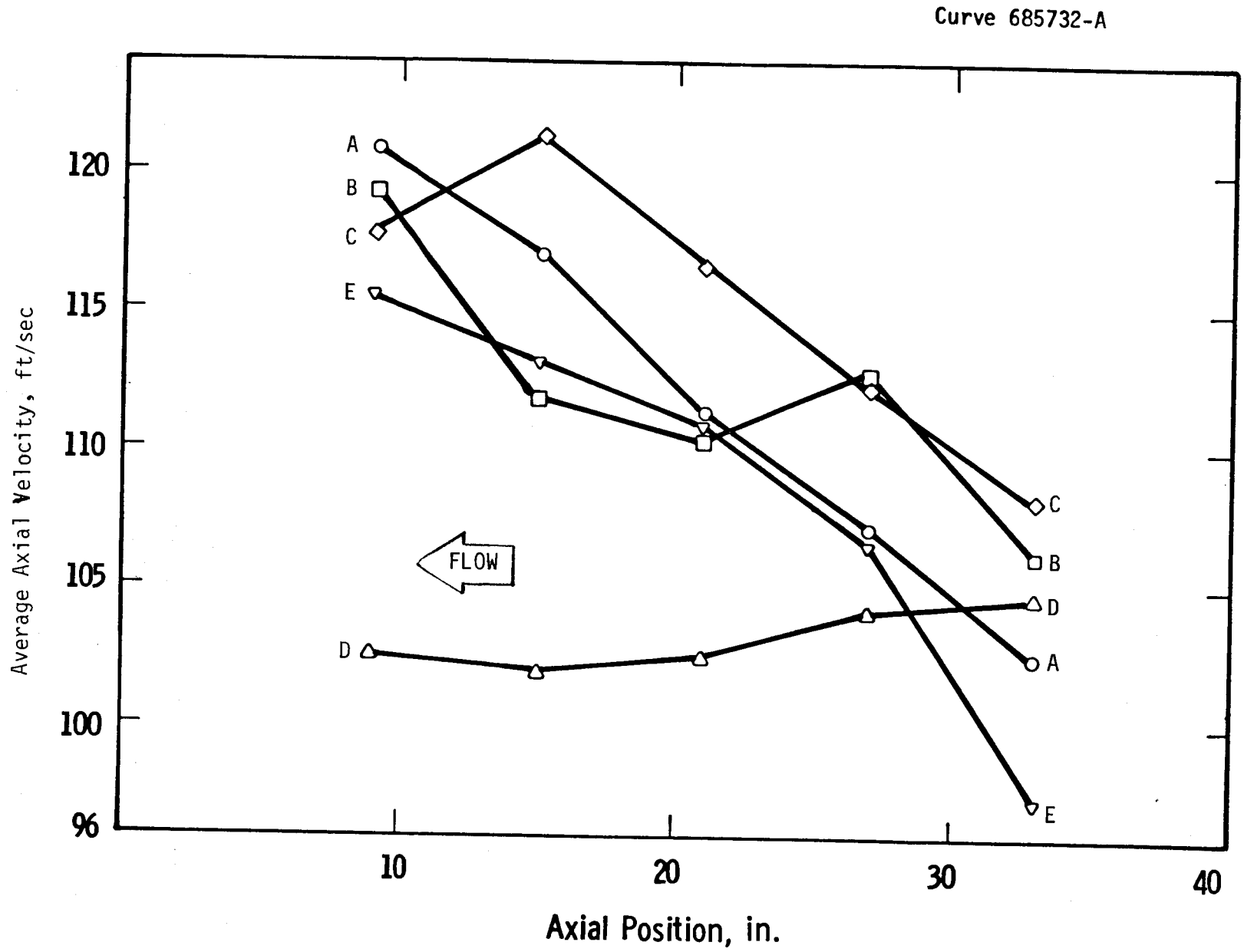

Fig. 6-1 — Subchannel average axial velocities at each axial plane

7.0 CONCLUSIONS

Flow development is the least definite in the corner subchannels when compared to interior and side subchannels. The axial velocity trace does not show any apparent pattern over the range of wire wrap angle investigated, $-79° \leq \alpha \leq 22°$ where $\alpha = 0°$ in the center of the corner subchannel. The friction factor is also the highest at 0.0388 compared to a range from 0.0251 to 0.0297 for side subchannels[2] and 0.0206 for interior subchannels[1]. The higher values for friction factors may indicate less flow development, effects of subchannel geometry on fully developed flow, or a combination of both. It should be noted, however, that this experiment has been conducted within one and one-half wire wrap periods of the rod bundle entrance. Such an axial zone represents only the initial entrance lengths of an actual fuel or radial blanket assembly. In this zone, slow flow development is the least significant since it occurs in a region of the fueled assembly where the temperature rise over the inlet temperature is minimal.

Tracer gas mixing tests again show strong crossflow behind the wire wrap as was seen in both interior and side subchannel test results[1,2]. Backflow in the gap between wire wrap and duct wall is not seen as was observed in side subchannels[2]. Whether or not this is attributable to circumferential swirl flow or not would depend on results of side and corner subchannel tests over other ranges of wire wrap angle.

Detailed profiles of crossflow in the three corner subchannel gaps (α = 0°, 30°, -30°) show a strong crossflow in the direction of wire wrap revolution with only minor and highly localized backflow. Gap averaged values for $\overline{\phi}(\alpha)$ compare favorably with the corresponding function for side subchannel gaps with two differences. A strong local minimum is observed at $\alpha = -52°$ for the central gap of the corner subchannel. This minimum had been observed at $\alpha = 30°$ for the side subchannel gap[2]. Also, the values of $\overline{\phi}(\alpha)$ just preceding the entrance of the wire wrap into the corner subchannel gap decrease sharply where it had continued to climb in the side subchannel gap[2]. The curves for $\overline{\phi}(\alpha)$ in the corner subchannel gaps at $\alpha = \pm 30°$ are similar to that in the central gap of the corner subchannel for an observed range of $-79° \leq \alpha \leq -44°$ with only a slightly stronger crossflow seen in the $\alpha = \pm 30°$ gaps.

Axial flow data in the corner subchannel appear as if that subchannel is serving as an extended connection between side subchannels involving a phase shift of sixty degrees in the wire wrap angle. Axial flow contours largely parallel the curvature of the rod surface and duct wall. Strong similarities are seen among axial flow patterns of interior and side subchannels adjacent to the corner rod and those in the previous side subchannel tests[2].

The average axial velocity of the corner subchannel has been calculated as 103.2 ft/sec compared to 104.5 ft/sec for interior subchannels[1] and 109.8 ft/sec for side subchannels and the assembly as a whole[1,2]. Since uncertainty in the axial velocity data has been estimated as $\pm$ 5 %[1,2], the ratio of average axial velocities among subchannel types appears to be unity or close to unity. In this range of wire wrap angle, however, the other subchannels adjacent to the corner rod average between 108.7 and 115.2 ft/sec - significantly higher than the corner subchannel itself.

REFERENCES

1. T. G. Bartholet, R. M. Roidt, and L. J. Harper, "11:1 Scale Wire Wrapped Rod Bundle Air Flow Test, Interior Subchannels", WARD-D-0108, November 1975.

2. T. G. Bartholet, R. M. Roidt, and J. E. Romano, "11:1 Scale Wire Wrapped Rod Bundle Air Flow Test, Side Subchannels", WARD-D-0129, January 1976.

APPENDIX A

Tracer Gas Distribution Contours

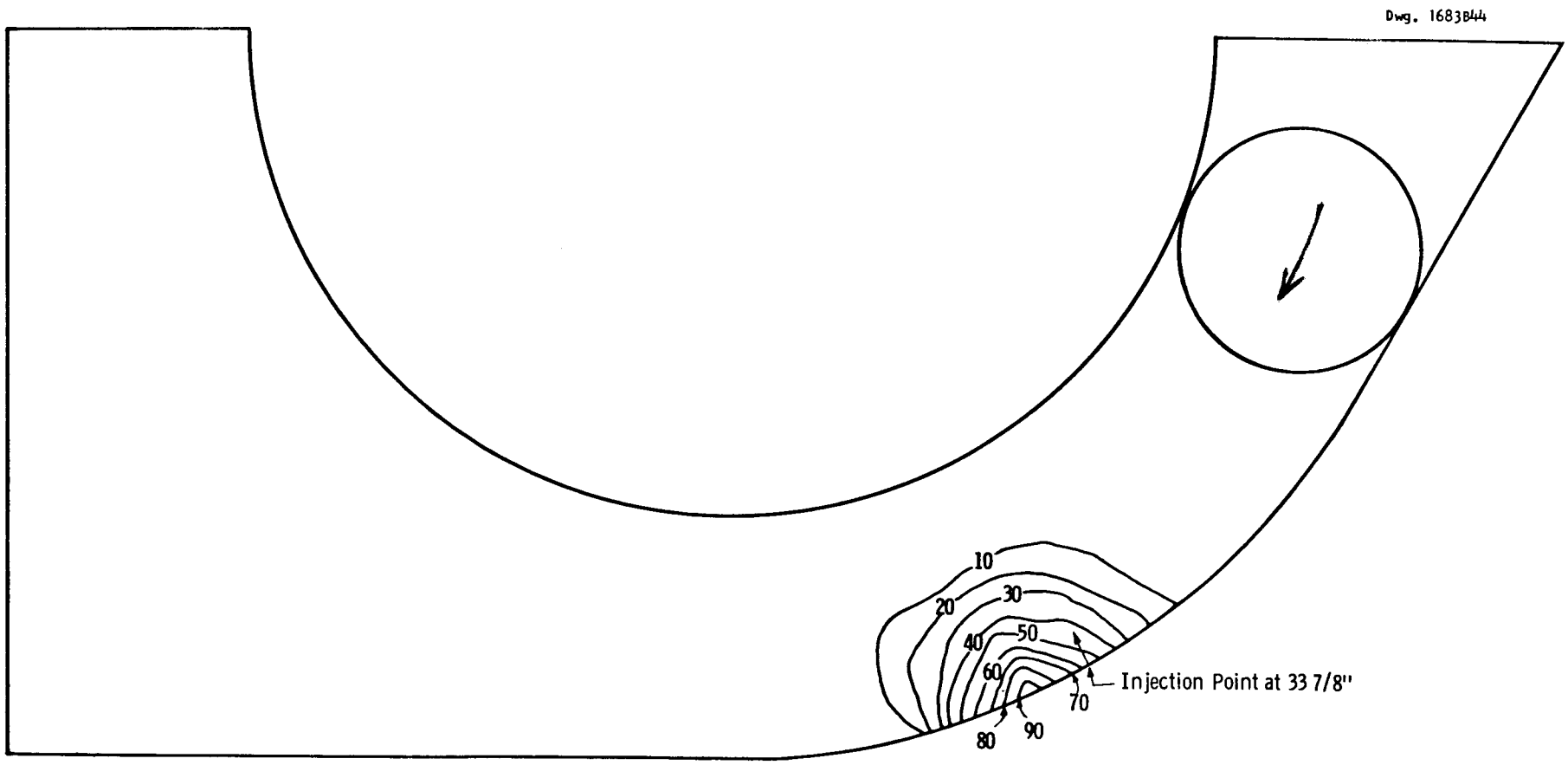

FIGURE A-1 Tracer Gas Experiment one, 27 Inch Axial Location

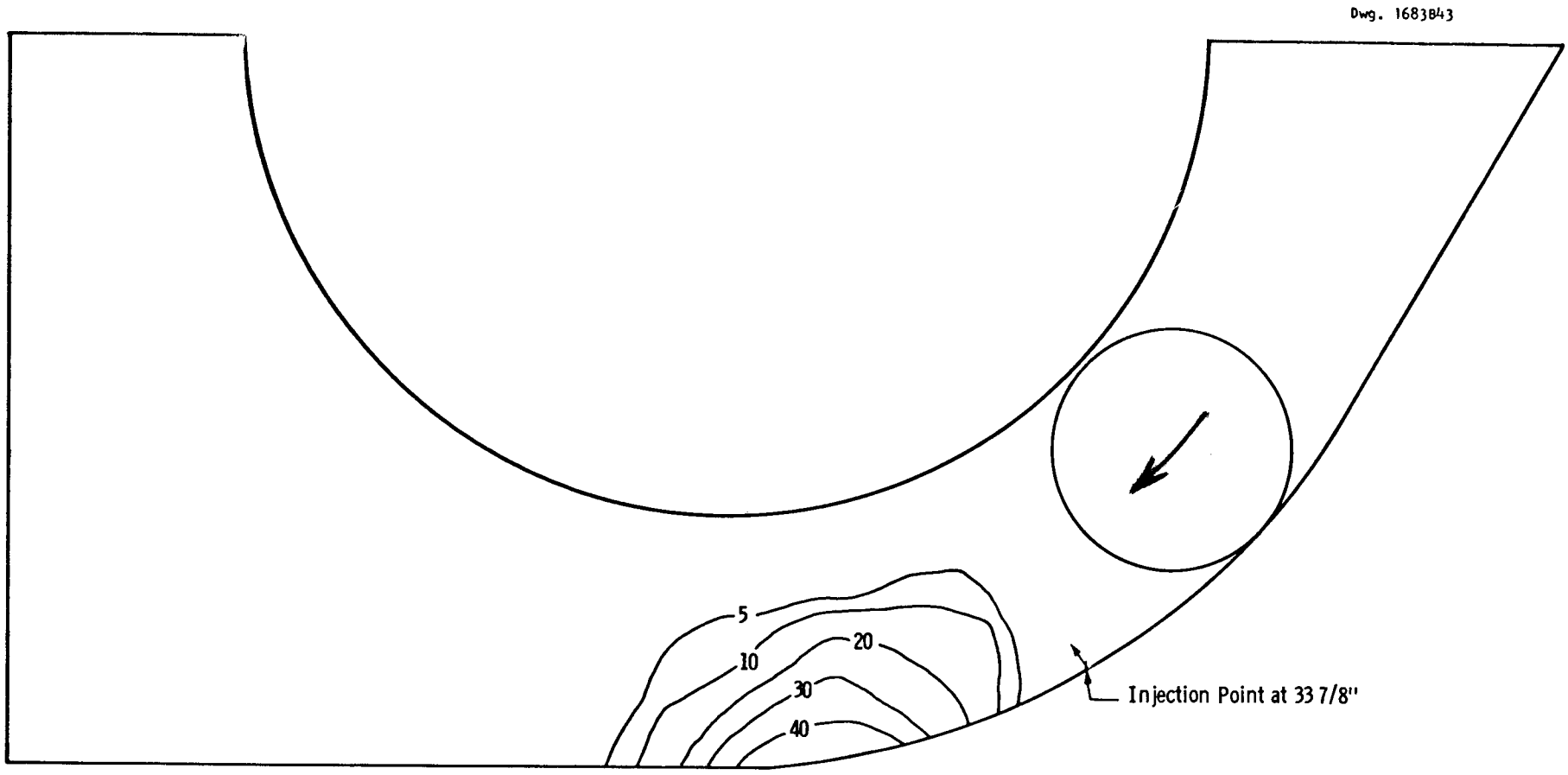

FIGURE A-2 Tracer Gas Experiment One, 21 Inch Axial Location

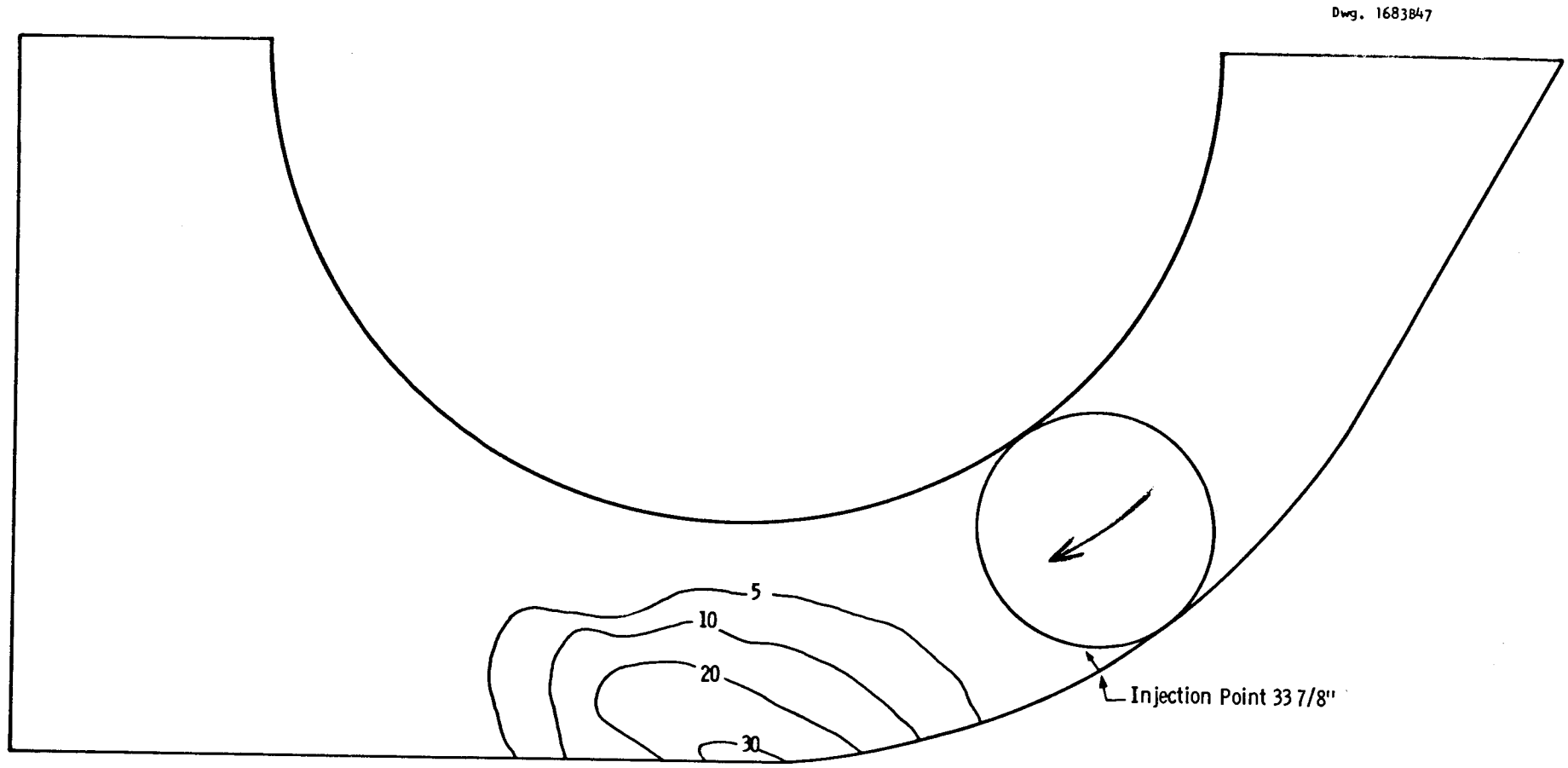

FIGURE A-3 Tracer Gas Experiment One, 15 Inch Axial Location

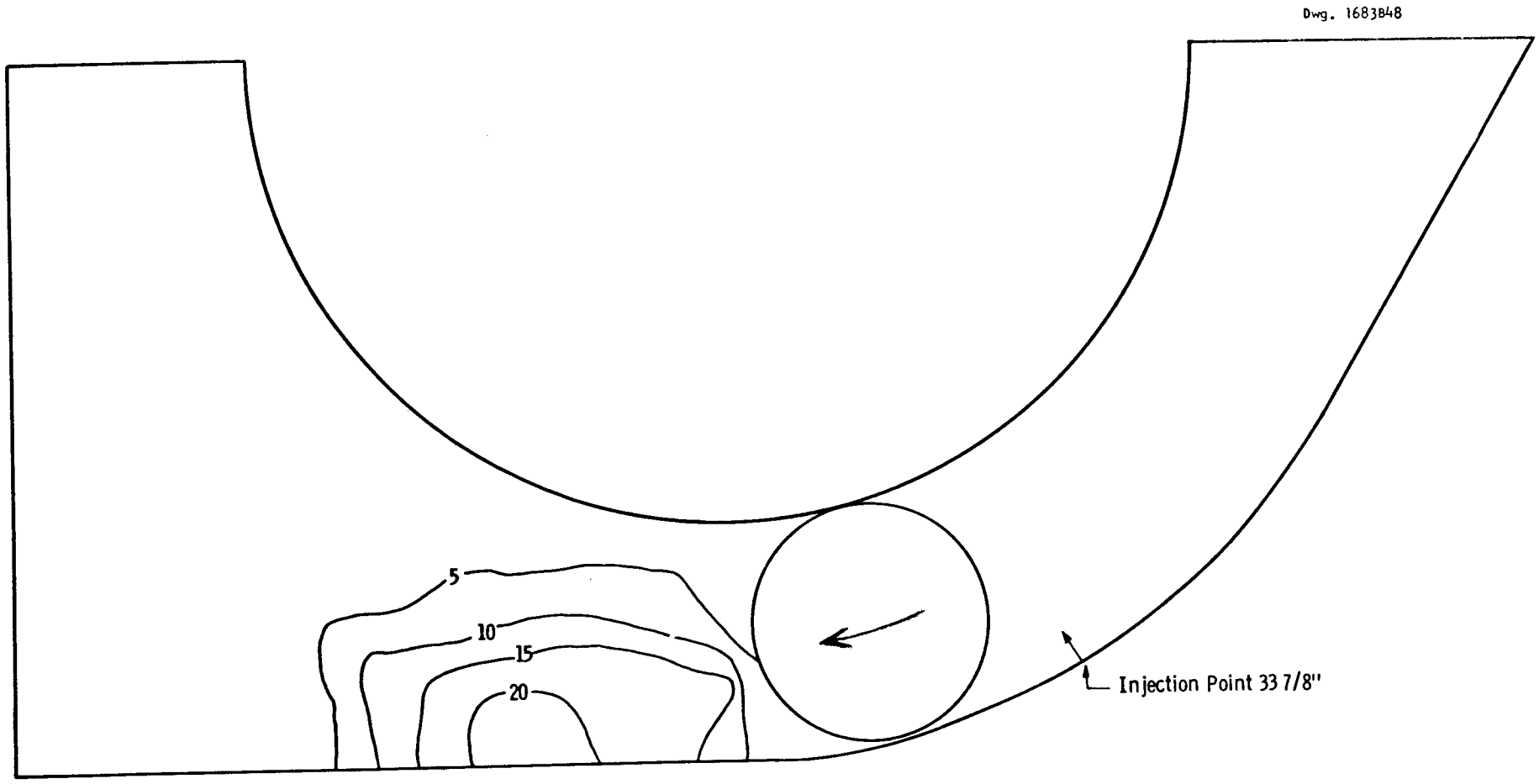

FIGURE A-4 Tracer Gas Experiment One, 9 Inch Axial Location

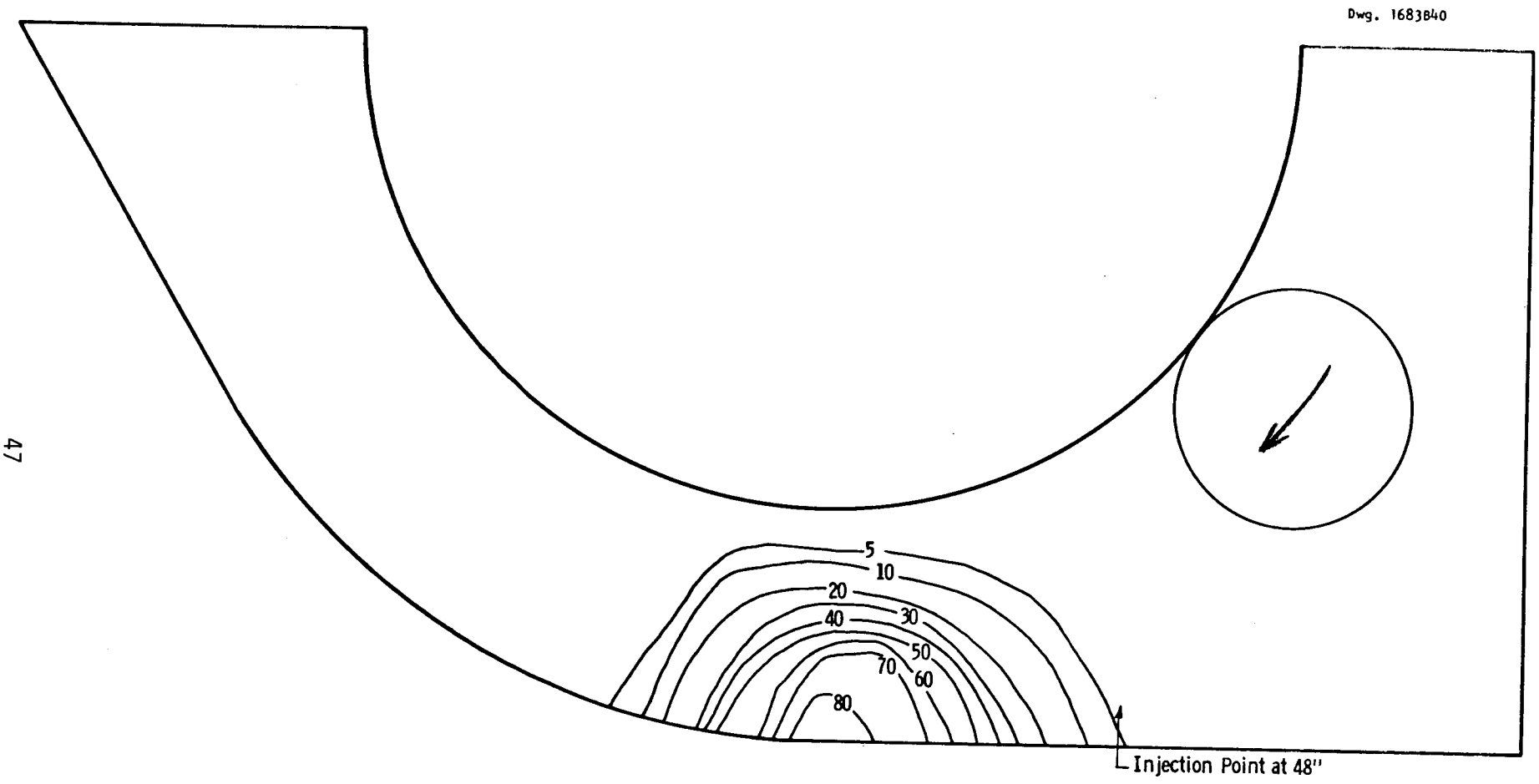

FIGURE A-5 Tracer Gas Experiment Two, 39 Inch Axial Location

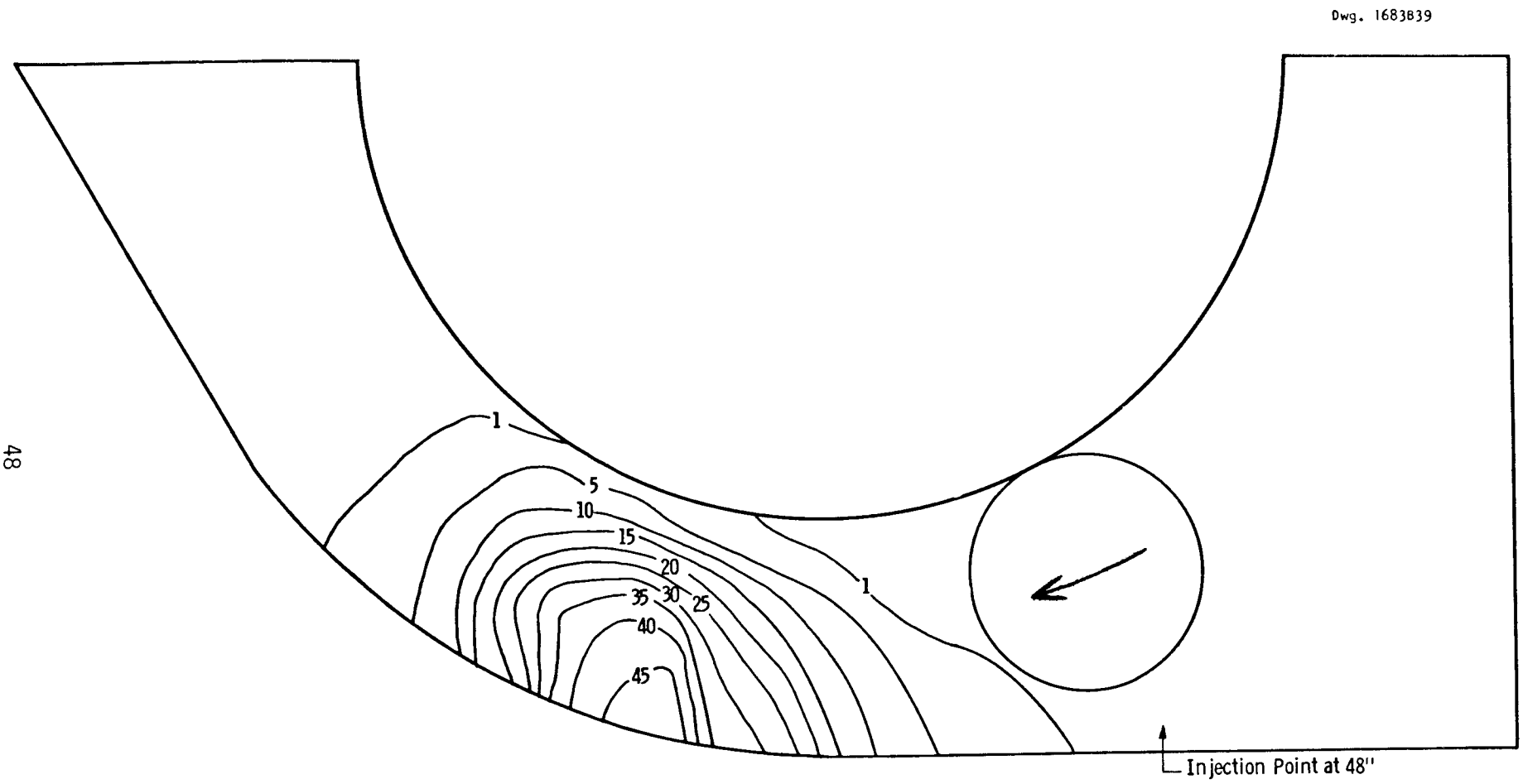

Fig. A-6 — Tracer gas experiment two, 33 inch axial location

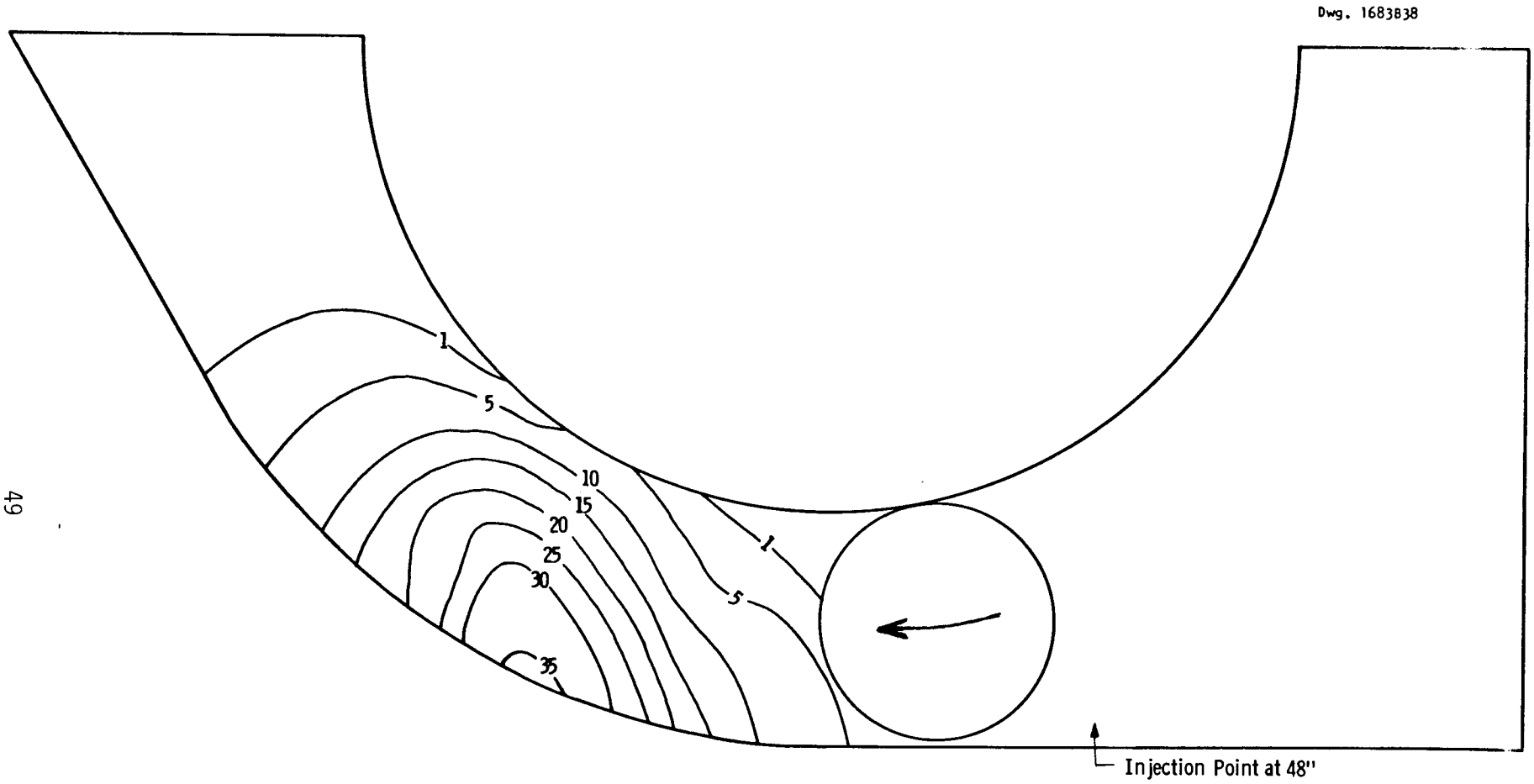

Fig. A-7 — Tracer gas experiment two, 27 inch axial location

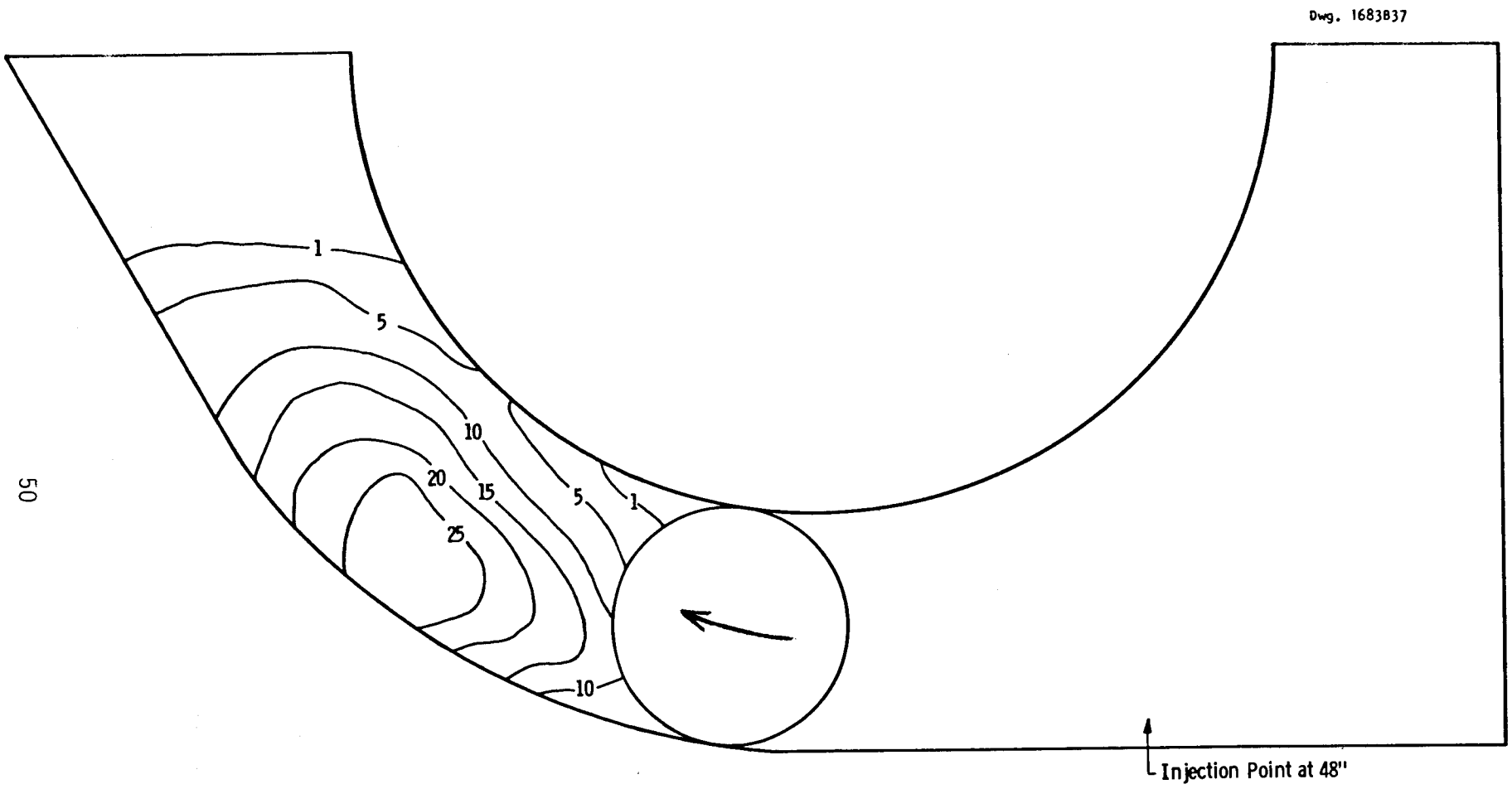

Fig. A-8 — Tracer gas experiment two, 21 inch axial location

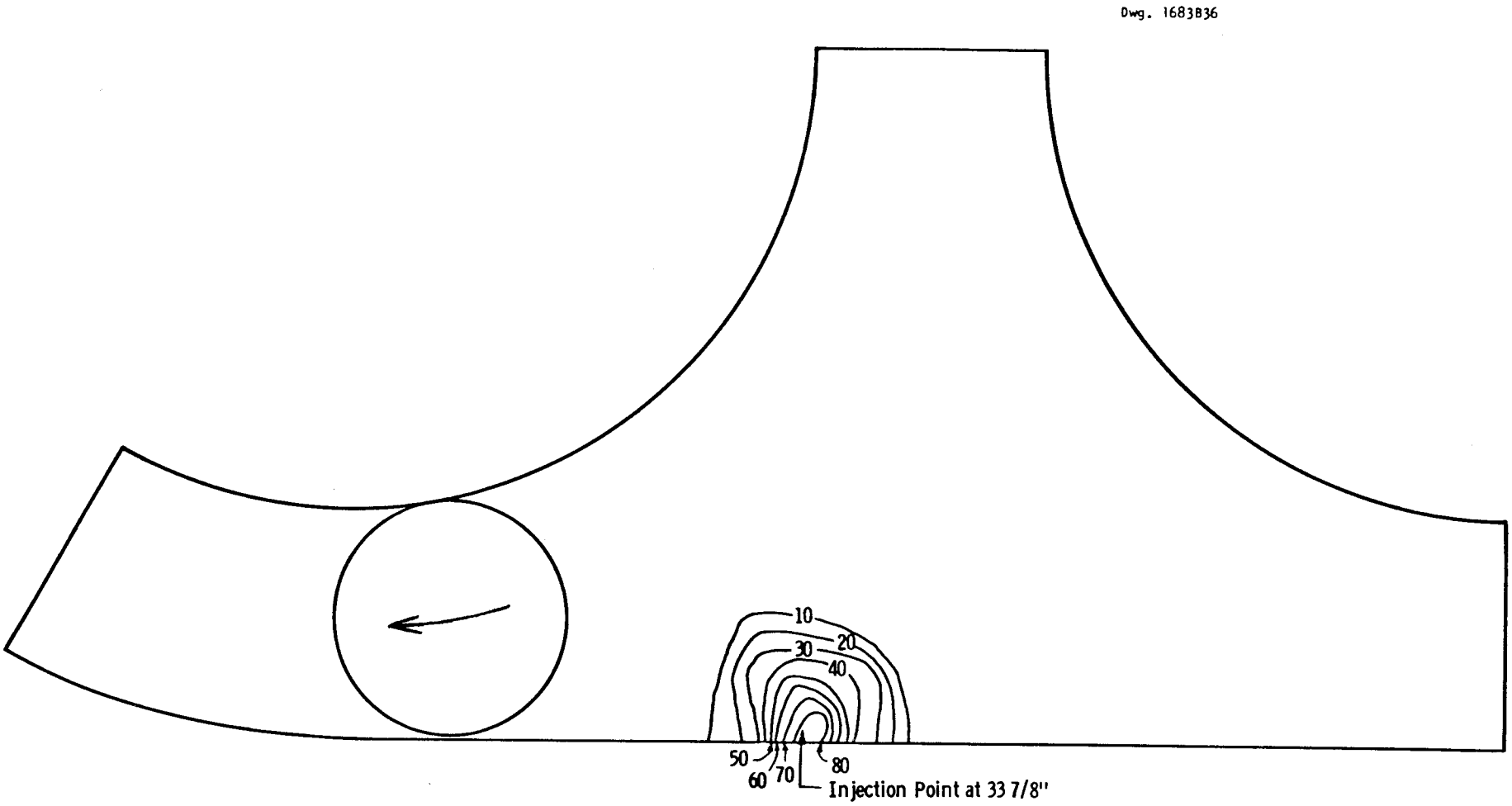

FIGURE A-9 Tracer Gas Experiment Three, 27 Inch Axial Location

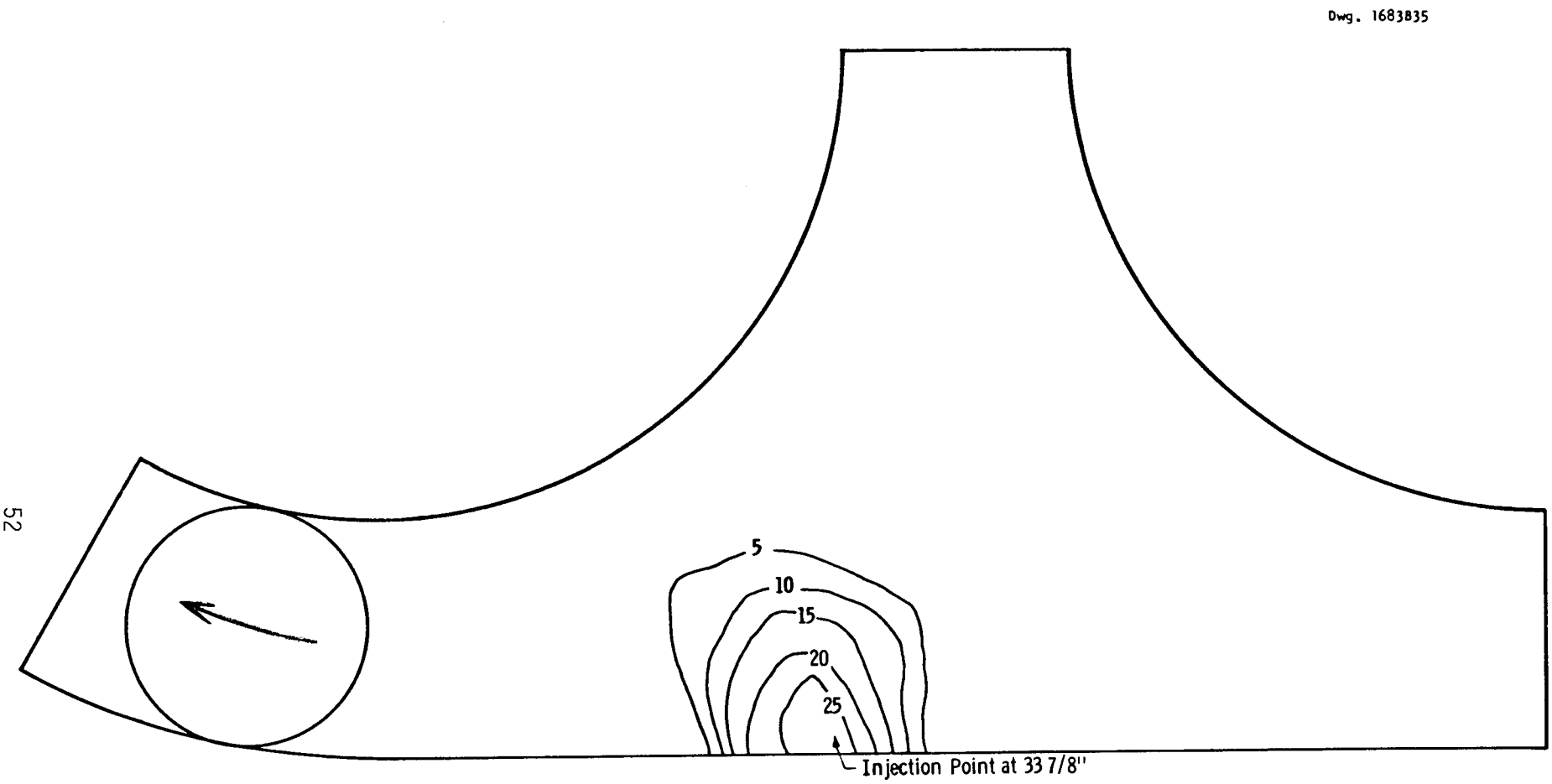

FIGURE A-10 Tracer Gas Experiment Three, 21 Inch Axial Location

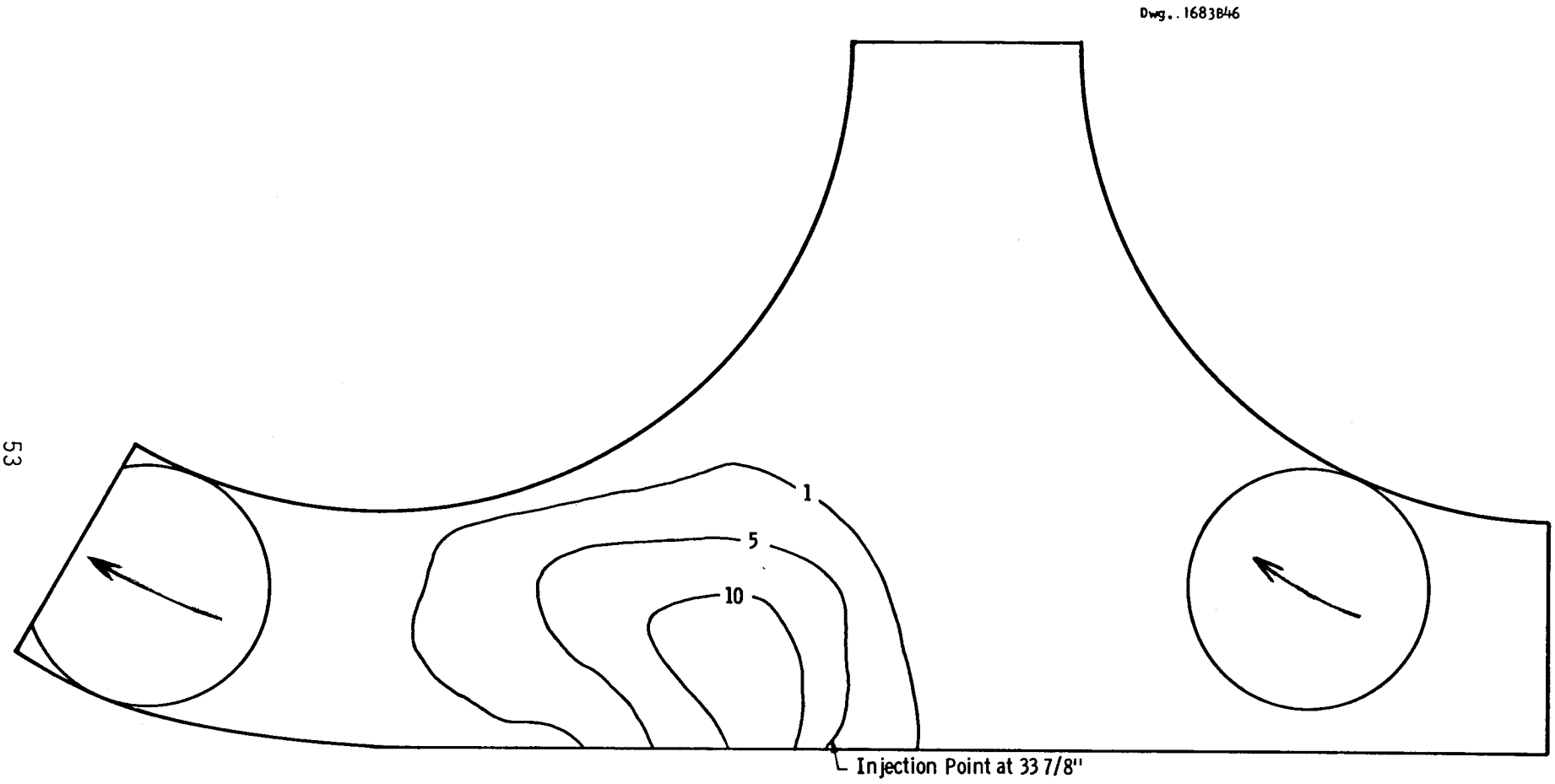

FIGURE A-11 Tracer Gas Experiment Three, 15 Inch Axial Location

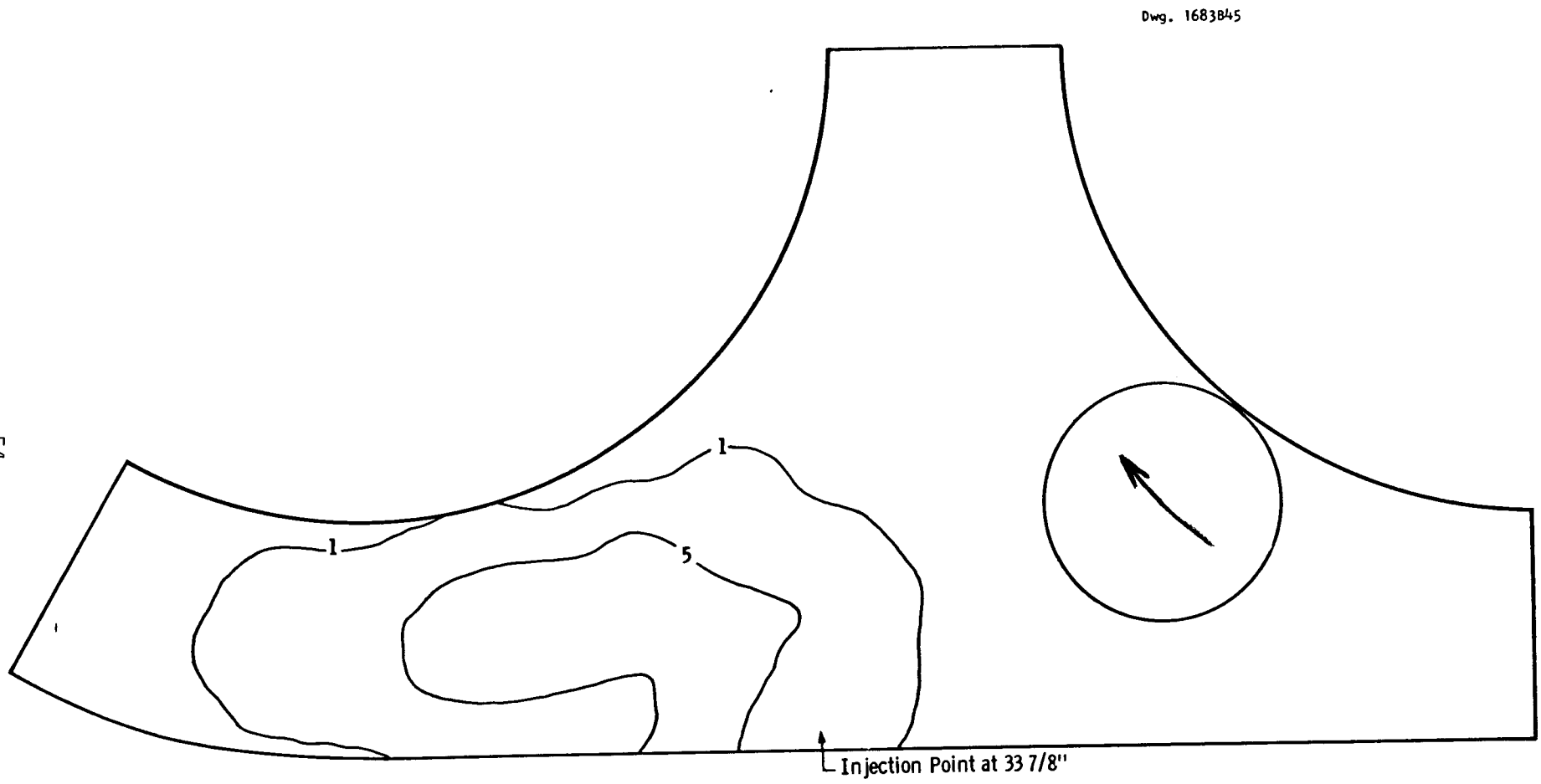

FIGURE A-12 Tracer Gas Experiment Three, 9 Inch Axial Location

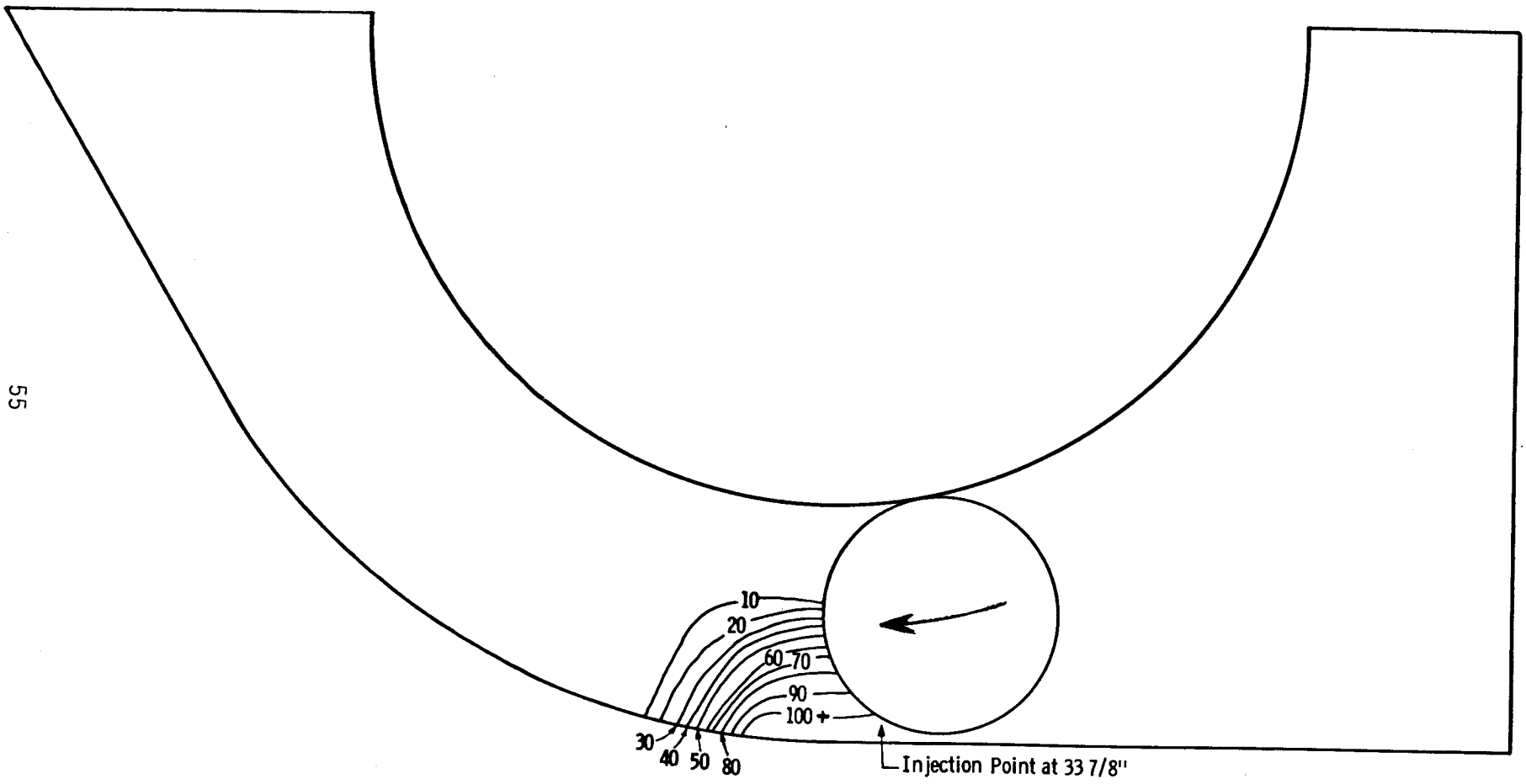

Fig. A-13 — Tracer gas experiment four, 27 inch axial location

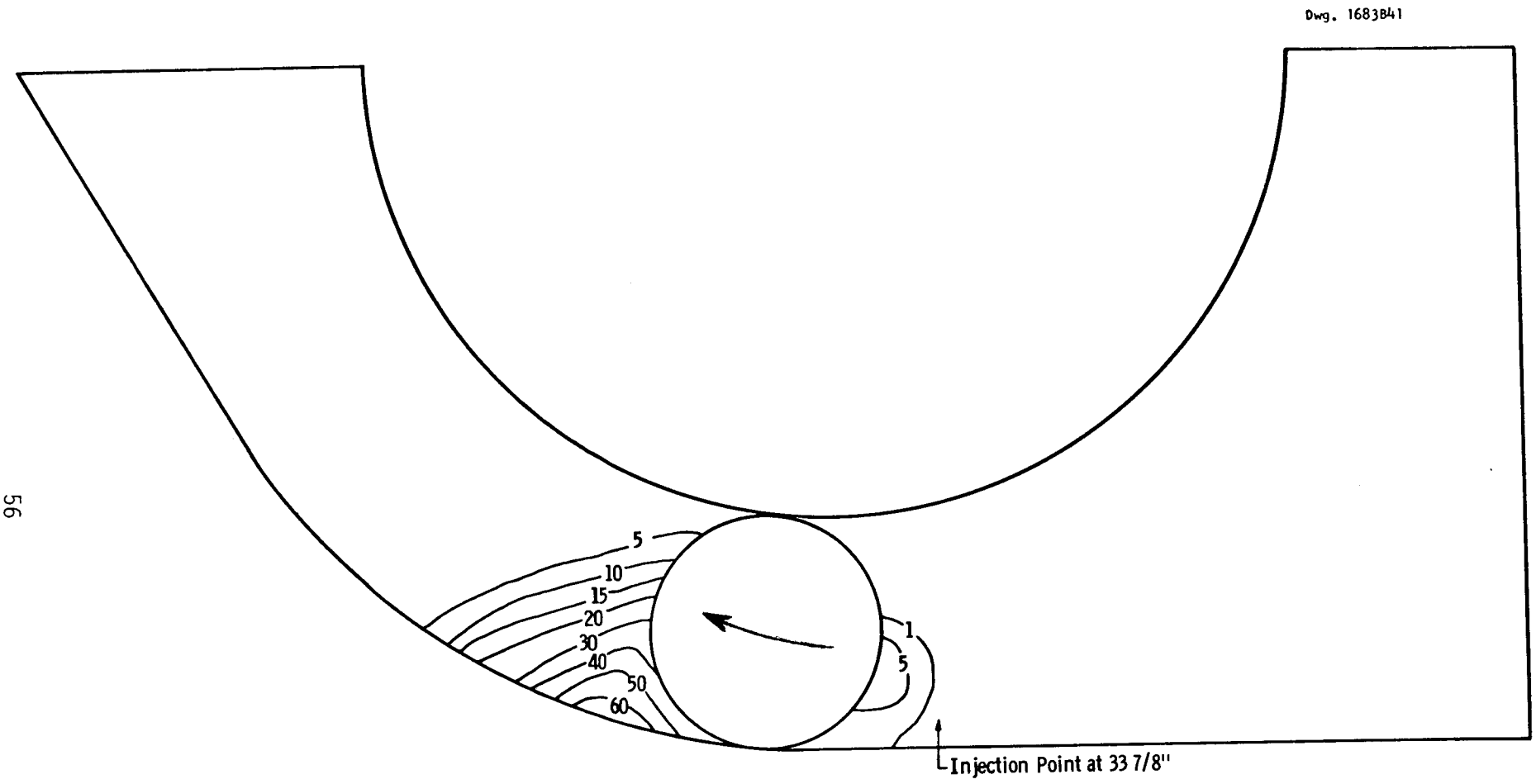

Fig. A-14 — Tracer gas experiment four, 21 inch axial location

APPENDIX B

Gap Crossflow Profiles

Curve 685700-A

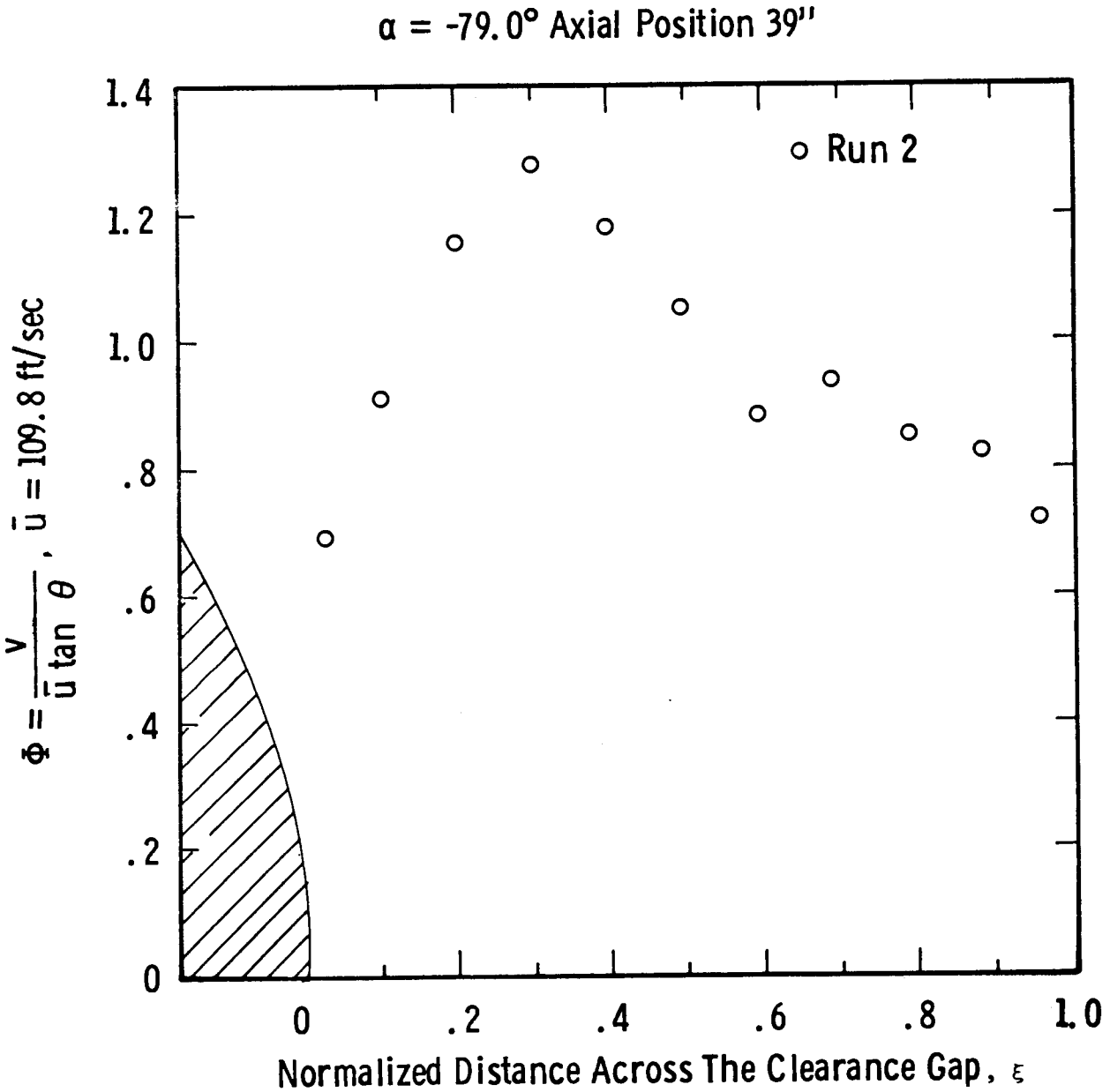

Fig. B-1 — Dimensionless crossflow coefficient $\Phi(\xi)$, $\alpha = -79.0°$

Curve 685702-A

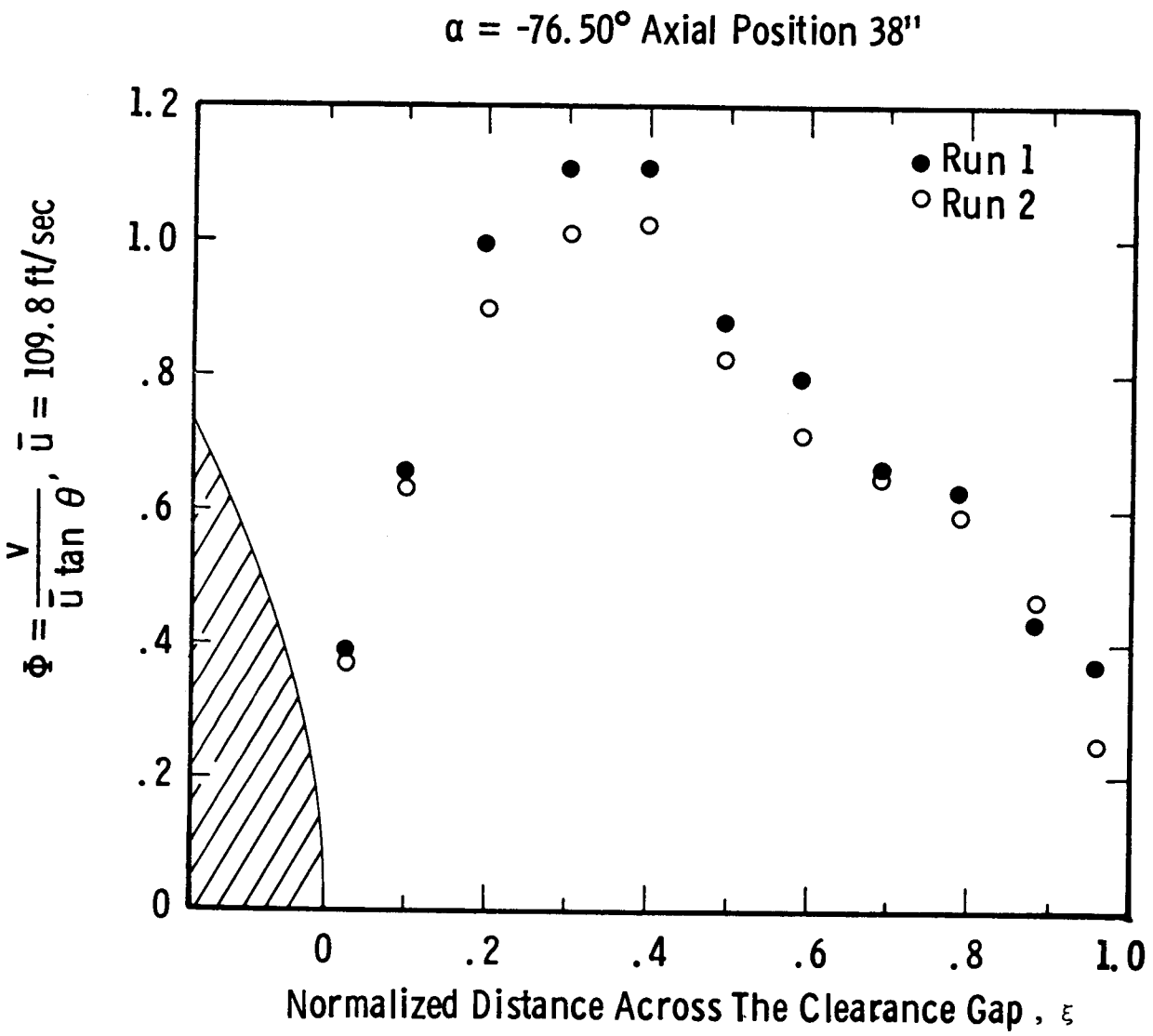

Fig. B-2 — Dinemsionless crossflow coefficient $\Phi(\xi)$, $\alpha = -76.5°$

Curve 685701-A

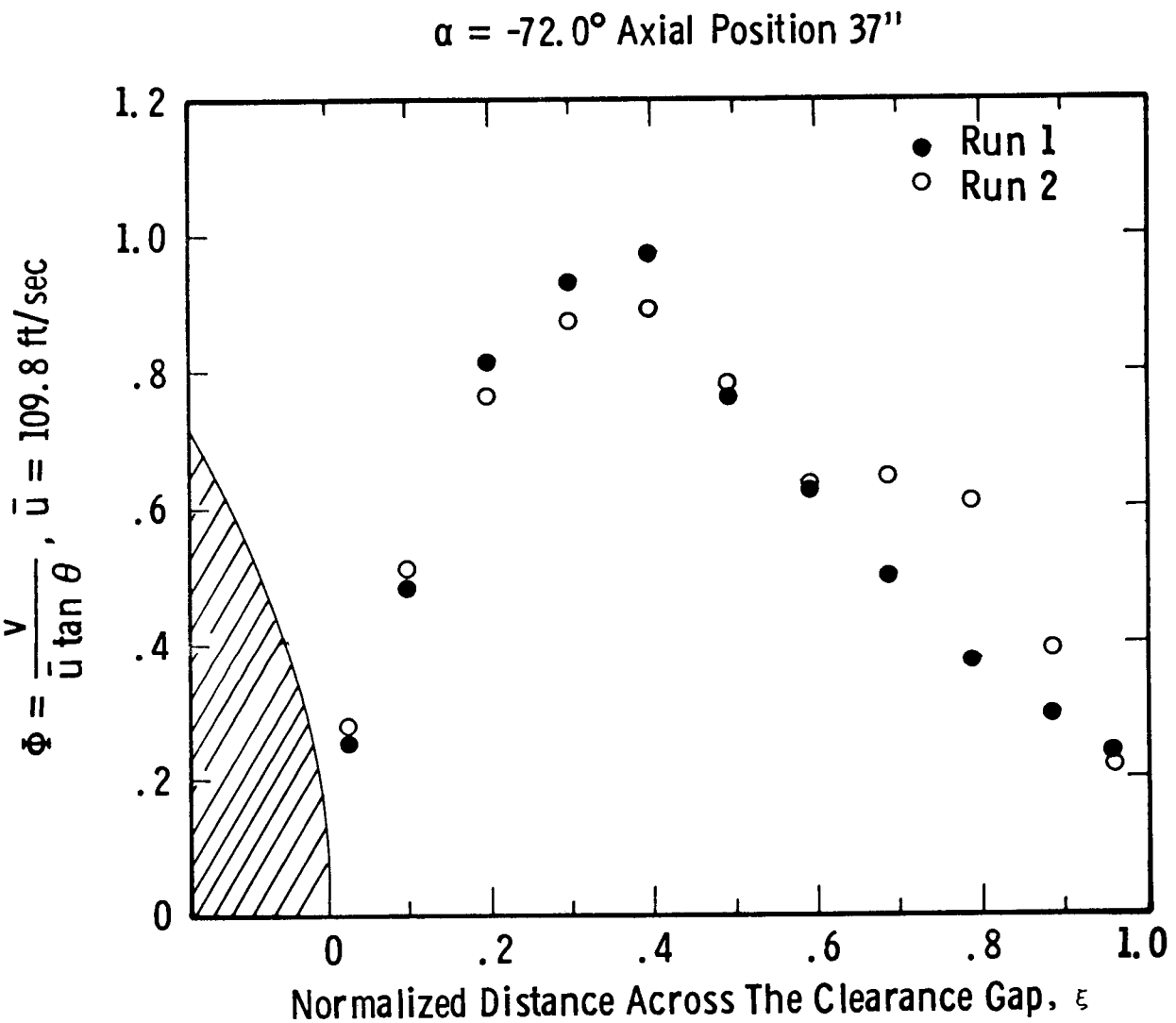

Fig. B-3 — Dimensionless crossflow coefficient $\Phi(\xi)$, $\alpha = -72.0°$

Curve 685703-A

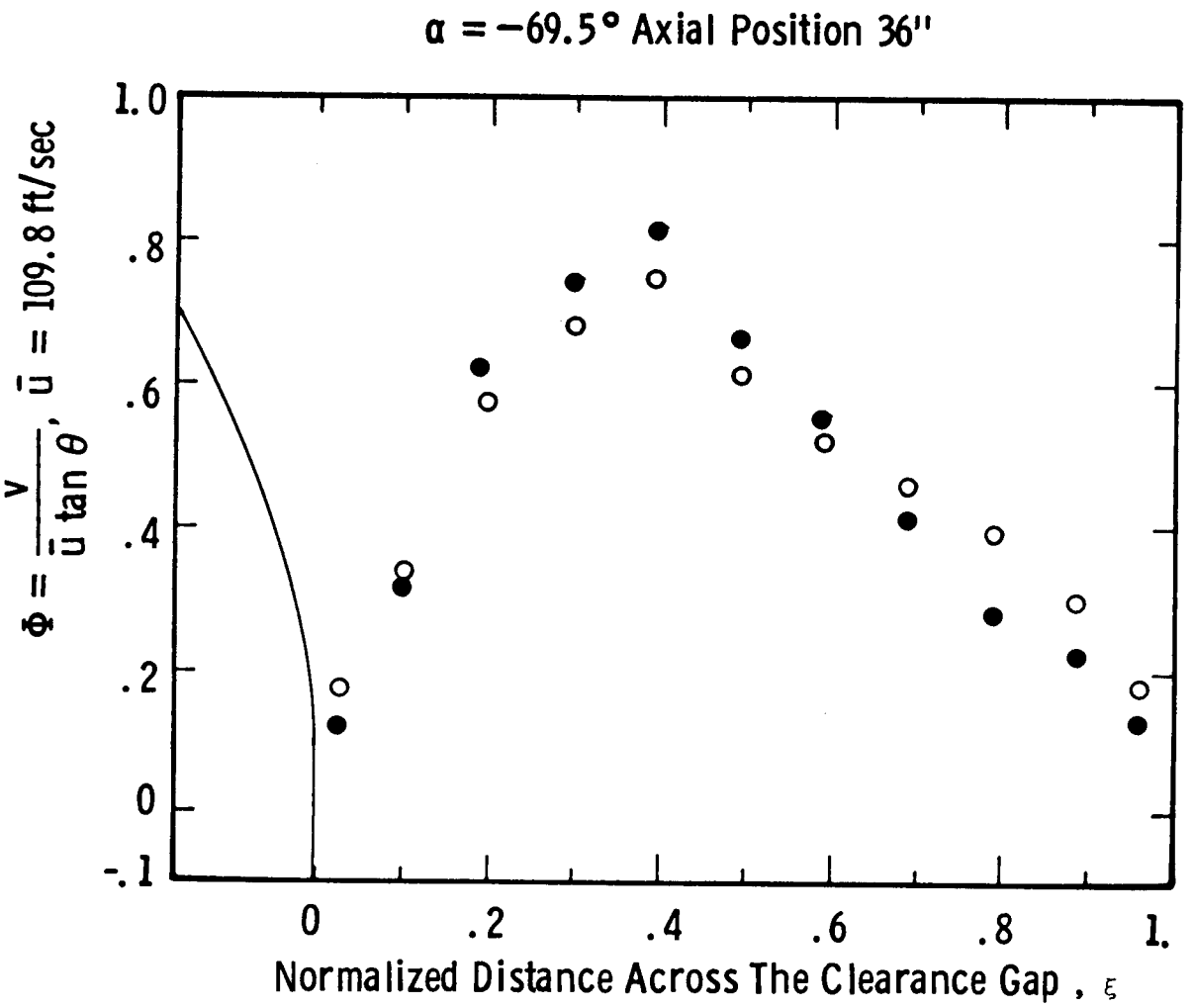

Fig. B-4 — Dimensionless crossflow coefficient $\Phi(\xi)$, $\alpha = -69.5°$

Curve 685704-A

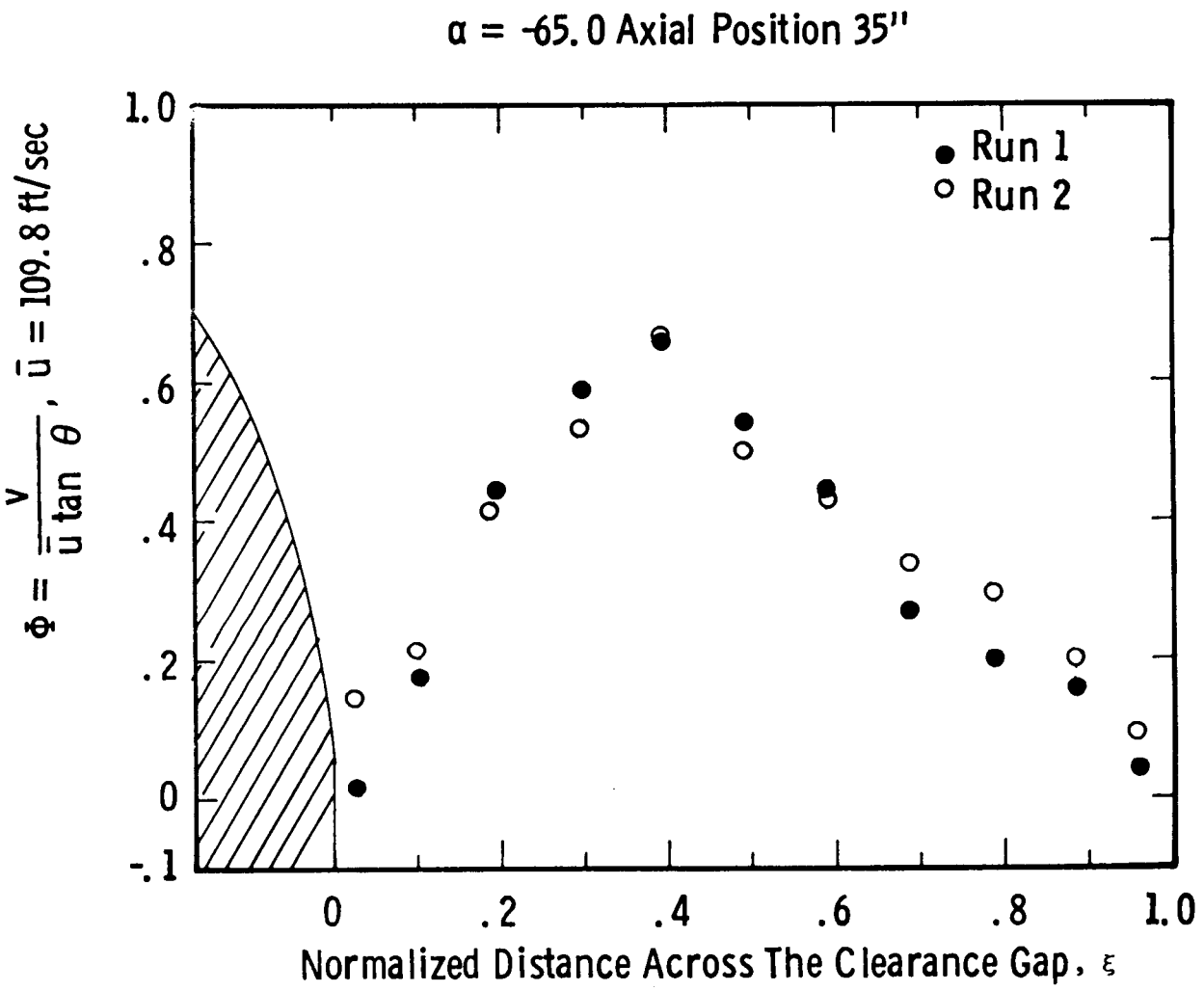

Fig. B-5 — Dimensionless crossflow coefficient $\Phi(\xi)$, $\alpha = -65.0°$

Curve 685705-A

$\alpha = -61.50°$ Axial Position 34"

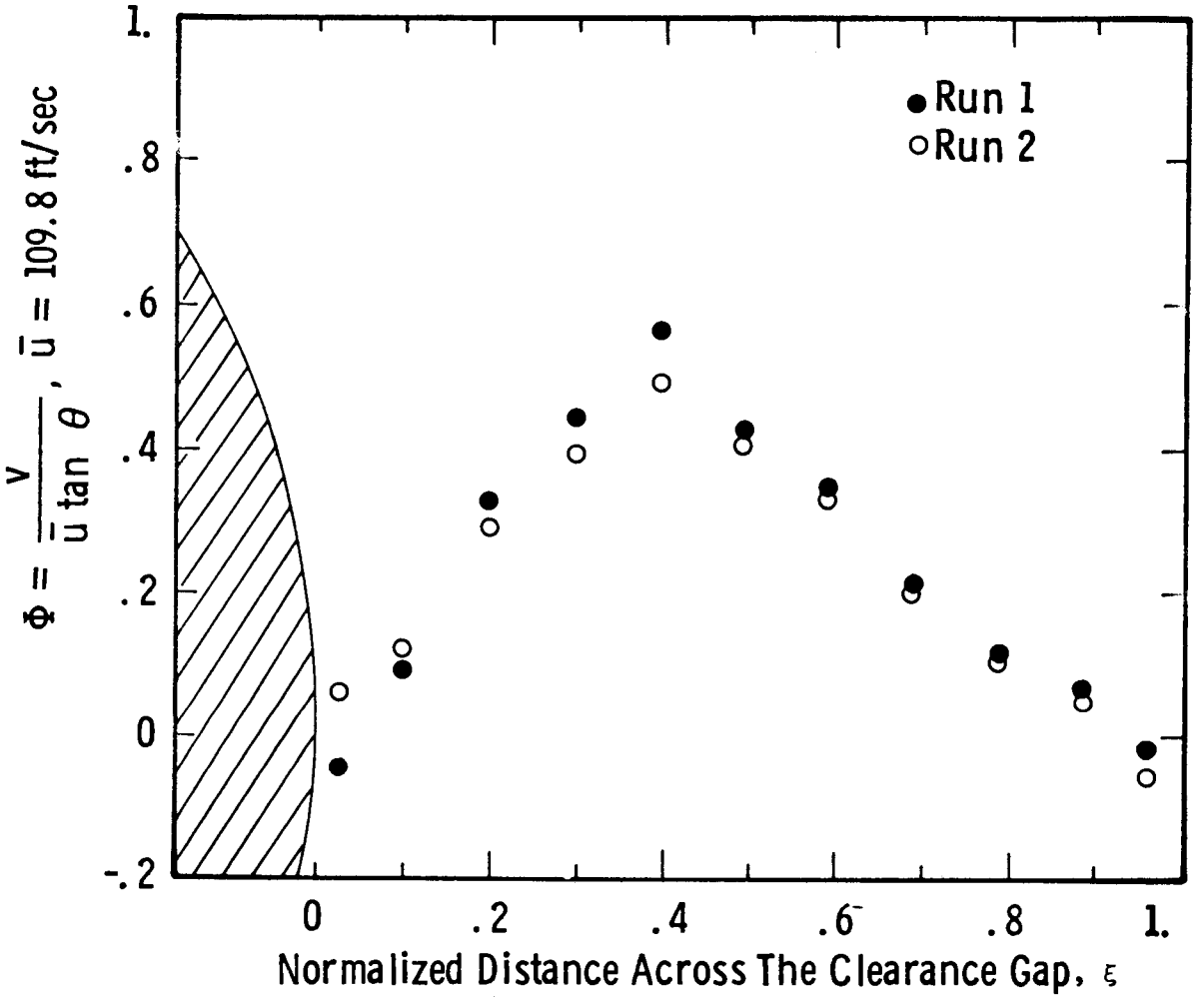

Fig. B-6 — Dimensionless crossflow coefficient $\Phi(\xi)$, $\alpha = -61.5°$

Curve 685706-A

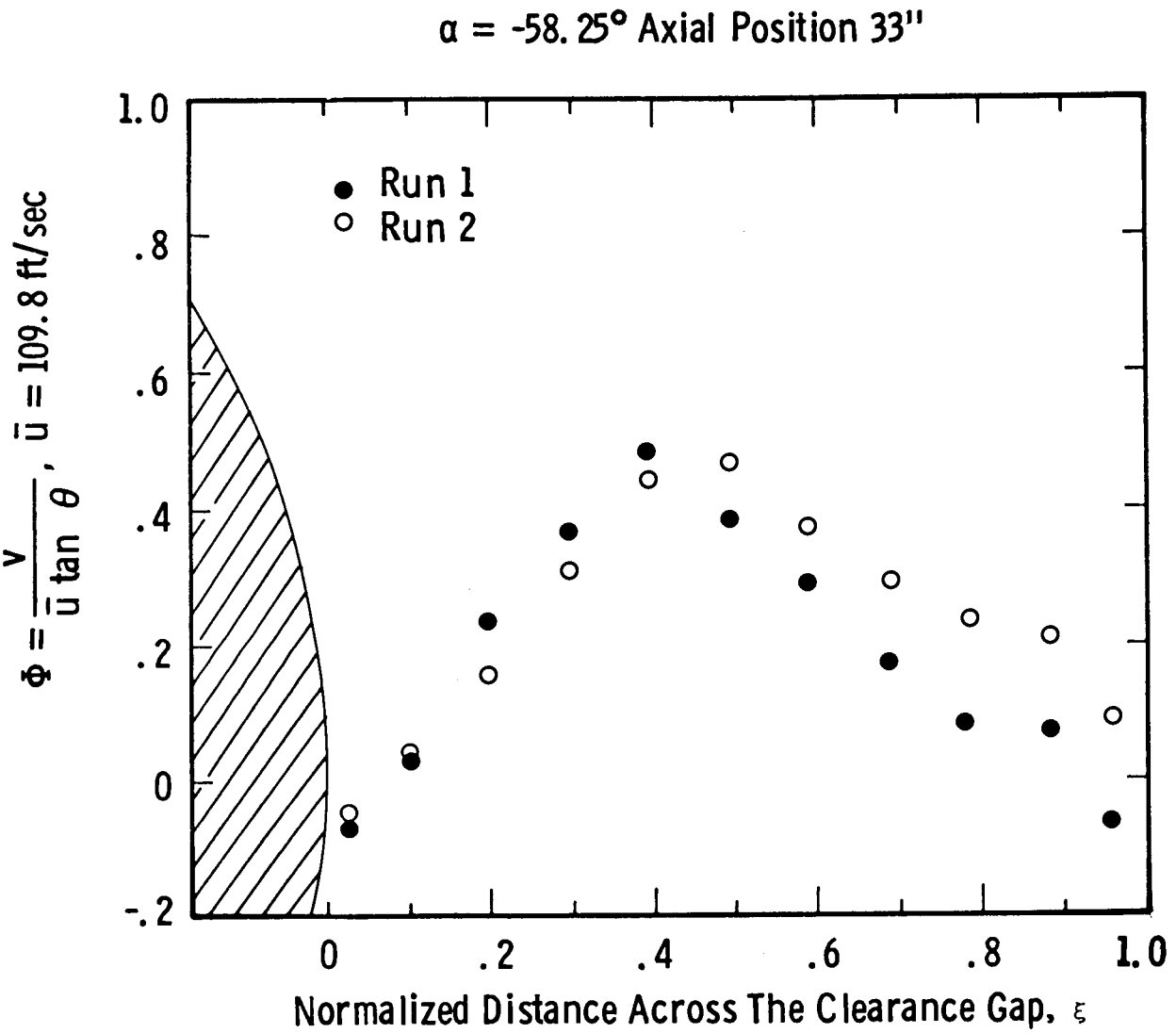

Fig. B-7 — Dimensionless crossflow coefficient $\Phi(\xi)$, $\alpha = -58.2°$

Curve 685707-A

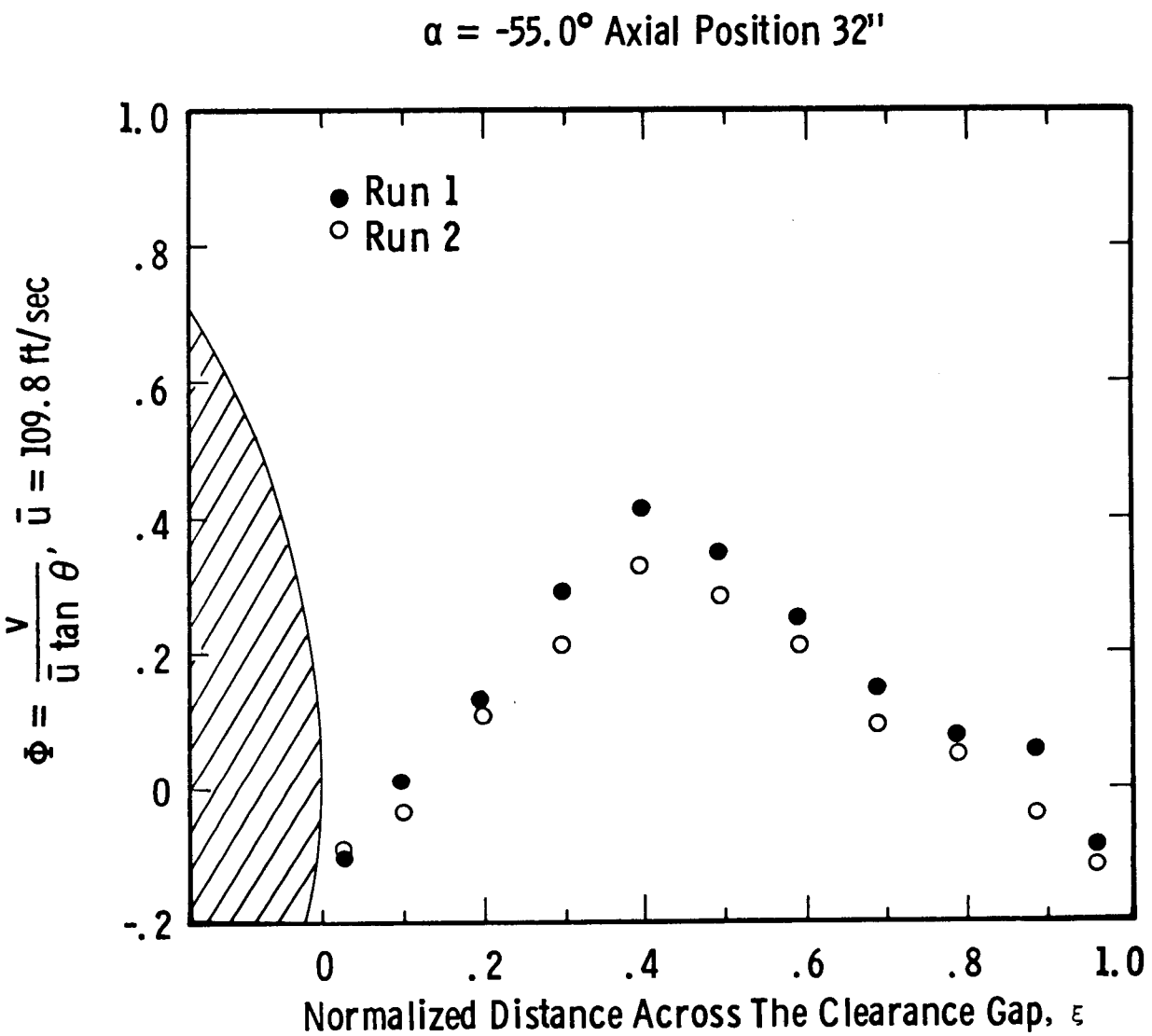

Fig. B-8 — Dimensionless crossflow coefficient $\Phi(\xi)$, $\alpha = -55.0°$

Curve 685708-A

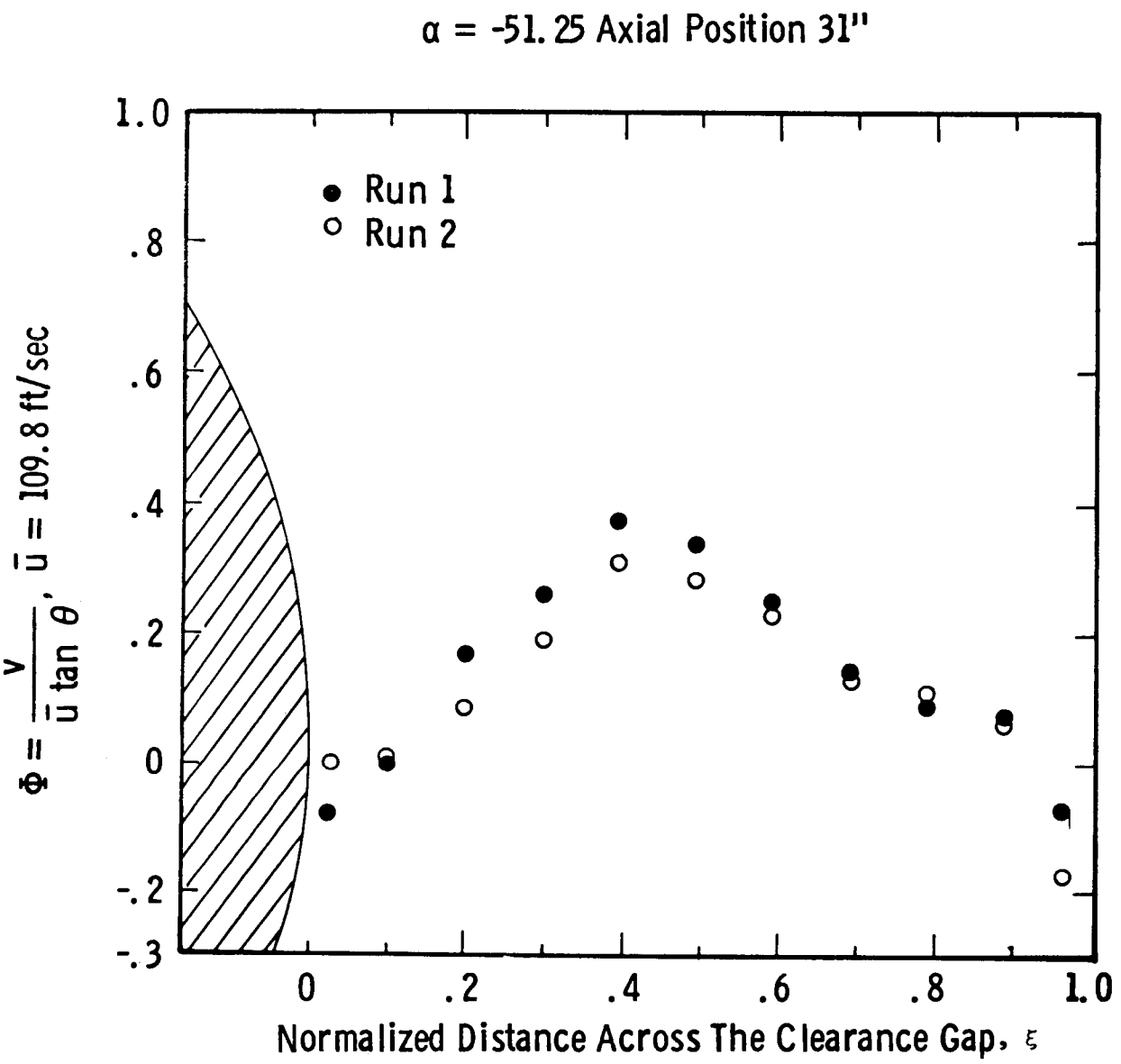

Fig. B-9 — Dimensionless crossflow coefficient
$\Phi = (\xi)$, $\alpha = 51.2°$

Curve 685709-A

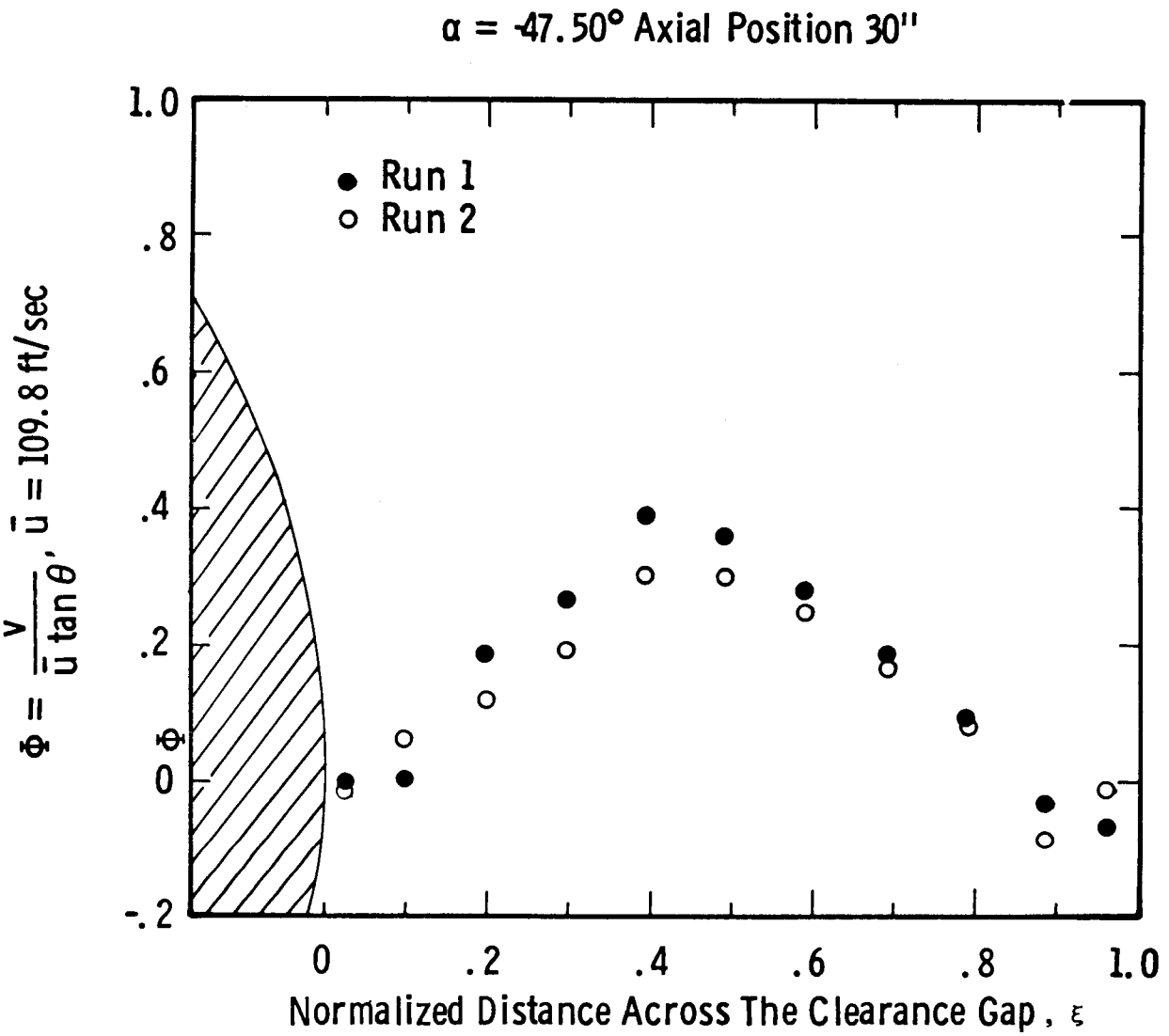

Fig. B-10 — Dimensionless crossflow coefficient $\Phi(\xi)$, $\alpha = -47.5°$

Curve 685710-A

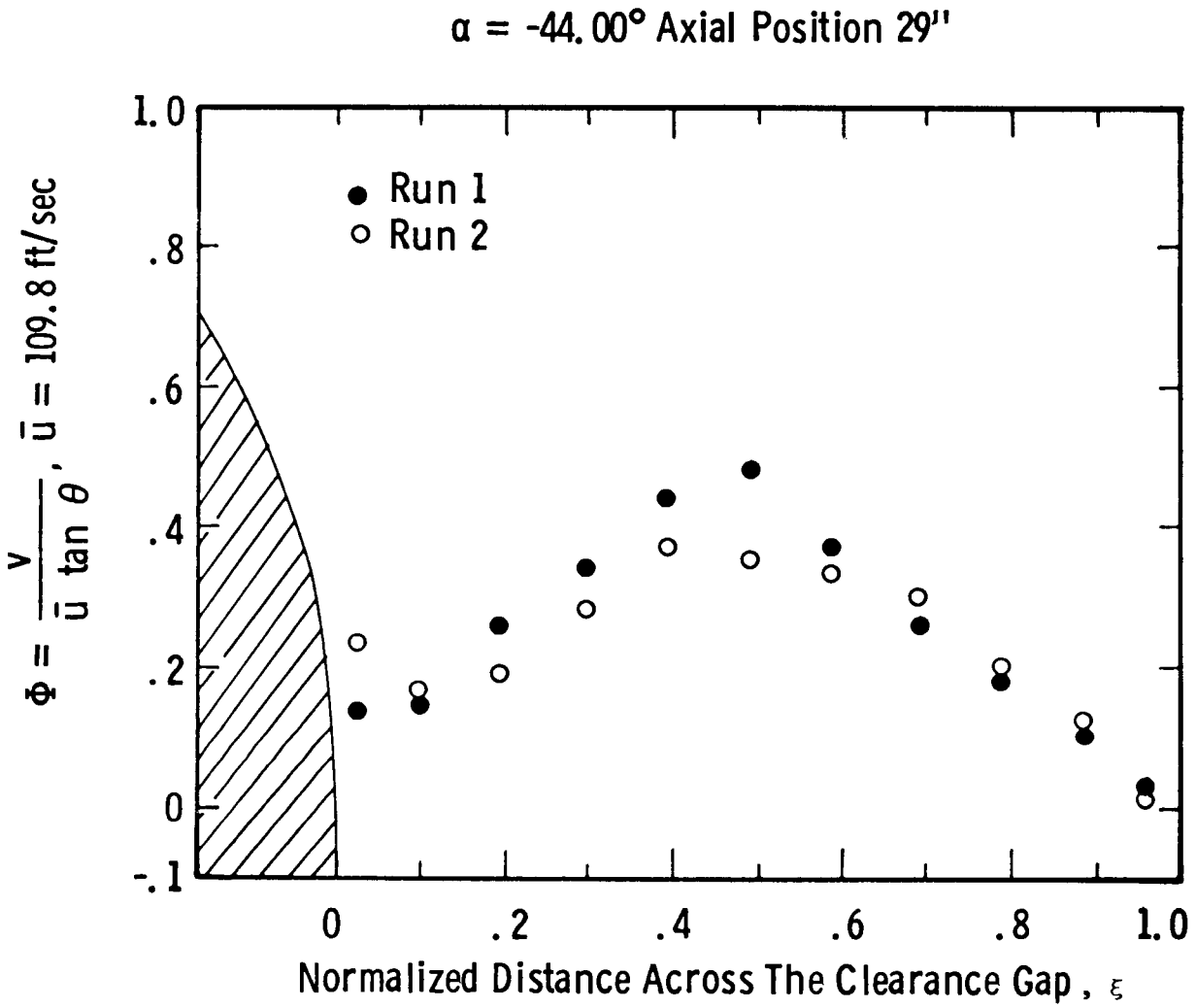

Fig. B-11 — Dimensionless crossflow coefficient $\Phi(\xi)$, $\alpha = -44.0°$

Curve 685711-A

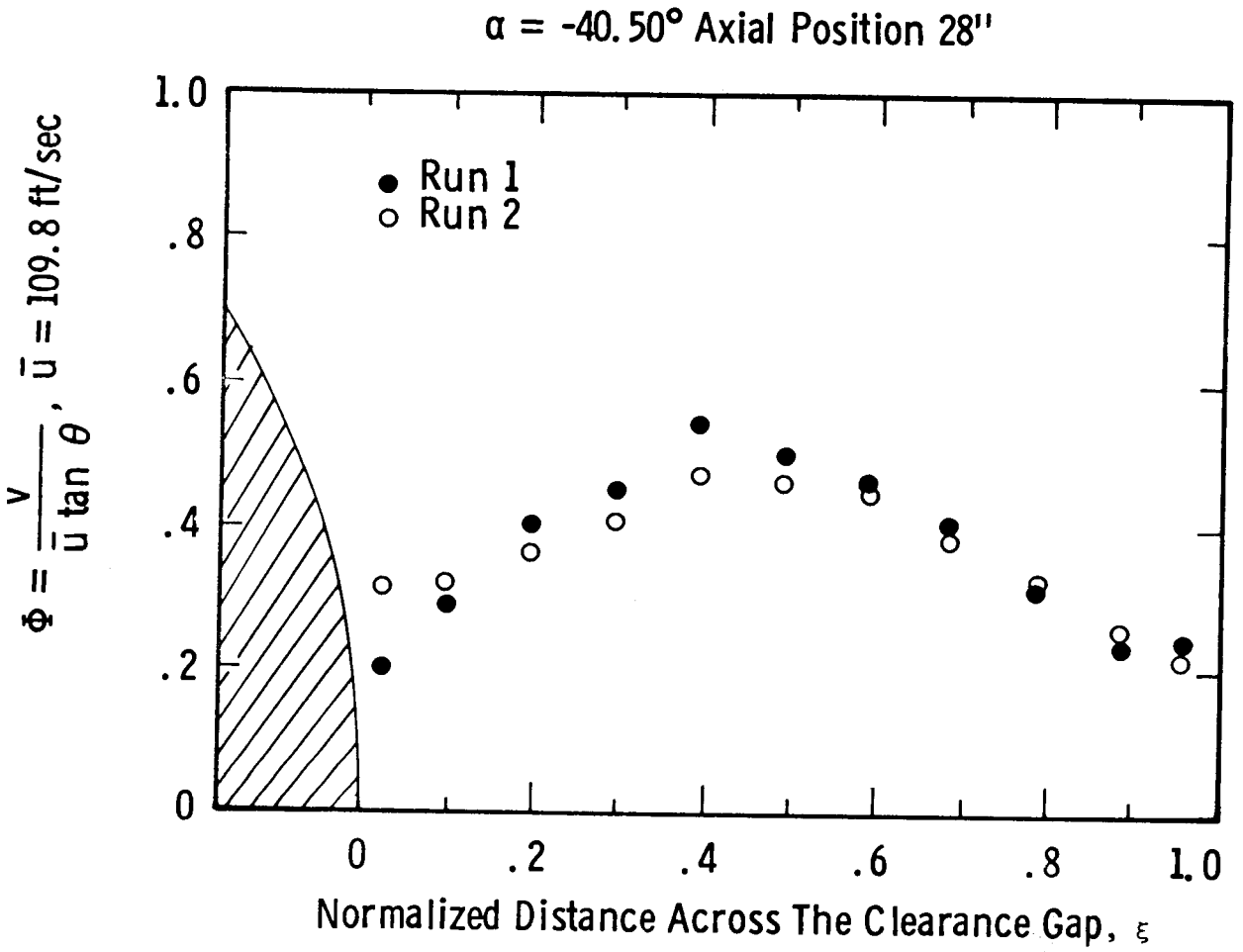

Fig. B-12 — Dimensionless crossflow coefficient $\Phi(\xi)$, $\alpha = -40.5°$

Curve 685712-A

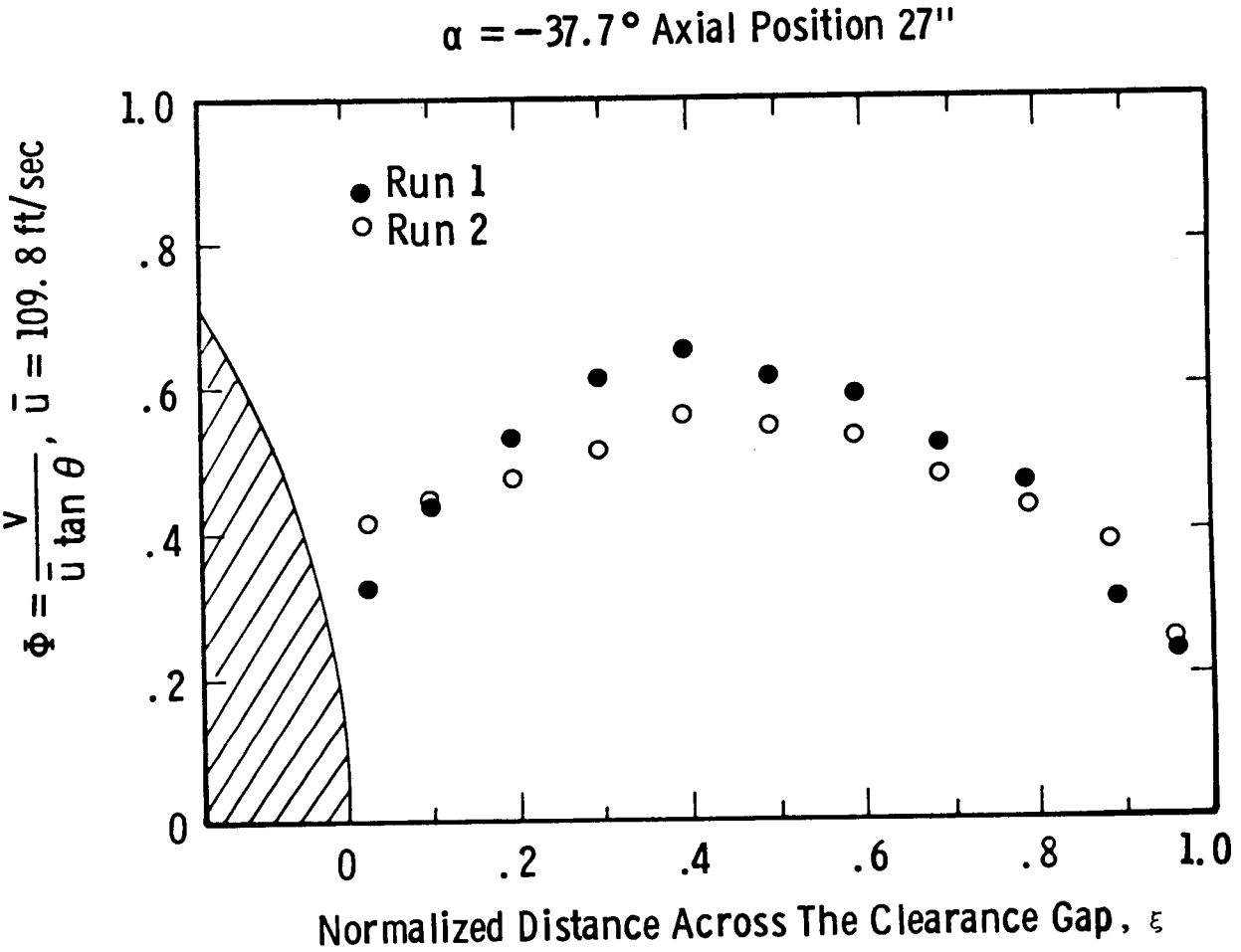

Fig. B-13 — Dimensionless crossflow coefficient $\Phi(\xi)$, $\alpha = -37.7°$

Curve 685713-A

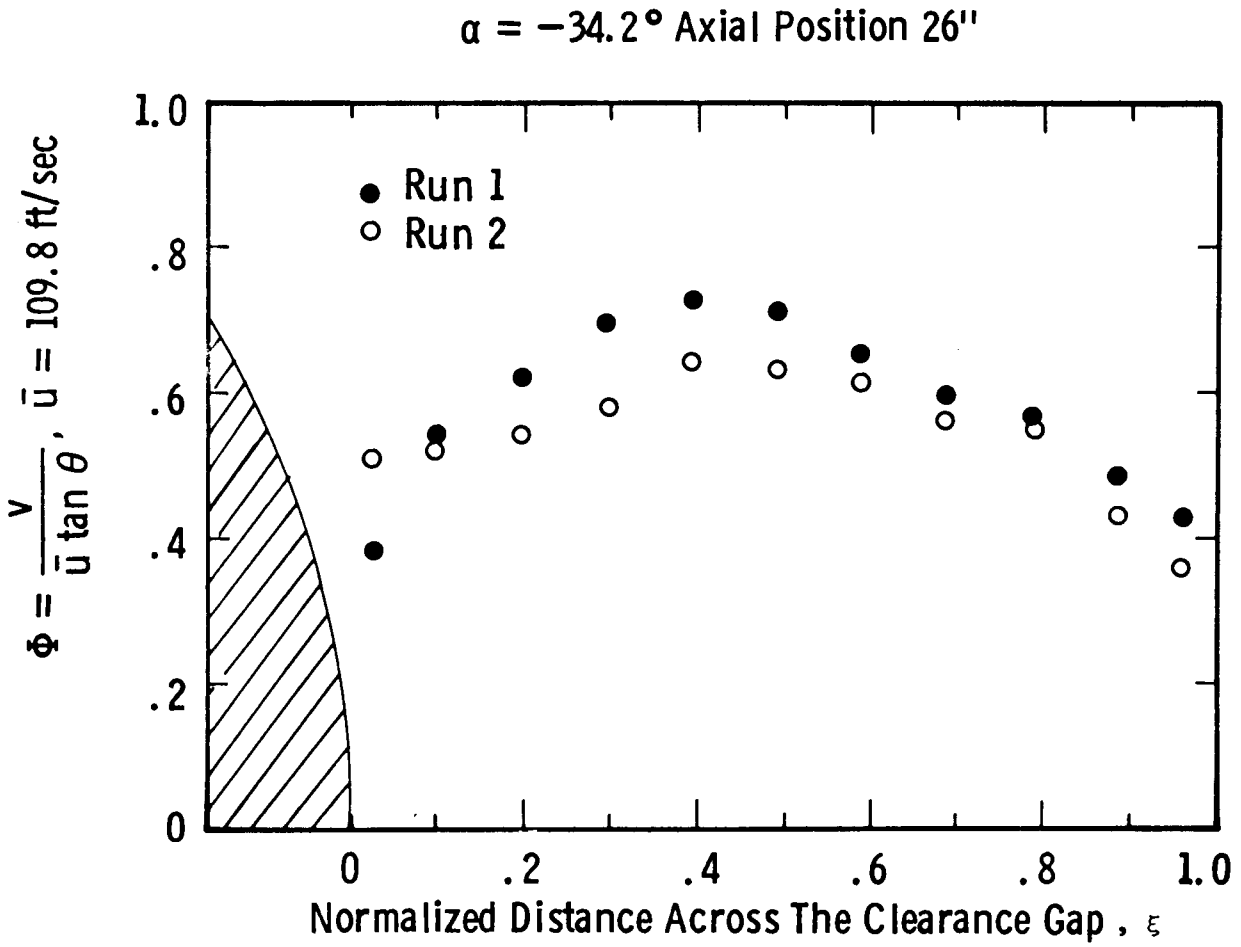

Fig. B-14 — Dimensionless crossflow coefficient $\Phi(\xi)$, $\alpha = -34.2°$

Curve 685715-A

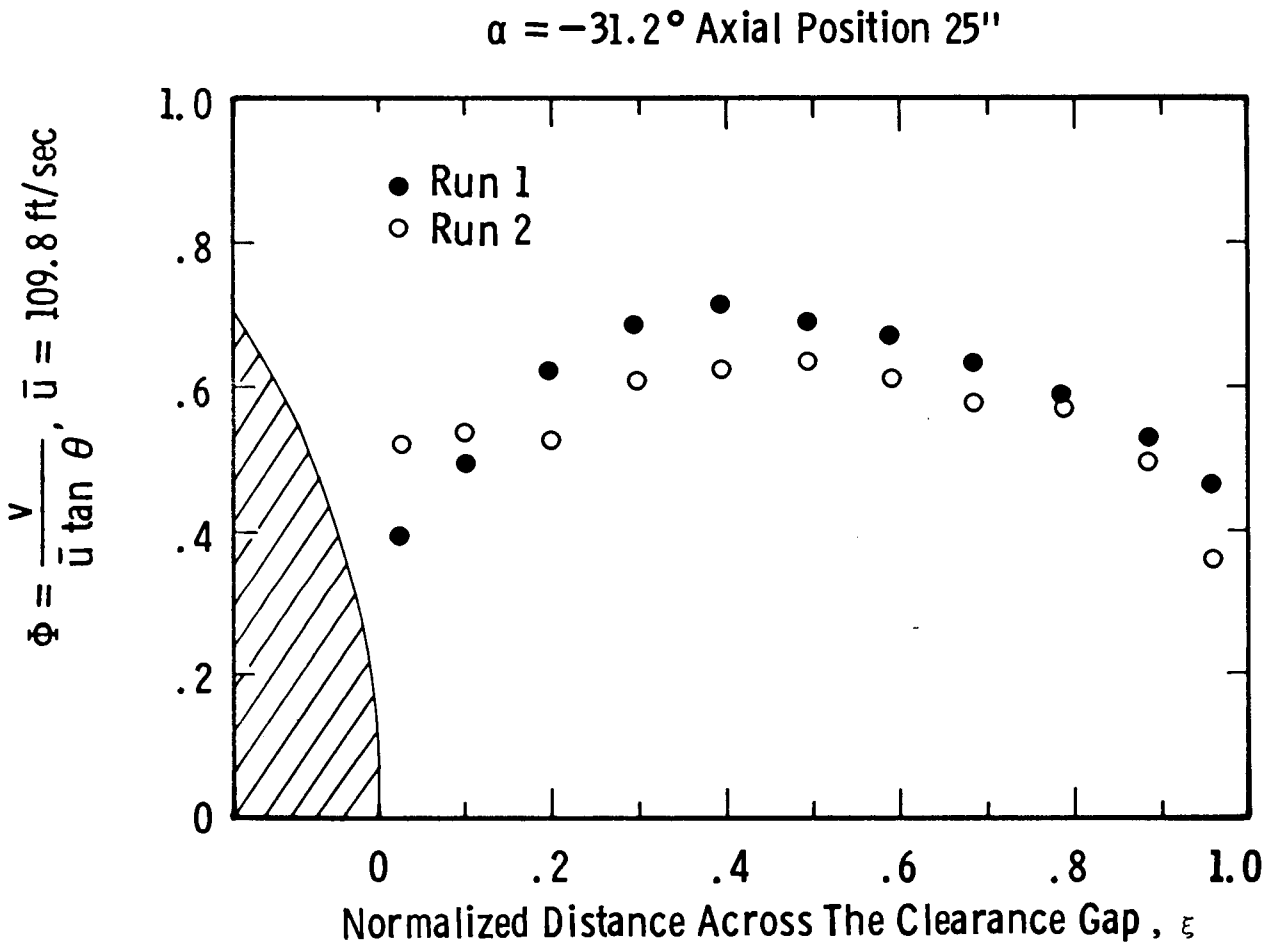

Fig. B-15 — Dimensionless crossflow coefficient $\Phi(\xi)$, $\alpha = -31.2°$

Curve 685714-A

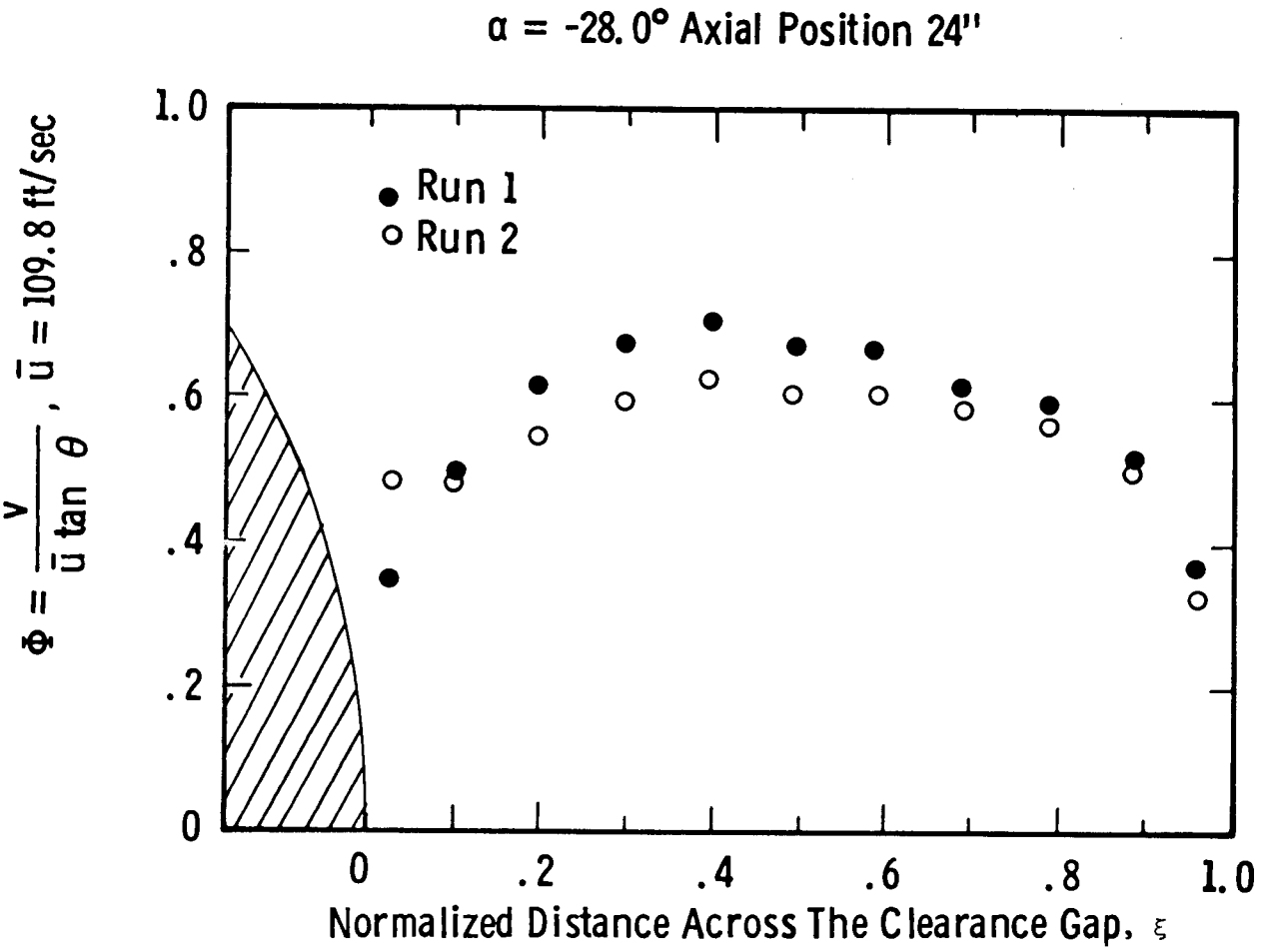

Fig. B-16 — Dimensionless crossflow coefficient $\Phi(\xi)$, $\alpha = -28.0°$

Curve 685717-A

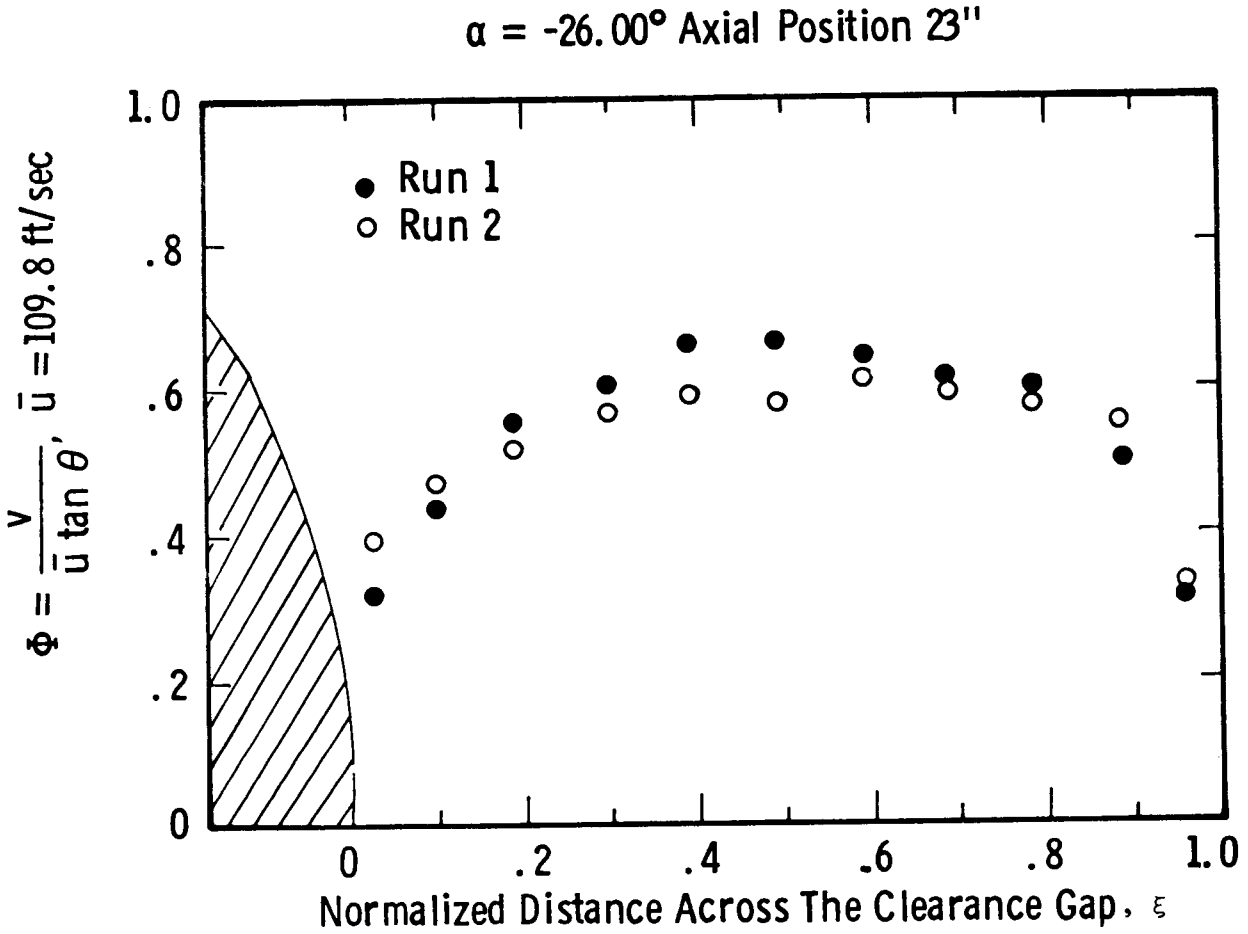

Fig. B-17 — Dimensionless crossflow coefficient $\Phi(\xi)$, = −26.0°

Curve 685716-A

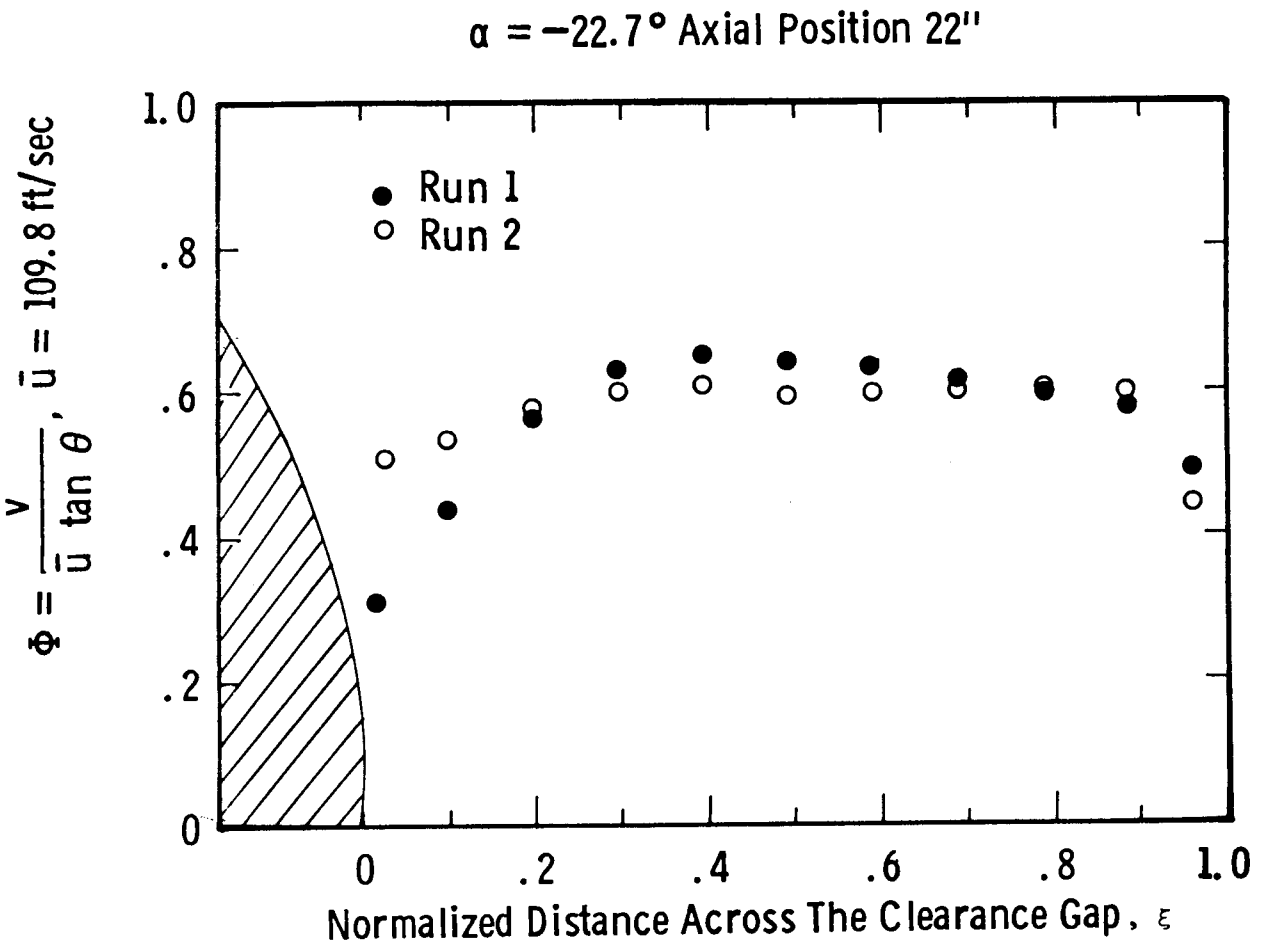

Fig. B-18 — Dimensionless crossflow coefficient $\Phi(\xi)$, $\alpha = -22.7°$

Curve 685718-A

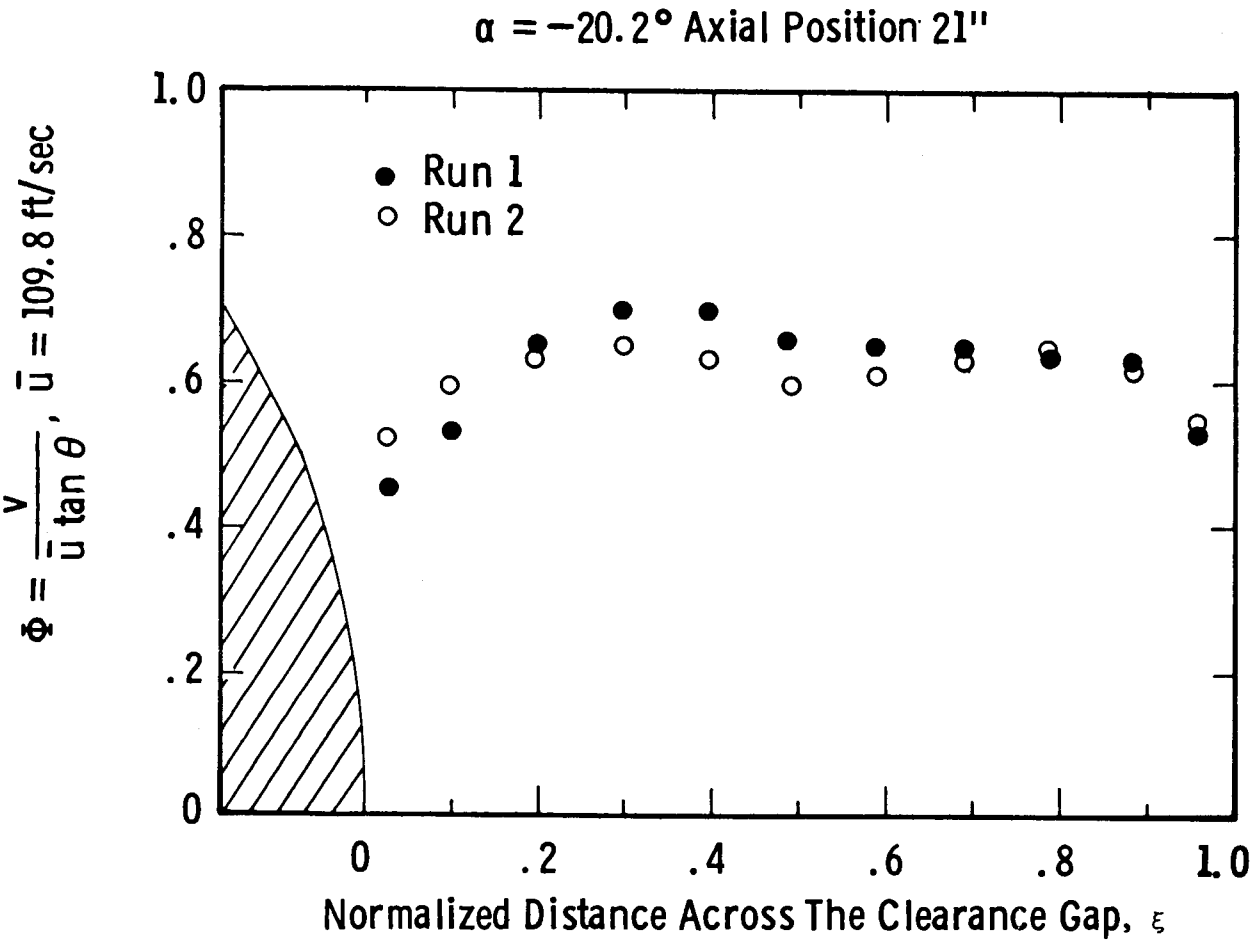

Fig. B-19 — Dimensionless crossflow coefficient $\Phi(\xi)$, $\alpha = -20.2°$

Curve 685720-A

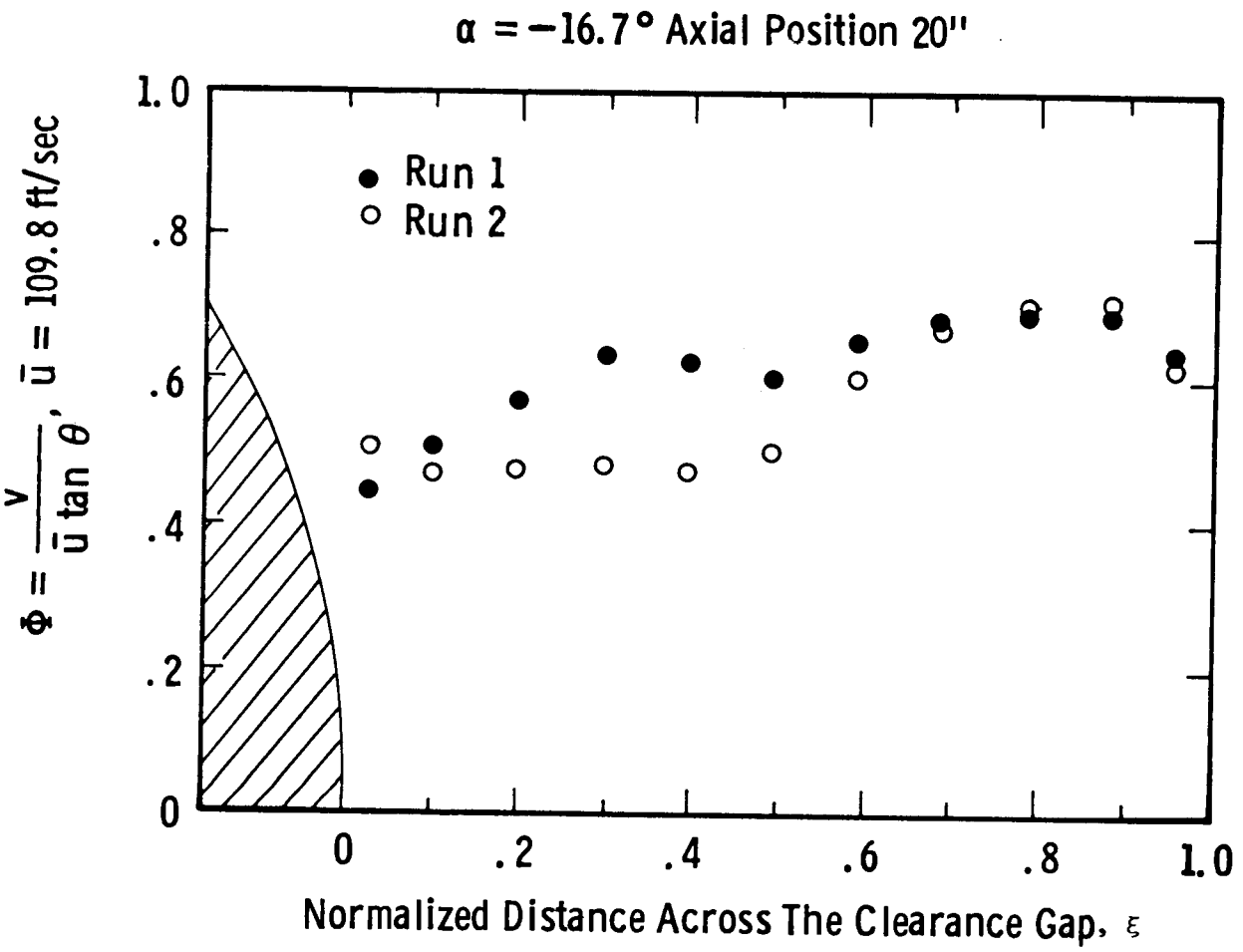

Fig. B-20 — Dimensionless crossflow coefficient $\Phi(\xi)$, $\alpha = -16.7°$

Curve 685721-A

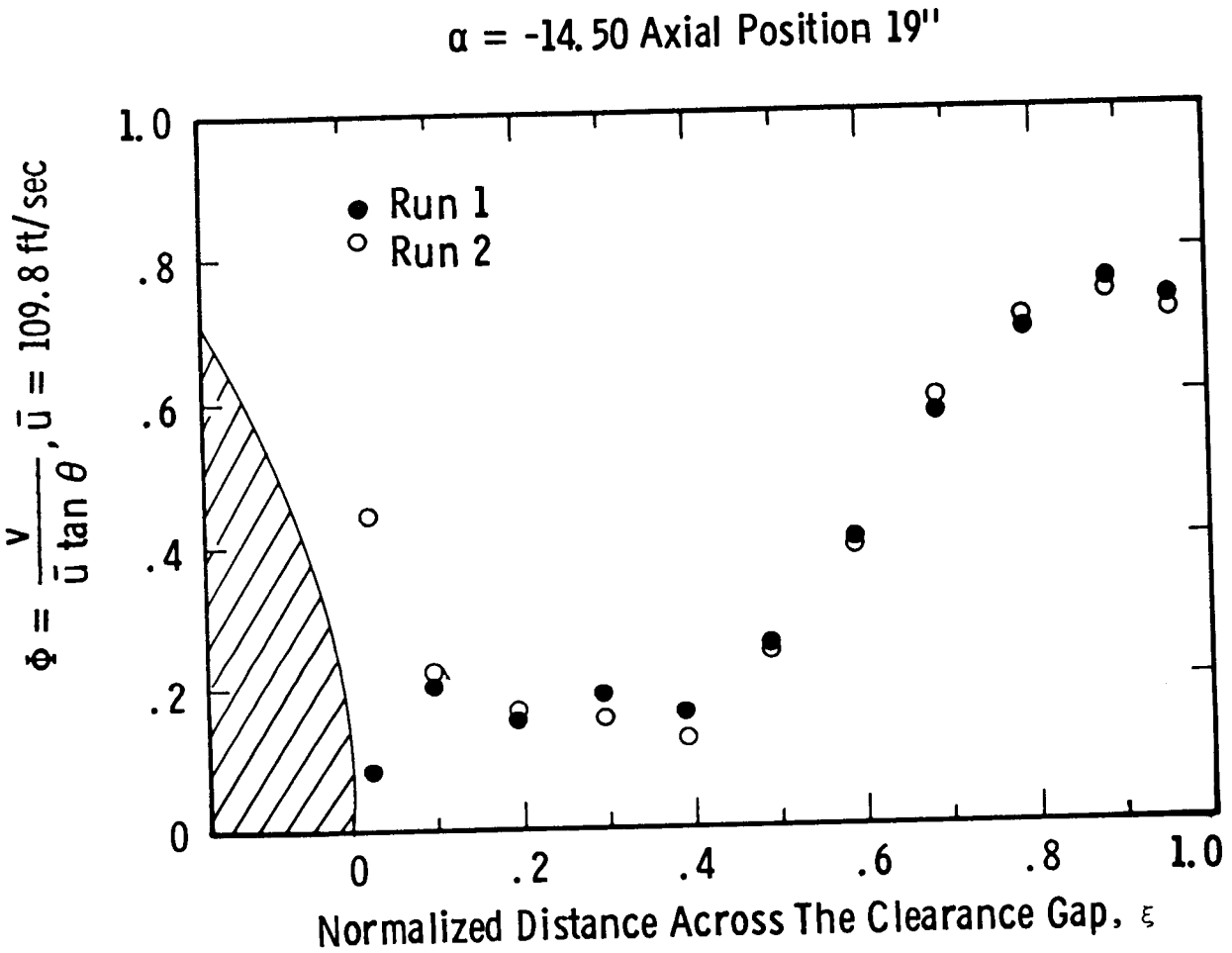

Fig. B-21 – Dimensionless crossflow coefficient $\Phi(\xi)$, $\alpha = -14.5°$

Curve 685719-A

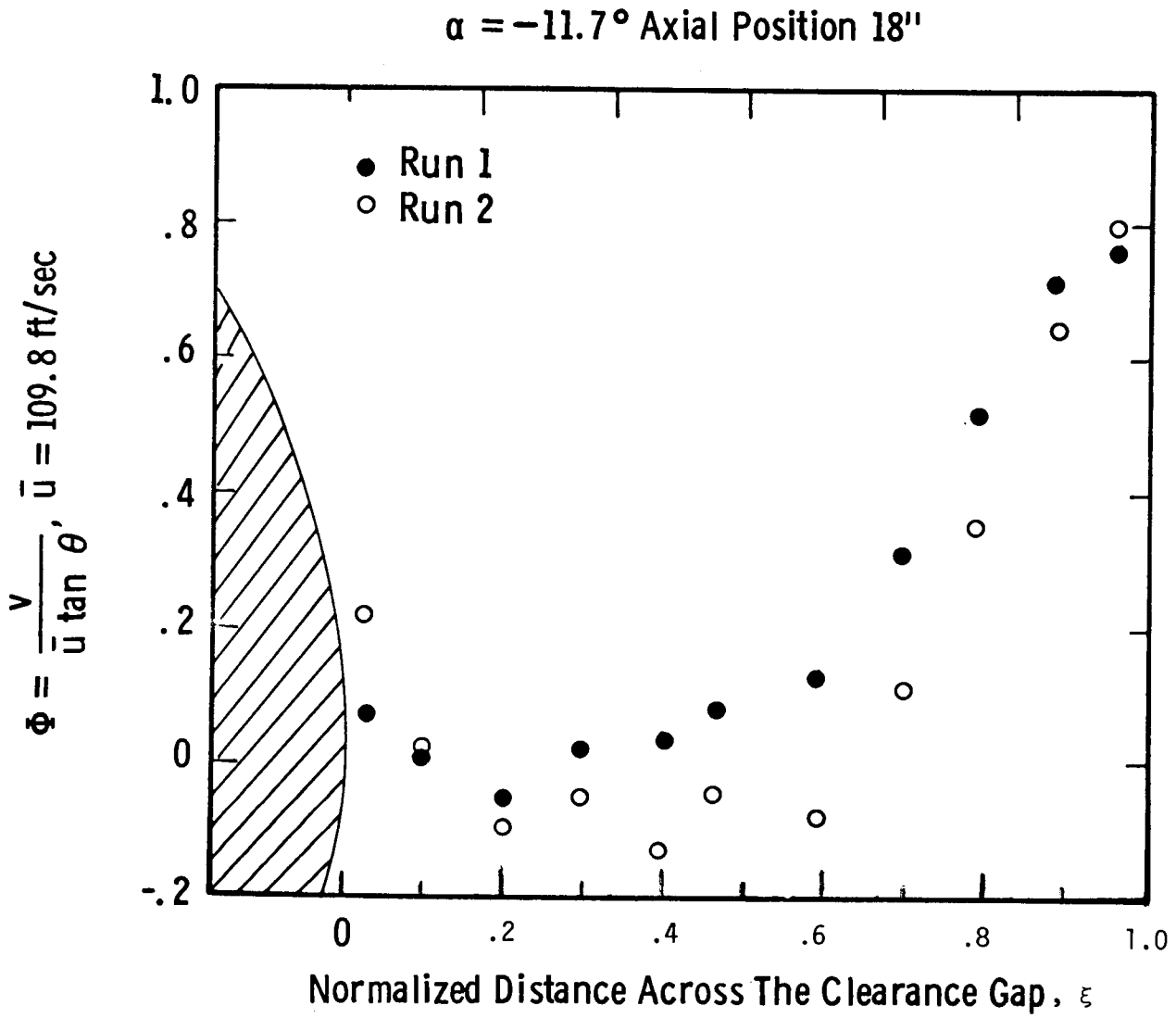

Fig. B-22 — Dimensionless crossflow coefficient $\Phi(\xi)$, $\alpha = -11.7°$

Curve 685720-A

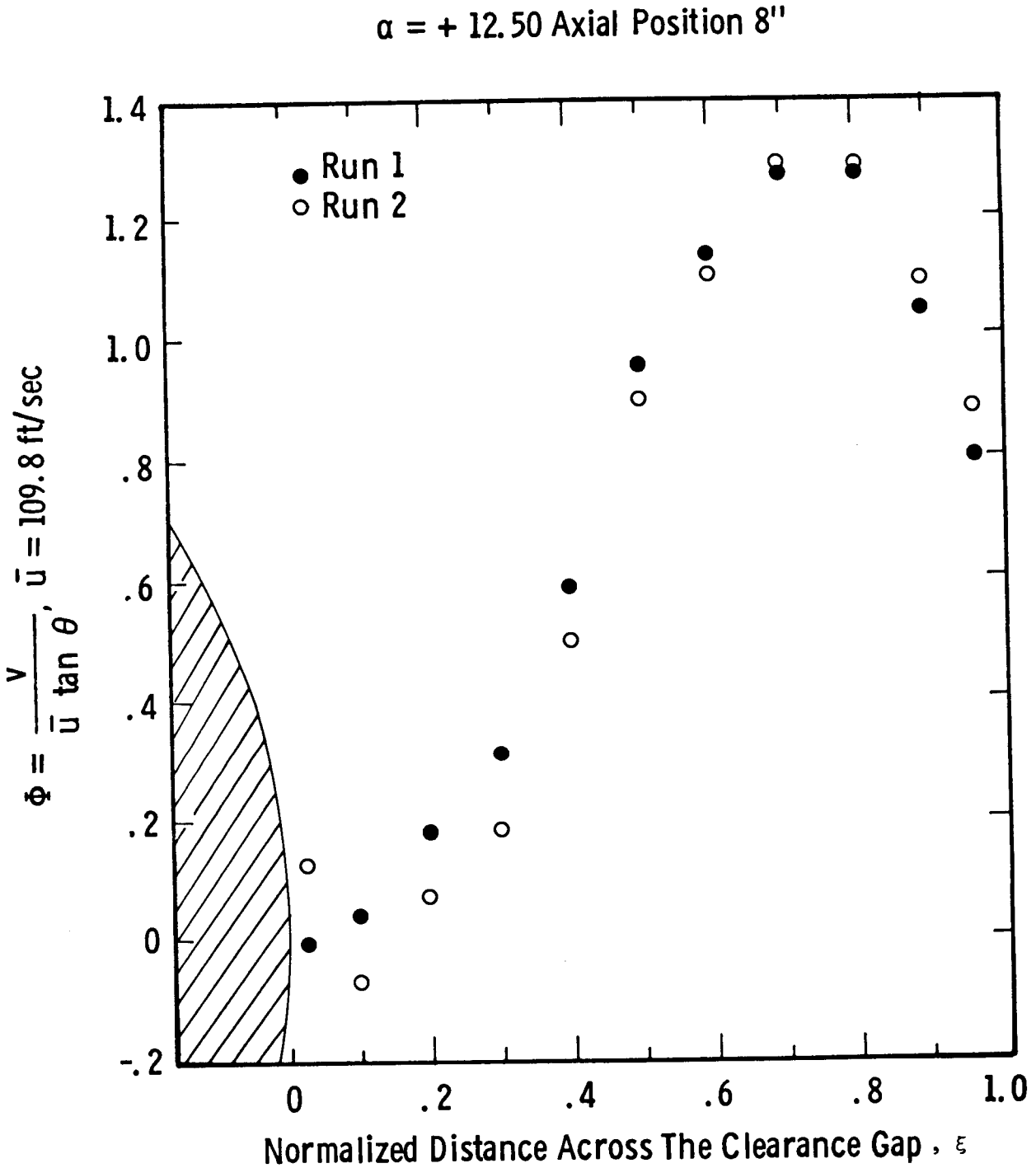

Fig. B-23 — Dimensionless crossflow coefficient $\Phi(\xi)$, $\alpha = 12.5°$

Curve 685723-A

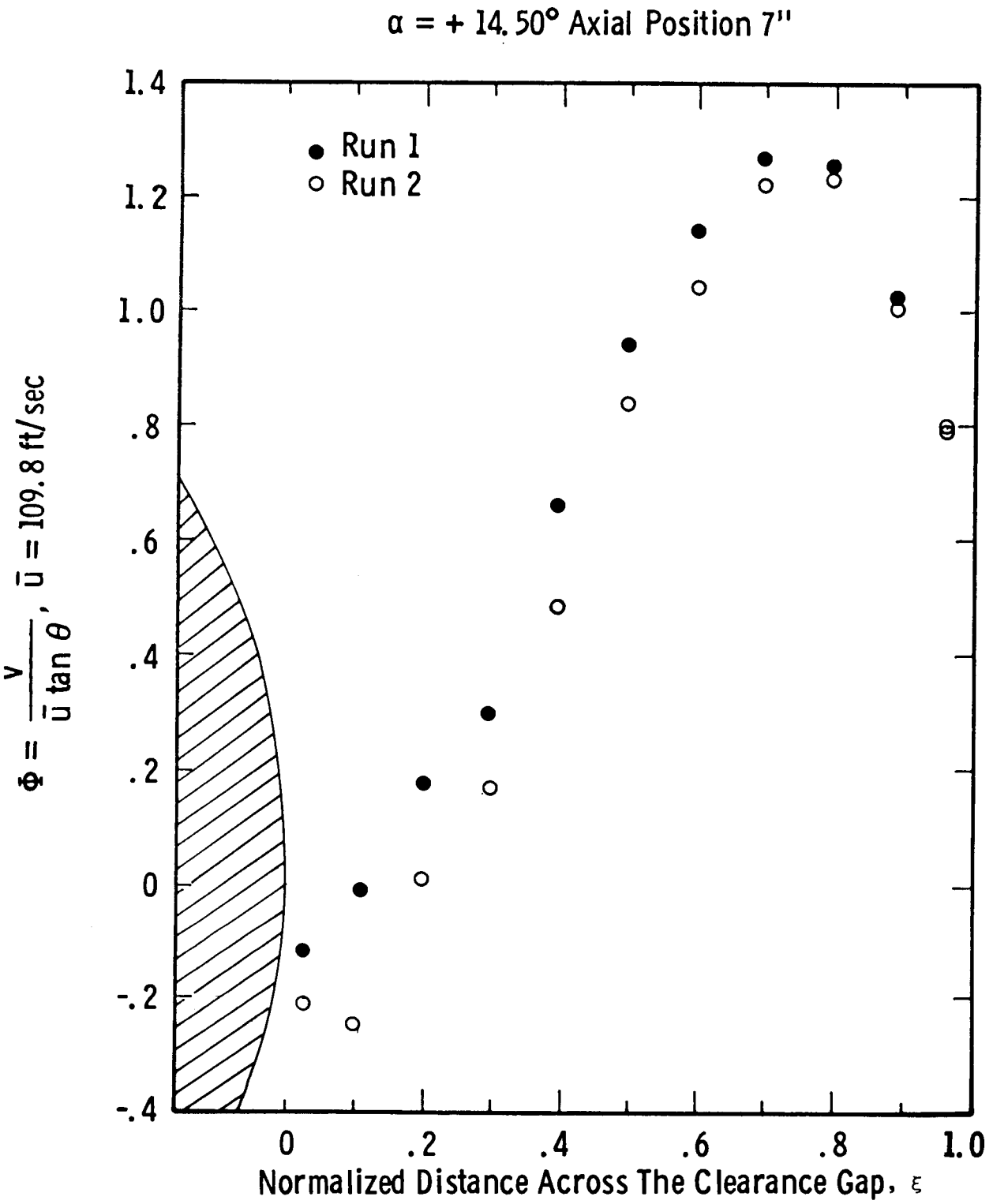

Fig. B-24 — Dimensionless crossflow coefficient $\Phi(\xi)$, $\alpha = 14.5°$

Curve 685724-A

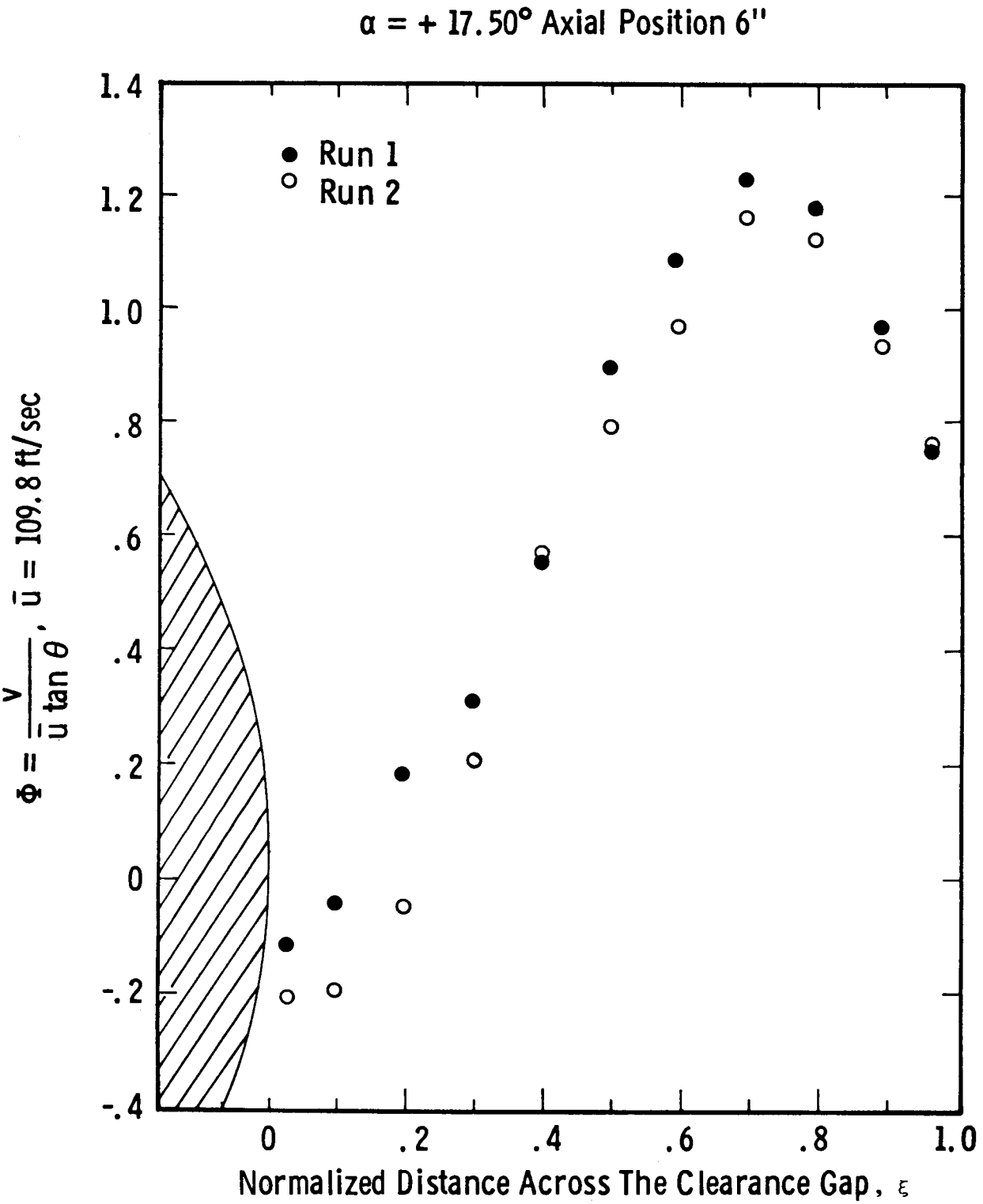

Fig. B-25 — Dimensionless crossflow coefficient $\Phi(\xi)$, $\alpha = +17.5°$

Curve 685725-A

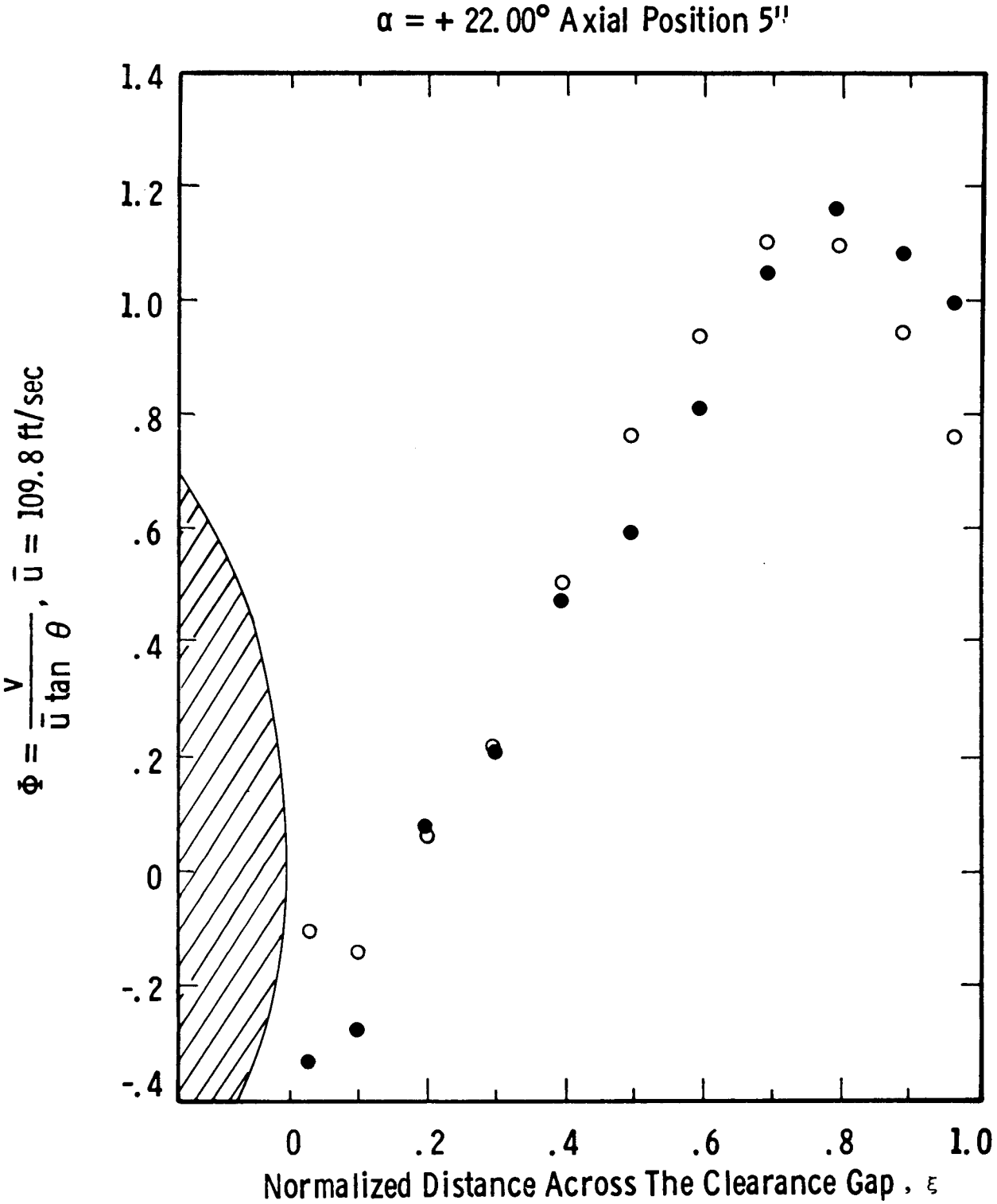

Fig. B-26 — Dimensionless crossflow coefficient $\Phi(\xi)$, $\alpha = 22.0°$

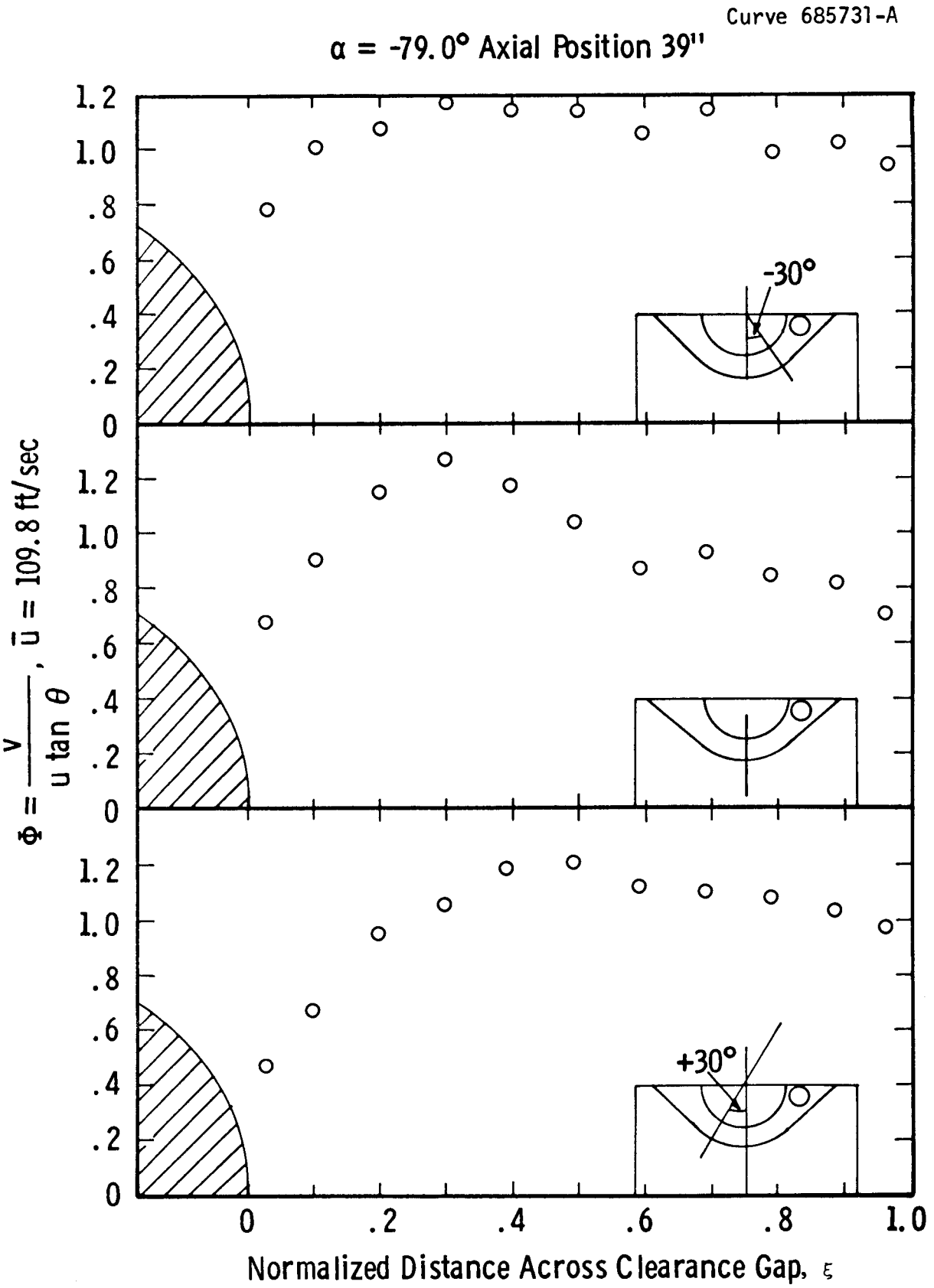

Fig. B-27 – Dimensionless crossflow coefficient $\Phi(\xi)$ for three gaps at $\alpha = -79.0°$

Curve 685730-A

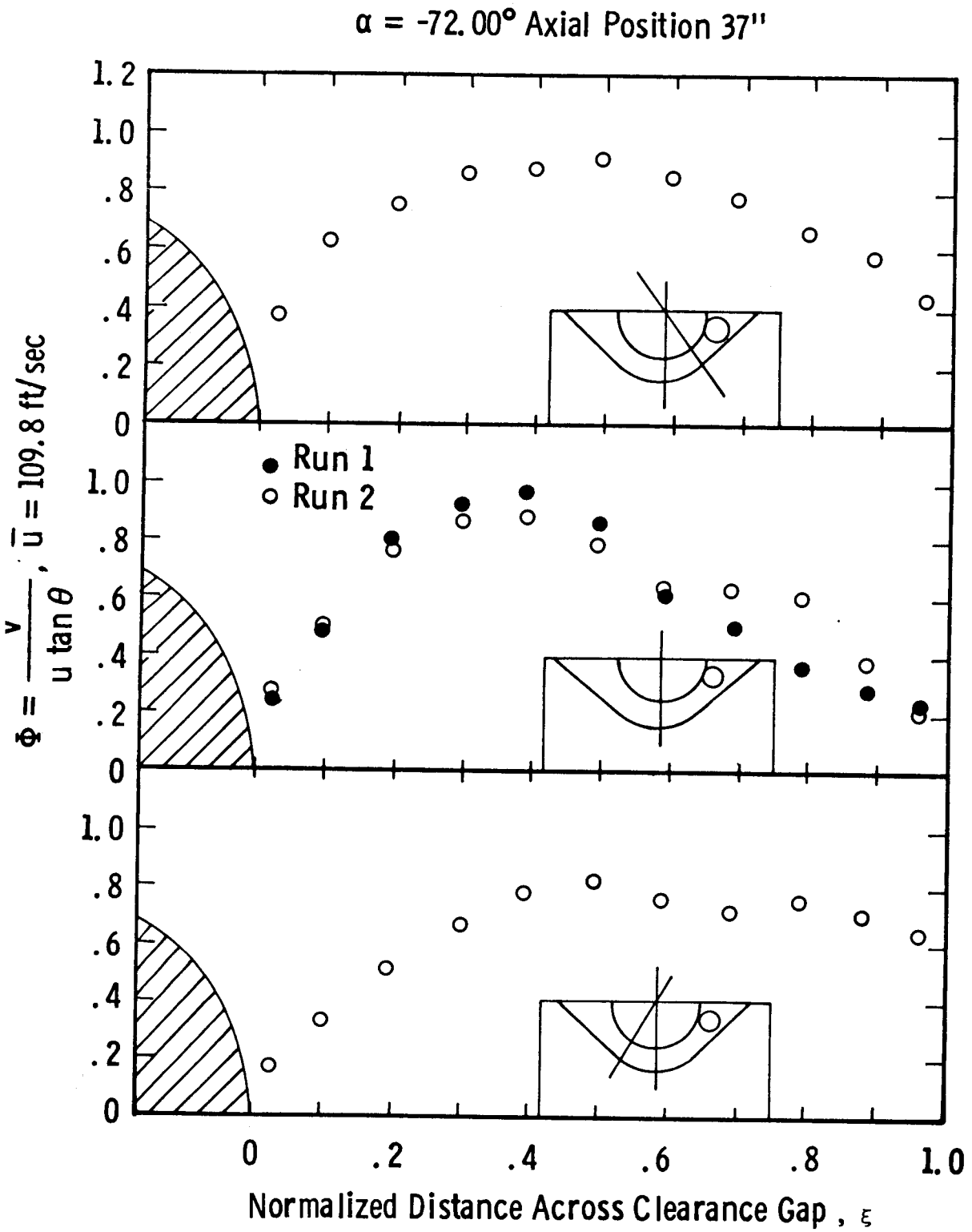

Fig. B-28 — Dimensionless crossflow coefficient $\Phi(\xi)$ for three gaps at $\alpha = -72.0°$

Curve 685729-A

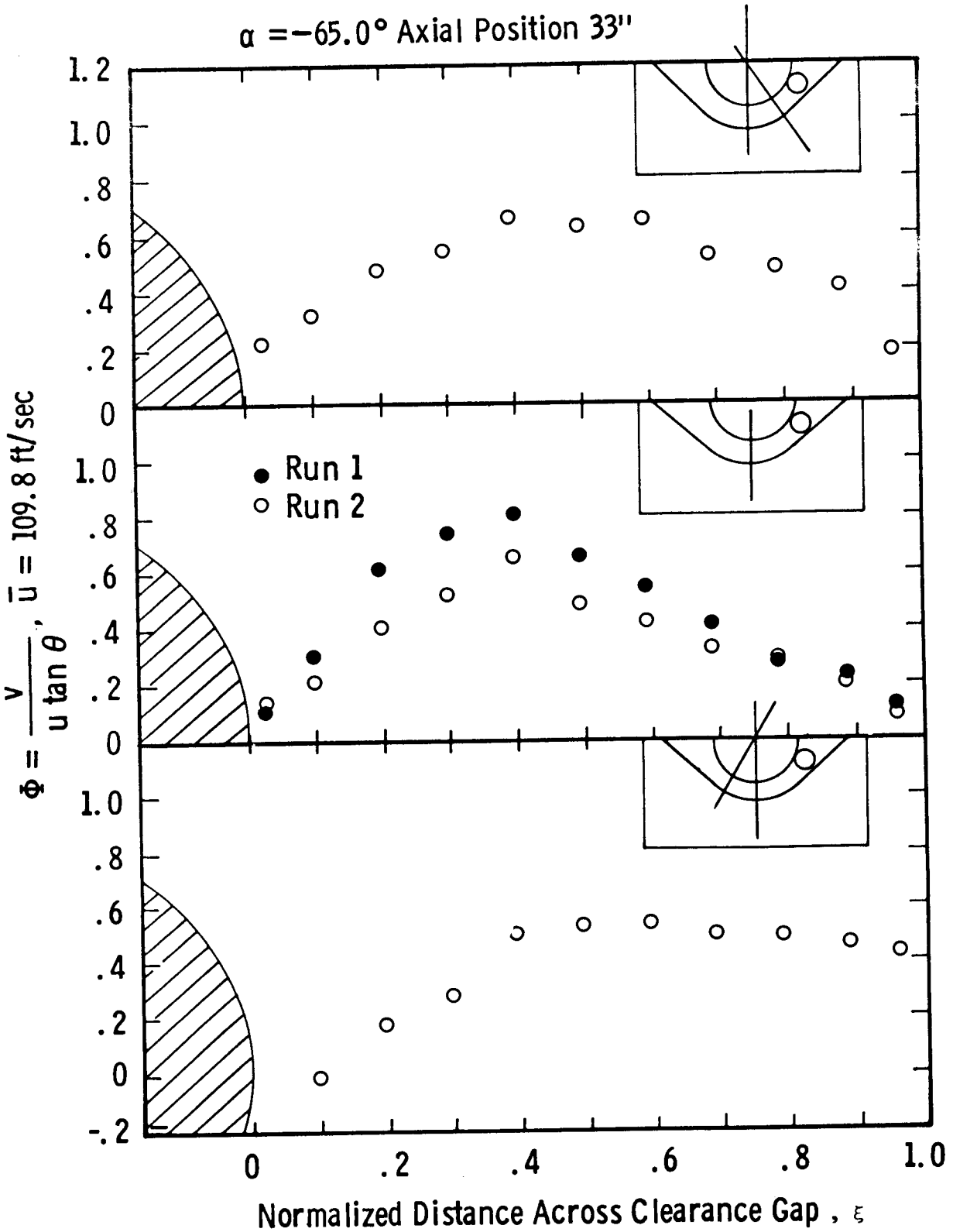

Fig. B-29 — Dimensionless crossflow coefficient Φ (ξ) for three gaps at α = −65.0°

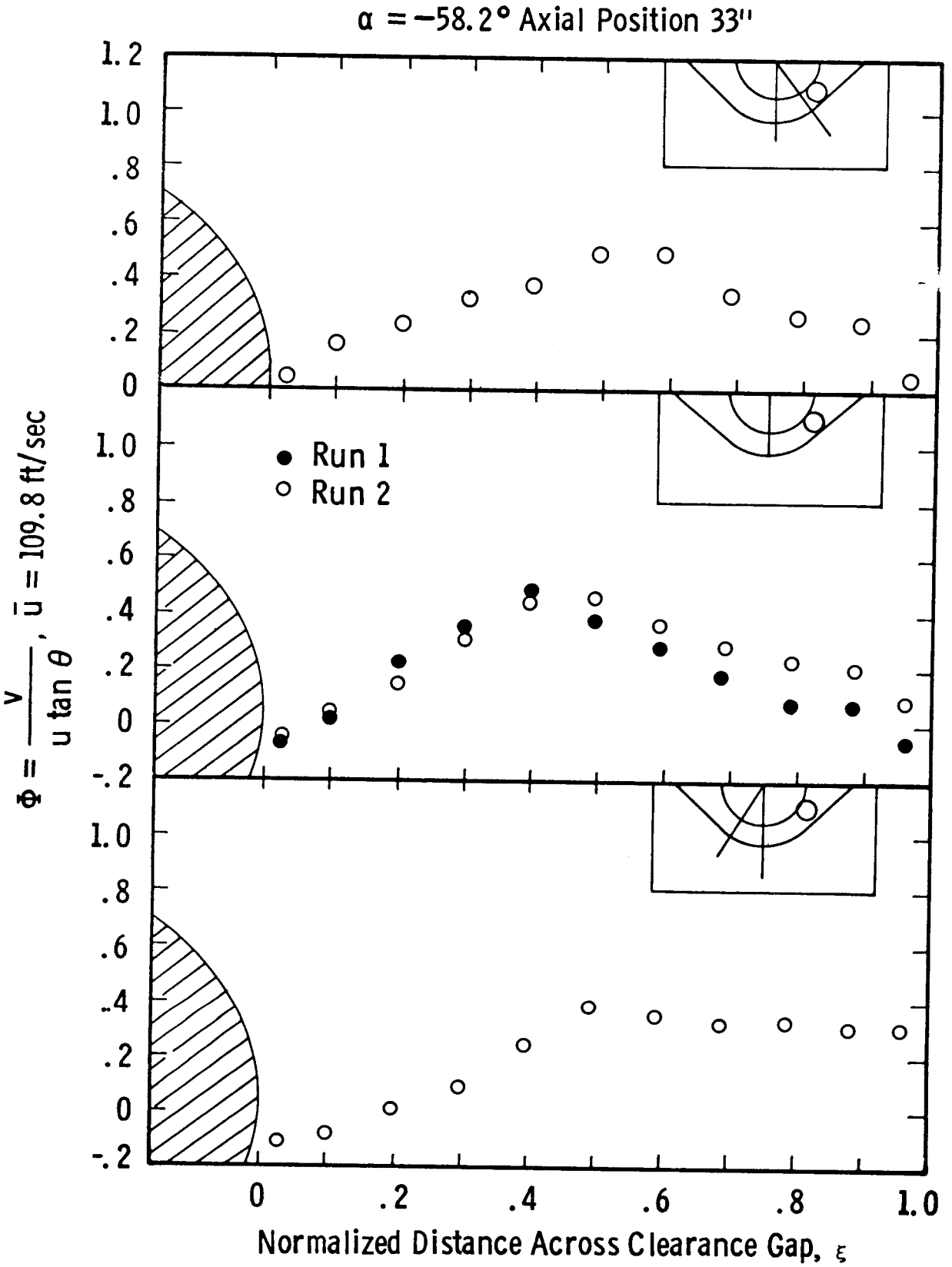

Fig. B-30 — Dimensionless crossflow coefficient $\Phi(\xi)$ for three gaps at $\alpha = -58.2°$

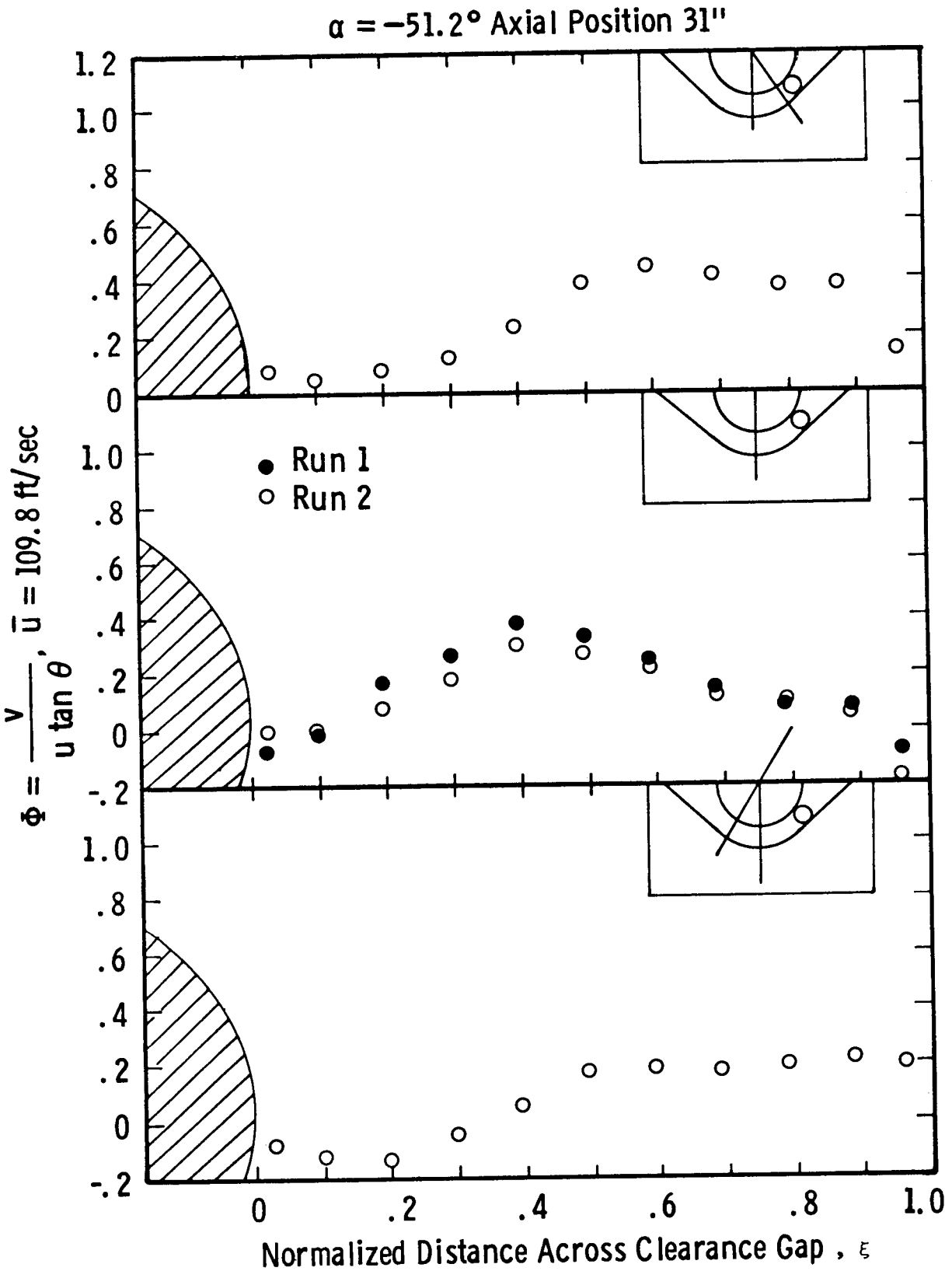

Fig. B-31 – Dimensionless crossflow coefficient Φ (ξ) for three gaps at α = −51.2°

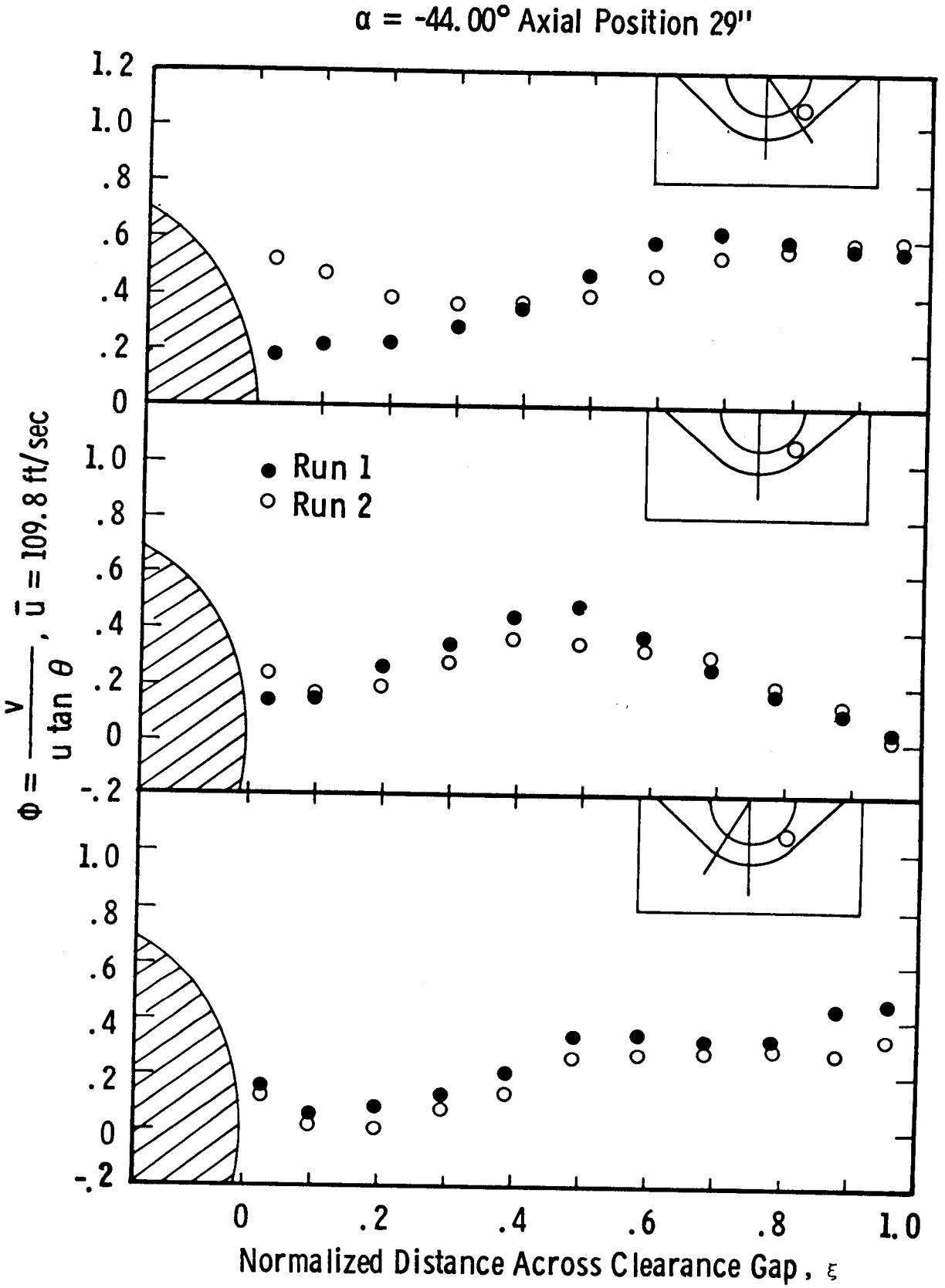

Fig. B-32 — Dimensionless crossflow coefficient $\Phi(\xi)$ for three gaps at $\alpha = -44.0°$

APPENDIX C

Axial Velocity Contours

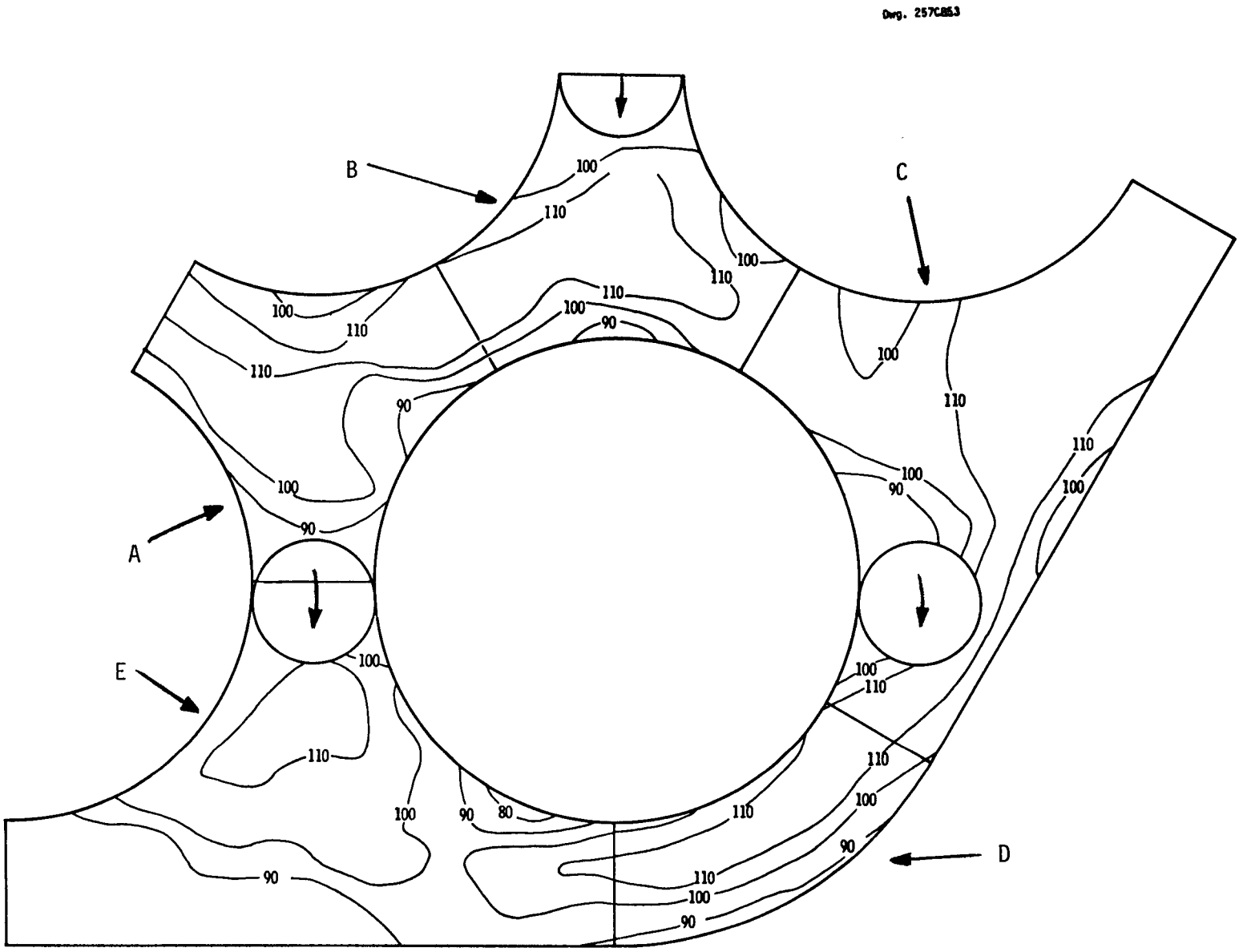

Fig. C-1 — Axial velocity distribution (ft/sec) 33 inches from downstream end of pitot tube travel

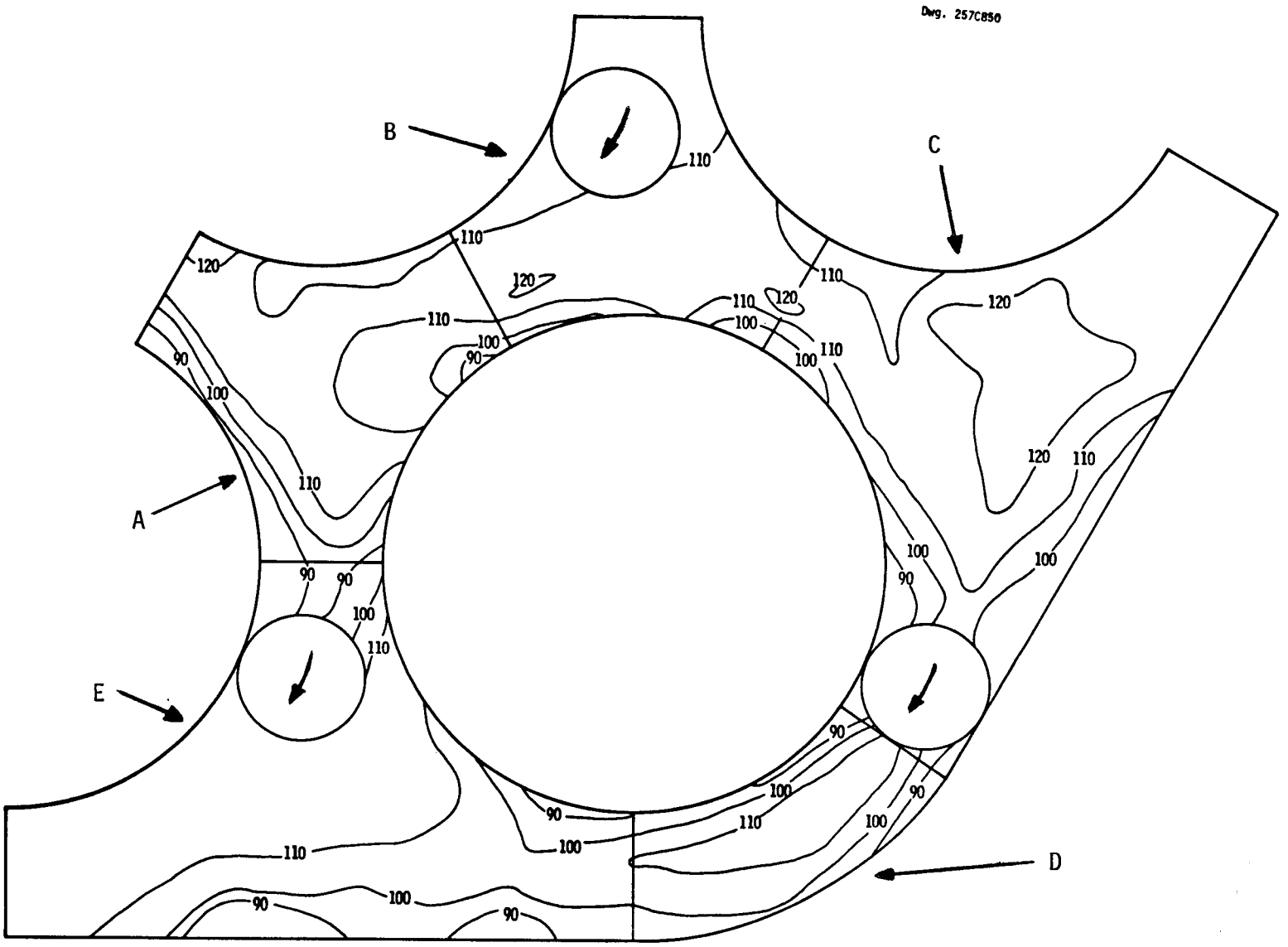

Fig. C-2 — Axial velocity distribution (ft/sec) 27 inches from downstream end of pitot tube travel

Dwg. 257C849

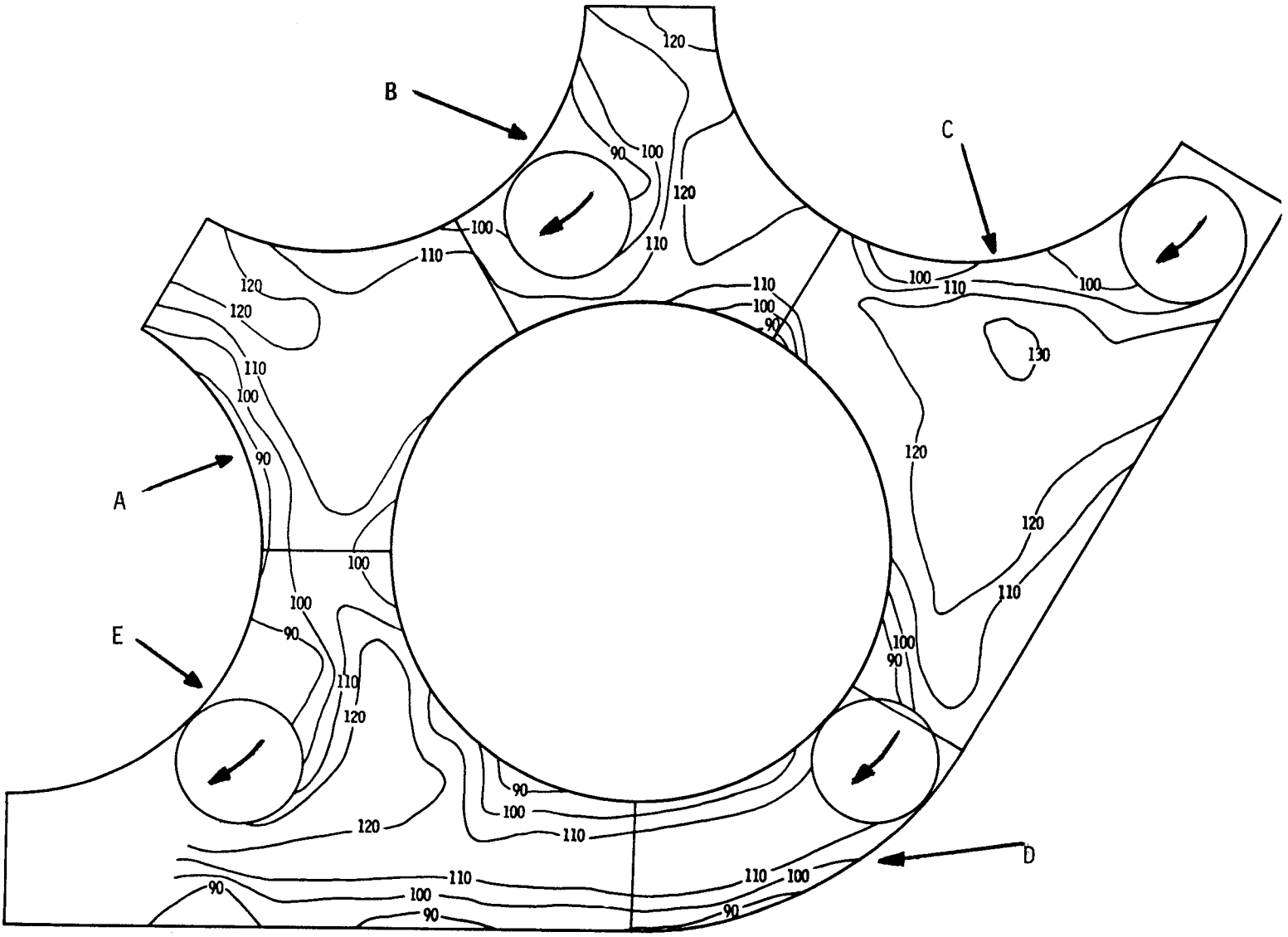

Fig. C-3 — Axial velocity distribution (ft/sec) 21 inches from downstream end of pitot tube travel

Dwg. 257C851

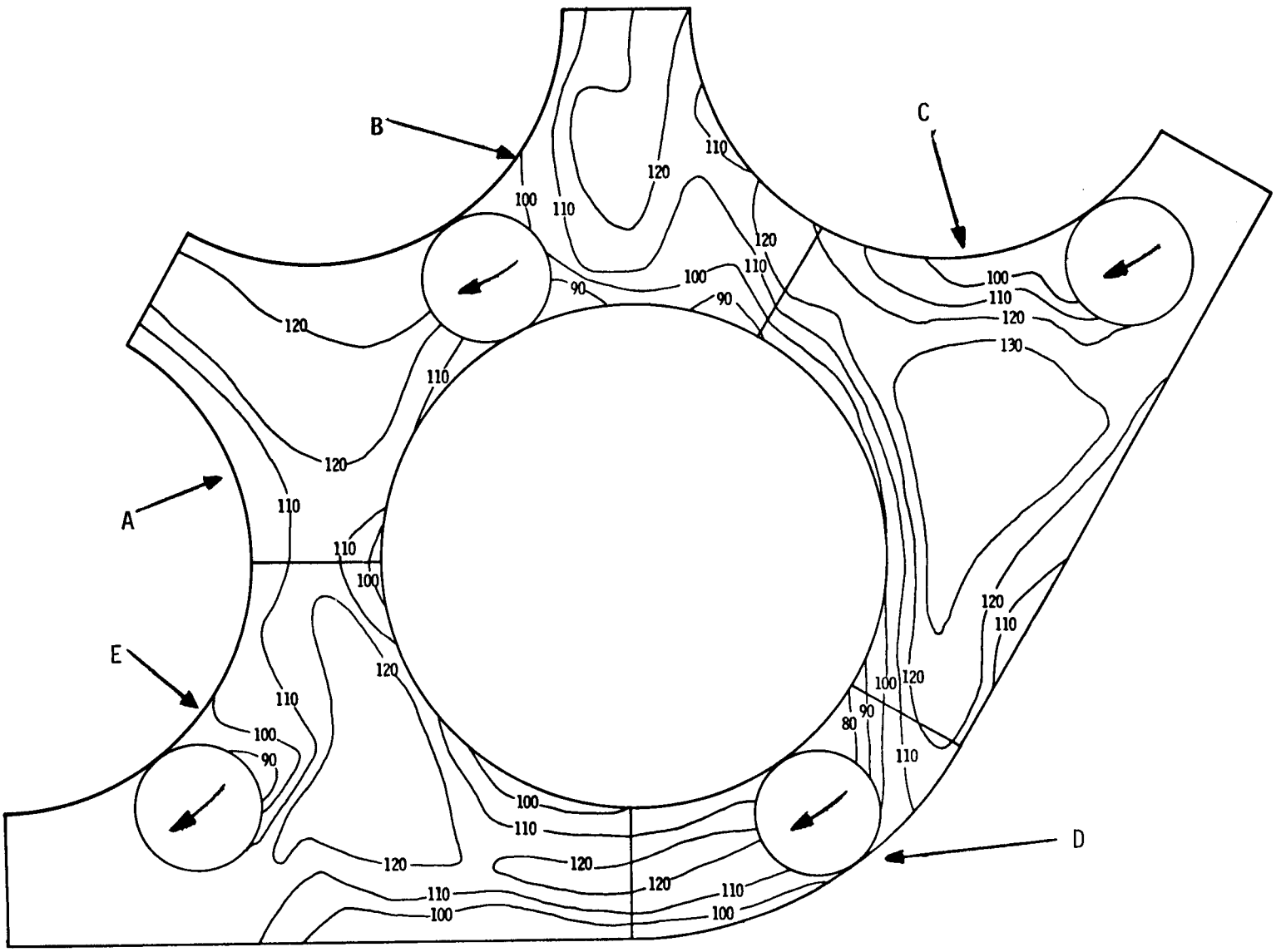

Fig. C-4 — Axial velocity distribution (ft/sec) 15 inches from downstream end of pitot tube travel

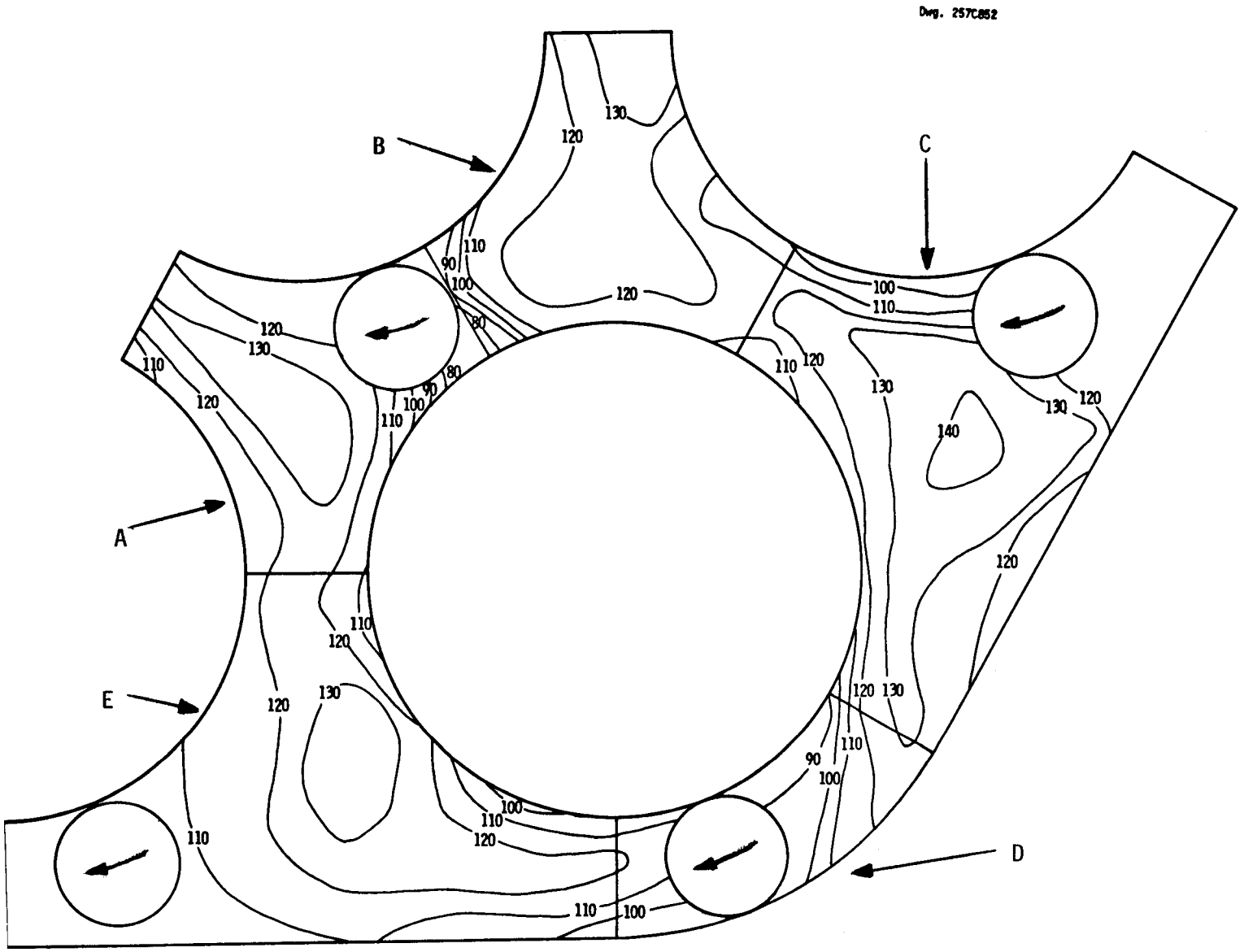

Fig. C-5 — Axial velocity distribution (ft/sec) 9 inches from downstream end of pitot tube travel